

# **Experimental Evaluation of Rover Mobility Prediction Methods using Single Wheel Experiments**

**Alexander Demishkevich**

**A Thesis  
in  
The Department  
of  
Electrical and Computer Science**

**Presented in Partial Fulfillment of the Requirements  
for the Degree of  
Master of Applied Science (Electrical and Computer Engineering) at  
Concordia University  
Montréal, Québec, Canada**

**March 2025**

**© Alexander Demishkevich, 2025**

CONCORDIA UNIVERSITY

School of Graduate Studies

This is to certify that the thesis prepared

By: **Alexander Demishkevich**

Entitled: **Experimental Evaluation of Rover Mobility Prediction Methods using  
Single Wheel Experiments**

and submitted in partial fulfillment of the requirements for the degree of

**Master of Applied Science (Electrical and Computer Engineering)**

complies with the regulations of this University and meets the accepted standards with respect to originality and quality.

Signed by the Final Examining Committee:

\_\_\_\_\_ Chair  
*Dr. Name of the Chair*

\_\_\_\_\_ External Examiner  
*Dr. Name of External Examiner*

\_\_\_\_\_ Examiner  
*Dr. Name of Examiner One*

\_\_\_\_\_ Supervisor  
*Dr. Name of Supervisor*

Approved by

\_\_\_\_\_  
Dr. Abdelwahab Hamou-Lhadj, Chair  
Department of Electrical and Computer Science

\_\_\_\_\_ 2025

\_\_\_\_\_  
Mourad Debbabi, Dean  
Faculty of Engineering and Computer Science

# Abstract

## Experimental Evaluation of Rover Mobility Prediction Methods using Single Wheel Experiments

Alexander Demishkevich

Multiple lunar exploration activities from around the world are driving the development of small skid-steer rovers for Moon missions. Single wheel experiments are commonly done to approximate the mobility of a rover design. This research aims to evaluate the limitations and accuracy of simple approximation models. In this work, single-wheel and full rover laboratory experimentation methods are described for systematic comparison of wheel designs in point turns and slope climbing. The effects of lunar gravity are accounted for using Granular Scaling Laws and GRC-1 lunar simulant in all experiments. Single wheel experiments are paired with simple theoretical models to predict full rover performance. The accuracy of the predictions are confirmed using scaled tests with a full rover. Slanted grousers are shown to be compared favorably against V-offset grousers for point turns, achieving successful point turning with approximately 30% slip in single-wheel and full rover experiments. This also showed that single wheel experiments can accurately predict full rover performance in point turns. On the other hand, slope climbing predictions had a substantial amount of errors. In part, this error was found to be explained by the diameter/width value of the wheel, with larger values being associated to a higher prediction error. To reduce prediction error a correction factor can be approximated from the experimental rigid wheel test datasets.

# Acknowledgments

I would like to express my sincerest gratitude to my supervisor, Dr. Krzysztof Skonieczny, for his invaluable guidance, support, and encouragement throughout my research. His expertise and insightful feedback have been instrumental in shaping this work, and I am truly grateful for the opportunity to learn under his supervision.

I am incredibly grateful to Pierre-Lucas Aubin-Fournier for his guidance and training on laboratory equipment, which played a crucial role in my research. Additionally, I am thankful for the support and collaboration of my lab colleagues, including Dr. Adriana Daca, Chantelle Dubois, Fauzi Ame, Jasim Usmani, Mohammad Azami, and Momtaz Abadir. Their insights, discussions, and teamwork have significantly enriched my research experience.

A special note of appreciation goes to my family for their unwavering support and encouragement. Their belief in me and my aspirations has motivated me throughout my academic journey.

Furthermore, I am profoundly grateful to my wife, Maria, for her support and motivation through every challenge and success during my research.

For their financial and technical contributions I would like to thank MDA Space and Mission Control Space Services. Moreover, funding from the Natural Sciences and Engineering Research Council of Canada and Concordia University has been crucial in enabling this research and advancing the study of planetary rover mobility.

To everyone who has contributed to this journey in any way, I extend my sincere gratitude. Your support, guidance, and encouragement have made this accomplishment possible.

# Contents

<b>List of Figures</b>	<b>ix</b>
<b>List of Tables</b>	<b>xi</b>
<b>1 Introduction</b>	<b>1</b>
1.1 Introductory concepts . . . . .	3
1.1.1 Rigid Wheels Characteristics . . . . .	3
1.1.2 Rigid Wheel Evaluation Criteria . . . . .	4
1.1.3 Skid-Steer Rover Mobility Metrics . . . . .	6
1.2 Research Problem . . . . .	7
1.3 Thesis Objective . . . . .	7
1.4 Contributions . . . . .	7
1.5 Publications . . . . .	8
1.6 Thesis Outline . . . . .	8
<b>2 Literature Review</b>	<b>10</b>
2.1 Soil Wheel Interactions . . . . .	10
2.2 Single Wheel Mobility . . . . .	11
2.2.1 Grousers . . . . .	11
2.2.2 Single Wheel Test Beds . . . . .	13
2.2.3 Evaluating Steering Ability Using SWTB . . . . .	14
2.2.4 Evaluating Slope Climbing Ability Using SWTB . . . . .	15

2.3	Full Rover Mobility Predictions	16
2.4	Effect of Reduced Gravity	17
2.4.1	Soil Simulants	18
2.4.2	Reduced-mass engineering models	19
2.4.3	Granular Scaling Laws	19
2.4.4	Geotechnical Magnetic Similitude Models	20
2.4.5	Soil modeling techniques	20
2.5	Simulations of Soil Flow Properties	21
<b>3</b>	<b>Research Methodology</b>	<b>23</b>
3.1	Experimental Apparatus	23
3.1.1	Single Wheel Gantry	23
3.1.2	Full Rover Test Environment and Data Gathering	24
3.1.3	Husky Rover	25
3.1.4	Soil Preparation	25
3.1.5	Experimental Wheel Design	26
3.2	GSL and Equal Load Approximations	29
3.3	Using Single Wheel Tests to Evaluate Mobility of a Wheel Design	30
3.3.1	Predicting Full Rover Point Turn Ability	31
3.3.2	Predicting Full Rover Slope Climbing Ability	32
3.3.3	Sub Surface Soil Flow Imaging	33
<b>4</b>	<b>Results</b>	<b>35</b>
4.1	Comparing Slanted and V-Offset Grouser Designs for Point Turns and Slope Climbing	36
4.1.1	Single Wheel Experiments	36
4.1.2	Single Wheel Results: Drawbar Pull Coefficient	37
4.1.3	Single Wheel Results: Sinkage	37
4.1.4	Single Wheel Results: Tangent Turning Force	38
4.2	Single Wheel Tests to Predict Point Turns	39
4.2.1	Full Rover Point Turn Results: Sinkage	40

4.2.2	Full Rover Point Turn Results: Slip . . . . .	41
4.3	Single Wheel Tests to Predict Slope Climbing . . . . .	42
4.3.1	Full Rover Slope Climbing Results: Slip . . . . .	43
4.3.2	Full Rover Slope Climbing Results: Sinkage . . . . .	44
4.4	Influence of Weight Distribution on Slope Climbing Predictions . . . . .	44
4.4.1	Weight Distribution Theory . . . . .	45
4.4.2	Slope Climbing Predictions . . . . .	46
4.4.3	Single Wheel Experiments . . . . .	47
4.4.4	Prediction Accuracy Evaluation . . . . .	54
4.5	Influence of Diameter over Width Ratio on Slope Climbing Predictions . . . . .	56
4.5.1	Diameter over Width Effect on Slope Climbing . . . . .	58
4.5.2	Improving Prediction Using Diameter/Width Value . . . . .	61
4.6	Single Wheel Experiments on Sloped Terrain . . . . .	63
4.6.1	Data Collection on Sloped Terrain . . . . .	63
4.6.2	Results: Drawbar Pull Coefficient . . . . .	64
4.6.3	Sinkage . . . . .	65
4.7	Soil Imaging Comparison between Flat and Sloped Terrain . . . . .	66
4.7.1	Drawbar Pull Equations . . . . .	67
4.7.2	Soil Imaging Experiments . . . . .	69
4.7.3	Soil Imaging Results . . . . .	71
<b>5</b>	<b>Conclusions and Future Work</b>	<b>74</b>
5.1	Advantages of Slanted Grousers over V-offset Grousers for Slope Climbing and Point Turns . . . . .	74
5.2	Predicting Full Rover Point Turns using Single Wheel Experiments . . . . .	75
5.2.1	Estimating Point Turn Performance . . . . .	76
5.3	Predicting Full Rover Slope Climbing using Single Wheel Experiments . . . . .	76
5.3.1	Single Wheel Experiments on Flat Versus Slope Terrain . . . . .	76
5.3.2	Evaluating Slope Climbing Ability using Single Wheel Experiments . . . . .	77

5.3.3	Influence of Vertical Load Distribution Methods on Slope Climbing Predictions . . . . .	77
5.3.4	Soil Imaging . . . . .	78
5.3.5	Estimating Slope Climbing Performance . . . . .	78
5.4	Diameter and Width Experiments and Influence on Slope Climbing Predictions . .	79
5.5	Sources of Error and Limitations . . . . .	79
5.6	Future Work . . . . .	80
	<b>Bibliography</b>	<b>81</b>

# List of Figures

Figure 1.1	Rigid wheel with grousers . . . . .	3
Figure 1.2	Grouser Parameter Diagram . . . . .	4
Figure 1.3	Forces and their Directions Acting on a Wheel in a Point Turn . . . . .	5
Figure 3.1	Single wheel test apparatus . . . . .	24
Figure 3.2	Husky rover test platform during experiments . . . . .	25
Figure 3.3	V-offset (left) and Slanted (right) grousers . . . . .	26
Figure 3.4	CAD drawing of original wheel used in single wheel experiments . . . . .	29
Figure 3.5	CAD drawing of GSL scaled wheel used in single wheel experiments . . . . .	29
Figure 3.6	Husky rover and wheel dimensions used during experimentation, scaled relative to the LRM CSA lunar concept rover . . . . .	32
Figure 3.7	Forces experienced by wheel on sloped terrain . . . . .	32
Figure 3.8	Soil Imaging Attachment to SWTB . . . . .	34
Figure 4.1	Drawbar pull vs Slip data for equal loading (upper bounds) and GSL (lower bounds) experiments for Slanted and V-offset grouser designs. . . . .	38
Figure 4.2	Sinkage obtained during single wheel experiments, with the higher sinkage corresponding to GSL conditions and lower sinkage to Equal Load . . . . .	38
Figure 4.3	Sinkage in point turn driving for single wheel tests, with the higher sinkage corresponding to GSL conditions and lower sinkage to Equal Load . . . . .	39
Figure 4.4	Tangent turning force generated by the wheel during single wheel tests with the GSL corresponding to the lower bound and equal load to the upper. . . . .	39
Figure 4.5	Grouser orientation (view from below the rover) . . . . .	40

Figure 4.6	Average sinkage obtained during point turn full rover test . . . . .	41
Figure 4.7	Average slip obtained during point turn full rover test . . . . .	42
Figure 4.8	Velocity and slip obtained during slope experiments . . . . .	43
Figure 4.9	Sinakge obtained during slope experiments . . . . .	44
Figure 4.10	Forces Acting on Vehicle on Slope Terrain . . . . .	45
Figure 4.11	Wheels used in experiments; Bare, Grouser, Husky from left to right . . . . .	48
Figure 4.12	Bare Wheel $DB.P_{coeff}$ vs slip . . . . .	50
Figure 4.13	Grouser Wheel $DB.P_{coeff}$ vs slip . . . . .	52
Figure 4.14	Husky Wheel $DB.P_{coeff}$ vs slip . . . . .	53
Figure 4.15	All Slip Data for Grouser and Bare Wheels (including edge values) . . . . .	58
Figure 4.16	Slip Data Trends, Mid vs Boundary . . . . .	59
Figure 4.17	Mild Slip Data for Grouser and Bare Wheels . . . . .	60
Figure 4.18	Mild Slip Data for Grouser and Bare Wheels . . . . .	62
Figure 4.19	Single Wheel Experiments on Incline Terrain . . . . .	64
Figure 4.20	Comparing Force Generated by Grouser Wheel on Flat and Slope Terrain . . . . .	66
Figure 4.21	Comparing Grouser Wheel Sinkage on Slope Terrain . . . . .	67
Figure 4.22	Terremechanic Model of Wheel . . . . .	68
Figure 4.23	Image Processing Applied to GreyScale Image . . . . .	70
Figure 4.24	Wheel Rim Found After Application of Hough Transform . . . . .	70
Figure 4.25	Wheel Rim Found After Application of Hough Transform . . . . .	71
Figure 4.26	Magnitude plot of theta vector with blue representing CCW motion and yellow CW motion . . . . .	71
Figure 4.27	Magnitude and Direction Plots for wheel movement from right to left . . . . .	72

# List of Tables

Table 3.1	Grouser height to slope angle relationship . . . . .	27
Table 3.2	GSL variables . . . . .	31
Table 3.3	Tuning Parameters used in the SOFT Algorithm . . . . .	34
Table 4.1	Single wheel experimental conditions . . . . .	36
Table 4.2	Full Rover Parameters . . . . .	46
Table 4.3	Vertical load on the front and rear axles on sloped terrain . . . . .	46
Table 4.4	Experiments Completed to Test Influence of Weight Distribution . . . . .	48
Table 4.5	Force Required to Climb the Slopes Tested for Bare Wheel . . . . .	49
Table 4.6	Bare Wheel Estimated Slip Compared to Actual Slip Required to Climb Slope	51
Table 4.7	Force Required to Climb the Slopes Tested for Grouser Wheel . . . . .	51
Table 4.8	Grouser Wheel Estimated Slip Compared to Actual Slip Required to Climb Slope . . . . .	51
Table 4.9	Force Required to Climb the Slopes Tested For Husky Wheel . . . . .	52
Table 4.10	Husky Wheel Estimated Slip Compared to Actual Slip Required to Climb Slope	53
Table 4.11	Single Wheel Prediction Error for Front & Rear Method: Absolute Difference	54
Table 4.12	Single Wheel Prediction Error for Front & Rear Method: Percent Difference	55
Table 4.13	Single Wheel Prediction Error for 1/4 Method: Absolute Difference . . . . .	55
Table 4.14	Single Wheel Prediction Error for 1/4 Method: Percent Difference . . . . .	55
Table 4.15	Diameter to Width Ratio of Wheel used Previously . . . . .	57
Table 4.16	Single Wheel Experiments Completed to Test Influence of Diameter over Width	57
Table 4.17	Full Rover Experiments Completed to Test Influence of Diameter over Width	58

Table 4.18 Anderson Darling Test for all Wheels . . . . .	61
Table 4.19 T-Test for all Wheels . . . . .	61
Table 4.20 Slip Error for Grouser Wheel 64 mm after Adding a Correction Factor . . . . .	63
Table 4.21 Single Wheel Test Data for Flat and Slope Terrain for 88N Verical Load . . . . .	64
Table 4.22 Single Wheel Test Data for Flat and Slope Terrain for 149N Verical Load . . . . .	65
Table 4.23 Single Wheel Test Data for Flat and Slope Terrain for 210N Verical Load . . . . .	65
Table 4.24 Single Wheel Test Completed for Soil Imaging Experiments . . . . .	69
Table 4.25 Single Wheel Test Results, Location in Angle of Flow Switch for 210N . . . . .	72
Table 4.26 Single Wheel Test Results, Location in Angle of Flow Switch for 88N . . . . .	73

# Chapter 1

## Introduction

Extra-planetary exploration missions have been ongoing topics of research for the past decades. These missions not only satisfy human curiosity about the universe around us but also contribute to significant advances in technology that can be applied in a variety of fields. Since the early days of space exploration, planetary rovers have played an important role in furthering our understanding of the celestial bodies that surround us. To succeed in their role, rovers are required to safely travel through difficult terrain to scientifically interesting locations. The ability of rovers to traverse difficult terrain is established in the initial engineering design. To reduce cost and mission risk, different techniques can be applied that approximate the maximum mobility of a prototype rover. This research focuses on how rover mobility can be estimated during the early engineering design phase of the project.

The ongoing NASA Artemis program and multiple other space agencies have placed high priority on the robotic exploration of the Moon and Mars surface. An example mission scenario is the Canadian Space Agency's (CSA) lunar rover mission; this work was carried out as part of a Phase A study for this mission with a team led by MDA. The robotic exploration of planetary surfaces faces two large challenges. The first challenge is navigating the surfaces that mainly consist of fine granular regolith embedded with rocks. The second is the influence of reduced gravity. Despite the large amount of progress made in these fields over the past decades, planetary exploration has many risks and difficulties. The Moon rovers Lunakhod 1, Lunakhod 2, Lunar Roving Vehicle (LRV) and Mars

rovers, Spirit, Opportunity and Curiosity all encountered challenges originating from soil-wheel interactions. Lunakhods faced highly deformable soils when operating near crater rims, this led to sinkage orders of magnitudes more than during normal traverses (over 20 cm vs. a few cm) (Ming, 1992). Furthermore, Lunakhod got stuck on a crater slope and was only freed after applying full power to the mobility system which had the consequence of the rover having to recharge for the rest of the month (Harvey, 2007). Spirit faced high slippage during its operations in loose sandy terrain, and became stuck in a sulfate sand-filled crater (Arvidson et al., 2010), which ended its mission. Similarly, Opportunity lost multiple weeks of progress due to high slip situations including being embedded in the "Purgatory Dune" (Sullivan, Anderson, Biesiadecki, Bond, & Stewart, 2011). The Lunar Roving Vehicle (LRV) (Costes, Farmer, & George, 1972; Ming, 1992) and Lunakhods (Harvey, 2007; Kassel, 1971; Ming, 1992) faced similar mobility challenges when operating on the lunar surface. These situations emphasize the importance of correctly understanding the mobility profiles of planetary rovers in all mission stages. Reduced gravity also influences the mobility of the planet's rover directly through the soil-to-wheel and soil-to-soil interactions. For exploration of any of the rocky bodies (i.e. except the gas giants) in the solar system, planetary rovers will need to contend with a reduction in the level of gravity. Recent advances in wheel-soil and soil-soil interactions have led to the development of more accurate rover testing methods that account for the effect of reduced gravity on soil behavior (Daca & Skonieczny, 2022b). Using these methods one can get an accurate profile of the mobility a rover can expect to achieve under different levels of gravity on flat terrain.

During the design of exploration rovers, their mobility can be approximated from single wheel tests (SWT) using linear gantries and full-rover tests (FRT) using rover prototypes. The primary differences between the tests are cost, availability of an accurate rover test prototype and full-rover experimental apparatus. Given the additional difficulty of full-rover tests, single wheel experiments are often used to get an initial idea of the rover mobility in early development. The interest in low cost rover missions for Lunar exploration leads to development of techniques that can be used to further our ability to predict rover mobility without raising costs and complexity. Furthermore, low cost rover missions motivate rigid wheel design research and development due to their simplicity and ease of manufacturing. The main focus of this work is to explore how single wheel test methods compare to full-rover test methods for rigid wheel skid steer rovers. Furthermore, this work

explores methods that use single wheel tests to approximate the mobility of a full rover platform, its limitations and accuracy. The concepts explored in this research can be extended to different wheel and rover designs that are used in planetary exploration rovers.

## 1.1 Introductory concepts

### 1.1.1 Rigid Wheels Characteristics

The wheels considered in this study are rigid wheels with grousers as illustrated in Fig. 1.1 and have the following general wheel characteristics.  $D$  denotes the wheel width,  $r$  denotes the wheel radius (to the wheel's inter-grouser surface),  $V$  denotes forward velocity of the wheel,  $\omega$  denotes the angular velocity of the wheel,  $h$  denotes the wheel sinkage below the soil surface and  $L$  denotes the wheel diameter.

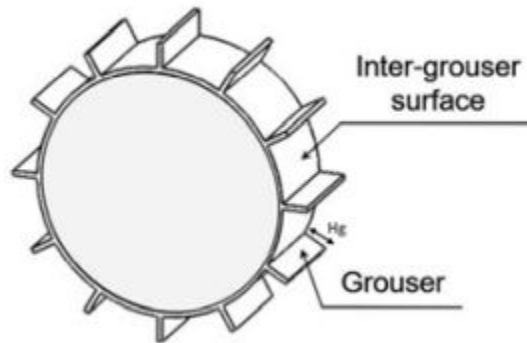


Figure 1.1: Rigid wheel with grousers

A critical part of planetary rover wheels are grousers, also known as lugs or cleats, that extend from the surface of the wheel. Grousers increase the forward force a wheel generates and reduce rolling resistance by preventing forward flow (bulldozing) of the soil ahead of the wheel (Nassiraei & Skonieczny, 2020). Grousers have seen wide use in exploration rovers for most extra-planetary exploration missions. As shown in Fig. 1.2 grousers are defined by the following geometric parameters: radius to wheel's surface ( $r$ ), grouser height ( $h_g$ ), grouser thickness ( $t$ ), grouser spacing (defined by the angle  $\beta$ ), grouser slant angle ( $\zeta$ ), grouser static sinkage angle ( $\theta_t$ ) and static sinkage ( $h$ ). Furthermore, grousers play an important role in the following maneuvers: slope climbing and point turns.

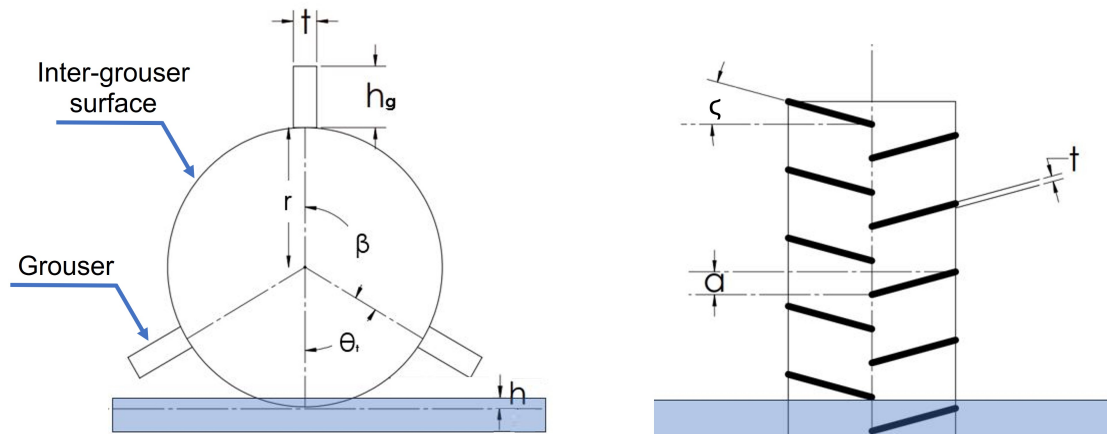


Figure 1.2: Grouser Parameter Diagram

### 1.1.2 Rigid Wheel Evaluation Criteria

The mobility of planetary rover wheels and full rover vehicles are defined and evaluated using the following metrics: drawbar-pull, wheel sinkage, tangent turning force, which are all dependent on wheel slip.

#### Drawbar Pull

A key terramechanics metric describing mobility performance is the drawbar pull (DB.P). The DB.P is defined as wheel thrust force ( $F_T$ ) generated in the desired direction of motion minus all the resisting forces ( $F_R$ ) acting on the wheel. The mobility of a vehicle is derived from the sum of drawbar pull generated by all of its wheels. The net force generated by the vehicle is the main force overcoming gravity resistance during slope climbing.

$$DB.P = F_T - \sum F_R \quad (1)$$

Drawbar pull to weight ratio ( $DB.P/W$ ), or commonly known as the drawbar pull coefficient  $DB.P_{coeff}$ , is approximately constant for a specific wheel design under a practical range of vertical loads. This relationship holds except in critical loads where additional sinkage starts to decrease the resulting drawbar pull.

#### Tangent Turning Force

The tangent turning force ( $F_{TTF}$ ), is the force that drives the rover during the point turn maneuver.

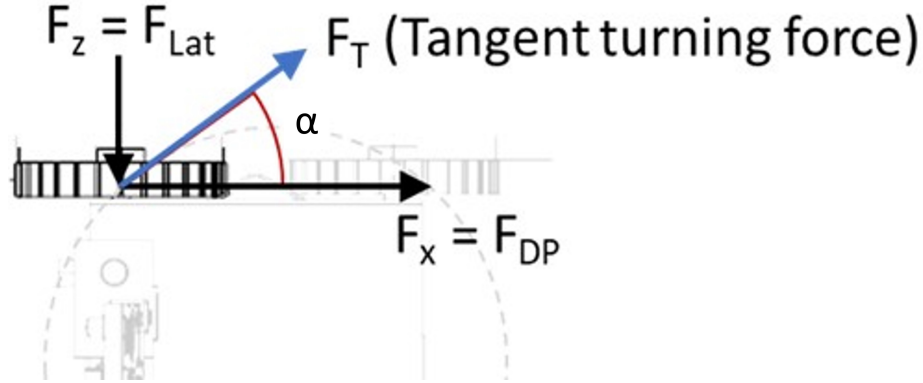


Figure 1.3: Forces and their Directions Acting on a Wheel in a Point Turn

This force acts in the direction of wheels' motion (which in skid-steering is different than the direction the wheel is pointing) and is composed of the tangential components of the net tractive force generated by the wheel, i.e. drawbar pull (DB.P), and the lateral resistance force ( $F_R$ ) as visualized in Fig. 1.3. The angle separating these forces is denoted as  $\alpha$ .

$$F_{TTF} = F_x * \cos(\alpha) - F_z * \sin(\alpha) \quad (2)$$

In order to achieve self-propelled point turning,  $F_{TTF}$  must be positive.

### Sinkage

Sinkage is the vertical displacement between the lowest point of the wheel's inter-grouser surface and the undisturbed soil surface. The sinkage depends on the vertical load applied on the wheel (static sinkage) and the slip (dynamic sinkage). Wheel sinkage also depends on soil characteristics such as cohesion, particle size and soil strength. Higher strength soils generate higher resistive forces under equal wheel sinkage. Therefore the amount of resistive forces acting on the wheel can be explained by different amounts of sinkage and/or soil characteristics. The resistive forces generated by sinkage are directly related to net vehicle traction. Sinkage can lead to traction loss or complete immobilization of the vehicle.

### Slip

Wheel slip is a ratio that relates the wheel's horizontal velocity to the wheel's rotational velocity. The drawbar pull produced by a wheel is related to wheel slip, with higher values of slip increasing DB.P until a peak value is hit. As slip is also directly associated to energy loss as well as dynamic sinkage, lower values of slip are desirable during vehicle operation. This drives wheel and grouser designs that are able to generate higher drawbar pull at all slip values. The definition of slip is shown below in Equation 3.

$$i_x = \frac{r\omega - V}{r\omega} \quad (3)$$

With  $\omega$  and  $V$  being the angular and horizontal wheel velocity, respectively and  $r$  being the wheel radius.

### 1.1.3 Skid-Steer Rover Mobility Metrics

#### **Point Turns**

A Point turn is a turn in place around the center point of a rover. Skid steering is commonly employed as a steering configuration for small rigid wheel rovers, but is associated with a high amount of loss. Large values of lateral resistance forces exerted on the wheels during point turns can result in high sinkage and high slip scenarios. Therefore, the ability to perform a point turn at operational slip values is an important metric used in wheel and rover design.

#### **Slope climbing**

Slope climbing is critically important for most planetary exploration rovers. From crater exploration to driving on uneven terrain, all previous Moon and Mars mission had to operate on sloped terrain. This results in planetary rovers having a slope climbing requirement in the initial phases of their design and mission planning. Drawbar pull combined with the vertical load acting on the wheel are commonly used to estimate the vehicle's ability to navigate sloped terrain. However, these slope approximation models often do not account for the normal force distribution acting on the rover when on a slope. Moreover, the specific soil-wheel and soil-soil interactions that change with respect to the gravity vector are also not taken into account in common approximation models.

## **1.2 Research Problem**

This research uses single wheel and full rover experimental data to improve current rover mobility predictions. Understanding limitations of single wheel tests and comparing them to full rover tests is a critical step required to achieve a higher accuracy rover mobility predictions.

Predicting rover mobility has been a recurring task for engineers since the start of extra-planetary rover programs. The best estimates are provided by having a complete rover prototype, but some critical mission decisions related to rover mobility need to be made prior to having a complete rover prototype built. With upcoming micro-rover missions to the Lunar surface, understanding the rover mobility profile in early design phases (prior to a complete prototype) can lead to the reduction of costs, timeline risk, and an increase in confidence in the final design. This drives experimental and theoretical work that will provide accurate predictions related to rover mobility from single wheel tests in the early phases of a rover design.

## **1.3 Thesis Objective**

This research showcases single wheel tests on flat terrain that can be used to replicate point turn and slope climbing rover maneuvers. This research then experimentally compares single wheel tests to full rover tests in both maneuvers. The gathered experimental data is used to validate and build on previous prediction methods to increase accuracy of estimates that use single wheel test data as an input to output the predicted rover mobility. The final goal of the research is to improve current full rover platform mobility prediction methods and models, used in early design phases when only a single wheel prototype is available.

## **1.4 Contributions**

The research presented in this thesis contributes to the field of robotic vehicle design and exploration. The contributions consist of novel experimental data collected for different wheel designs and evaluating the accuracy of simple prediction models to estimate the mobility of rover platforms. The contributions are shown in the list below in the same order they are presented in the thesis.

1. Identifying the advantages of Slanted grousers for skid-steer point turns and slope climbing for skid steer micro rovers.

2. Characterizing the impacts diameter-to-width ratio on slope climbing prediction using the equally distributed loading method, and evaluating the influence of using equally vs unequally distributed vertical weight loading for slope climbing predictions.

## 1.5 Publications

A part of the research material included in this thesis has been or could be published in the following papers in the future:

Journal Article: 1. A. Demishkevich\*, K. Skonieczny, B. Thai, "Advantages of slanted grousers for skid-steer planetary rovers with rigid wheels" Submitted to Mechatronics (Elsevier Journal) on October 2, 2024.

Conferences(\*indicates presenting author)

-Oral presentation with peer-reviewed papers:

- (1) A. Demishkevich\* and K. Skonieczny, "Estimating Rover Slope Climbing Ability from Single Wheel Experiments," 2024 International Conference on Space Robotics (iSpaRo), Luxembourg, Luxembourg, 2024, pp. 91-97
- (2) A. Demishkevich\* and K. Skonieczny, "Experimental Evaluation of Grouser Designs for Efficient Skid Steering," 2024 31st Annual Conference of the Computational Fluid Dynamics Society of Canada CSME/CFD2024, Toronto, Ontario, Canada

Conference Poster Presentations: 1. ECE graduate student research conference

## 1.6 Thesis Outline

The thesis is structured as follows. In Chapter 2, relevant literature is reviewed and sections are identified that this work aims to address. Chapter 3 describes single wheel, full rover and soil imaging experimental apparatus used in this research. It covers two different reduced gravity approximation methods (GSL and Equal Load) and their application in approximating rover mobility

in point turn and slope climbing. Then Chapter 4 presents how single wheel test approximations compare to results from full rover experiments. Finally, Chapter 5 summarizes key findings, future avenues of research and recommendations to be combined with common slope climbing approximations.

## Chapter 2

# Literature Review

The following chapter reviews relevant literature regarding soil wheel interactions, experimental methods for single wheel testing, full rover testing and prediction models to estimate full rover mobility.

### 2.1 Soil Wheel Interactions

Research on soil-wheel interactions rise from the terramechanics field, including all vehicle-terrain interactions. The cornerstone of modeling in classical terramechanics is a one-dimensional pressure-sinkage model established in the 1960's ([Bekker, 1956](#)), which describes the interaction between objects (wheels, plates, tracks) and soil through soil bearing and shearing capacities. Bekker's model assumes the soil to have homogeneous behavior and it does not account for dynamic sinkage during wheel motion. Some of the limitations were addresses in ([Reece, 1965](#)) that modeled sinkage as a combination of static sinkage and dynamic sinkage. Furthermore, the Bekker and Wong models have been commonly used as an initial point for the development of more complex models to describe wheel-soil interactions for rigid wheels ([Gao et al., 2013](#); [Irani, Bauer, & Warkentin, 2011a](#); [Lyasko, 2010](#)). While models derived from terramechanics theory require knowledge of soil-specific parameters, they provide prediction capability with computational efficiency. This has lead to their active use in the design and analysis of planetary rover mobility systems ([Ishigami, Miwa, Nagatani, & Yoshida, 2007](#); [Meirion-Griffith & Spenko, 2011](#); [Schäfer,](#)

Gibbesch, Krenn, & Rebele, 2010; J. Y. H. Wong & Reece, 1967; F. Zhou et al., 2014). Furthermore, current research investigates models to predict single wheel and full rovers mobility using the fundamentals from terramechanics (Deng, Gao, Tao, Iagnemma, & Liu, 2014; Irani, Bauer, & Warkentin, 2011b; Senatore & Iagnemma, 2014)

## 2.2 Single Wheel Mobility

Single wheel mobility research is often done at the start of planetary rover designs, since the mobility of a wheel and full rover depends on their ability to generate positive forward traction (drawbar pull). The main factors that influence a wheel's trust generating capabilities are its physical dimensions, the soil properties the wheel is driving on, the shape and type of the wheel (rigid, mesh, hybrid) and the presence of grousers. A common way to evaluate the mobility of a rover platform is to evaluate the characteristics of a single wheel using single wheel test beds (SWTB) and use them to derive the mobility of the full platform. SWTB are often used to determine the best performing grouser for a specific wheel and its performance in key rover maneuvers such as slope climbing and turns.

### 2.2.1 Grousers

Drawbar pull, defined in 1.1.2 as wheel thrust force generated minus all the resisting forces, is a key terramechanics metric describing mobility performance. Grousers increase drawbar pull by increasing thrust and/or decreasing resistance. Nassiraei and Skonieczny (2020) showed that, for rigid wheels, 80% of the improvement in drawbar pull is accomplished by the grousers at the front of the wheel, as opposed to grousers in the soil below the wheel. This is partially a result of reduced resistance forces; instead of soil in front of the wheel being pushed (bulldozed) forward inducing resistive reaction forces, a grouser rotating (toward the back of the wheel) as it enters the soil blocks forward flow and instead redirects soil back and captures it between the grouser and wheel rim. Once the space between grouser and rim is filled, the grouser then acts like an excavation blade pushing on a surcharged mass of soil. This shearing action generates a reaction force on the grouser along a vector that has a forward direction (i.e. along the wheel's direction of motion) component,

thus contributing to thrust. This latter aspect is consistent with how grousers have been traditionally understood in the literature (Iizuka, Yoshida, & Kubota, 2011; Irani et al., 2011a; Sutoh, Yusa, Ito, Nagatani, & Yoshida, 2012; J. Wong, 2022), though earlier work had assumed the main region of this thrust effect was directly below the wheel, while the more recent research suggests the main thrust generation also happens at the front of the wheel, when the grouser-rim gap is first filled.

Grousers can differ in their orientation with respect to the wheel surface, their spacing (and hence, the number of grousers), their height, and their shape. Grouser parameters affect drawbar pull, sinkage, lateral forces (perpendicular to the wheels forward direction), and point turn performance. Past studies have shown that drawbar pull rises with an increase in the number of grousers (Bauer, Leung, & Barfoot, 2005; Liu, Gao, & Deng, 2008; Sutoh et al., 2012; Watyotha, Gee-Clough, & Salokhe, 2001) and/or grouser height (Ding, Gao, Deng, Nagatani, & Yoshida, 2011; Iizuka et al., 2011; Liu et al., 2008; Nakashima et al., 2007) until a saturation point. It was also shown that grousers provide more traction gains than simply increasing the wheel diameter (Ding et al., 2011). Literature has shown that there is an optimal number of grousers that will ensure continuous and steady grouser-soil interactions for a given wheel. (Sutoh, Nagaoka, Nagatani, & Yoshida, 2013) proposed empirical guidelines using static wheel sinkage to derive the maximum grouser interval angle to ensure at least two grousers are in contact with the area on which normal and shear stresses are. (Skonieczny, Moreland, & Wettergreen, 2012) developed a parametric grouser spacing formula, based on rover/wheel design specifications (weight, diameter), in combination with the target mission operation parameters (slip, sinkage) to find grouser spacing/height that reduces the resistive force generated in the soil ahead of the wheel. However, both these approaches were limited to the longitudinal motion of the wheels and did not investigate steering.

The effect of different types of grousers (parallel, Slanted, V, V-offset) on planetary rovers traversing side-slopes has been studied by (Nagaoka, Sawada, & Yoshida, 2019). Each grouser type was tested using single wheel experiments as well as a 4-wheeled rover platform. The grouser types were evaluated on metrics including slip ratio, wheel sinkage, wheel driving torque, lateral force, and side-slip. The conclusion was that the V-offset and Slanted grousers provided the best resistance to side-slip while also maintaining longitudinal drawbar pull. Slanted grousers were highlighted as a particularly promising candidate for exploration rovers on sandy terrain (Nagaoka et al., 2019).

In addition to grousers, wheel diameter and wheel width play an important role in rover mobility on loose soil. The influence of wheel parameters on mobility have initially been studied on large vehicles (Pandey & Ojha, 1978). Further studies by K. Iizuka et al performed experiments on the influence of grouser length but did not include wheel width or diameter (Iizuka, Kunii, & Kubota, 2008). Sutoh et al, reported the influence of both grousers, wheel width and wheel diameter on the mobility of a two wheeled rover (Sutoh, Yusa, Nagatani, & Yoshida, 2010). This research showed that wheels with a small diameter to width ratio require have higher slip when climbing slopes compared to those with a higher ratio. This finding was consistent across different diameter to width ratios for the same wheel.

This research seeks to expand on this topic to evaluate if the conclusions of Sutoh et al true for wheels with different surfaces and if there is a consistent performance decreases when reducing the diameter to width ratio (Sutoh et al., 2010). This work examines wheels with low width to diameter ratio, similar to wheels on the NASA JPL CADRE rovers and the Astrobotic Cuberover. The performance of wheels with a small ratio are compared to those with a medium diameter to width ratio, which are used on rovers such as Curiosity, Lunakhod and Yutu. This is an important class of wheel designs to consider among the suite of skid-steer micro-rovers envisioned in the coming years.

### **2.2.2 Single Wheel Test Beds**

Single wheel test beds (SWTB) using linear gantries are commonly used to understand wheel mobility and soil wheel interactions of terrestrial off-road vehicles and extra-planetary rovers.

SWTBs have seen wide use around the world for design and research of wheels for planetary rover usage. These linear gantries are normally split into two different classes: slip controlled or free-slip systems. Slip controlled systems, the most common configuration used in SWTBs, control the slip ratio of the experimental wheel by adjusting the ratio of the wheel's angular and linear velocities. These systems are normally constrained in the direction of the wheel's linear and lateral motion but are unconstrained in the vertical direction of motion to allow for different vertical loads to be applied. On the other hand, free slip systems are systems where the slip ratio of the wheel is measured by controlling the wheel's angular velocity. These systems are constrained in only the

lateral direction to the wheels motion, with free motion in vertical and forward directions.

Many SWTB use dead weight to apply specific vertical loads. Motion is often constrained along the vertical axis using a linear rail using a deadweight system. Many SWTB that use this method of vertical force application have shown normal force oscillations (Irani et al., 2011b; Männel, 2016) in experiments encompassing wheels with (Niksirat, Daca, & Skonieczny, 2020) and without grousers (Daca, Nassiraei, Tremblay, & Skonieczny, 2022). Another possible way to apply the vertical load is by using a counterweight system, which uses a 4-bar mechanism that ensures a constant vertical load. The 4-bar mechanism is also designed to address the issue of normal force oscillations. However, SWTB with this method of vertical force application has also shown normal force oscillations (Daca, Nassiraei, et al., 2022; Niksirat et al., 2020).

Another feature that has been observed in SWTBs is the glass wall that can be used to record soil interactions using soil imaging tools (Moreland, Skonieczny, Inotsume, & Wettergreen, 2012; Skonieczny et al., 2012; Skonieczny, Niksirat, & Nassiraei, 2019).

Slip controlled SWTBs gather force and torque data that a wheel produces under controlled experimental conditions. Furthermore, sinkage is also commonly measured using potentiometers. The gathered data can be used to gain direct insight into the wheel's mobility in straight line flat and sloped motion. However, some SWTBs also have the ability to replicate steering motions especially, but not exclusively, skid steer (Effati, Fiset, & Skonieczny, 2020; Flippo, Heller, & Miller, 2009). This is done by rotating the wheel in the yaw direction around the vertical axis (Ishigami et al., 2007; Yoshida & Ishigami, 2004).

Lastly, some SWTBs can evaluate single wheel slope climbing ability by adjusting the angle of the test bed with respect to the horizontal (Iizuka, Sato, Kuroda, & Kubota, 2006a, 2006b).

### **2.2.3 Evaluating Steering Ability Using SWTB**

Predicting the behavior of rovers during a skid steer maneuver can be difficult due to the large amount of losses and skidding that occurs. A common way to research and evaluate the ability of a rover wheel to perform the skid steer maneuver is to use SWTB (Ding et al., 2017; Ishigami et al., 2007; Yoshida & Ishigami, 2004). Most SWTB rotate the wheel in the yaw direction around the vertical axis and linearly move the wheel in the x direction to simulate the forces it would experience

during a turn. Other SWTBs allow the motion in both x and y direction underneath the test stand to study the forces during skid steer motion (Flippo et al., 2009). To evaluate skid steering ability the forces that the wheel generates during the experiments are captured using a force torque sensor. For motion on even hard terrain, forces from SWTB experiments paired with a mathematical model can accurately predict the turn rate of a full rover platform (Flippo et al., 2009). However, hard terrain conditions do not accurately capture the soil-wheel interactions in rover operating conditions in loose soil. Terremechanics models have been used to describe soil wheel interactions during skid steer maneuvers, and the resultant forces. These models show the forces acting on the wheel during skid steer motion and can be used to estimate the slip required for a full rover platform to complete a successful point turn. (Flippo & Miller, 2014) has used single wheel experiments to estimate full rover turn rate on non loose soil. However, there is currently little experimental validation for methods that use the forces generated from single wheel experiments to predict the slip a rover with those wheel required to complete a point turn on loose soil. This thesis aims to address this by completing single wheel experiments to estimate the point turn ability of rover platforms.

#### **2.2.4 Evaluating Slope Climbing Ability Using SWTB**

Predicting the behavior of off-road vehicles on sloped terrain dates back to research in the 1950s completed for military vehicles ascending loose soil terrain. SWTB have been used to experimentally evaluate the slope climbing ability of wheels designed for the NASA LRV program (Freitag, Green, & Melzer, 1970). Experimental work (Freitag & Knight, 1964) provided an empirical model to estimate the slope climbing capabilities of all-wheel drive vehicles in loose soils such as sand using 4x4 or 6x6 trucks. Further work was done by Klaus (Wiendieck, 1971), which combined the theory of flexible wheels on unyielding slopes with the experimental performance of rigid wheels on yielding flat terrain to create a semi-empirical model to predict the slope climbing capabilities of wheels. Recently, a simple force approximation model has been used to estimate the drawbar pull required for a rover to successfully climb a slope (Sutoh, Yajima, Nagatani, & Yoshida, 2011). These tests used a full rover model operating on flat terrain combined with a pulley system that was used to approximate forces that would act against the rover on a slope. The results showed that this

setup conservatively predicts the slip required for the rover platform to climb slopes of different inclination. Furthermore, Sutoh's research highlighted the influence of adjusting the width of wheels while keeping the same diameter and tractive surface on DB.P. The reduction or increase in wheel width was seen to be directly associated with an increase or decrease in drawbarpull.

Furthermore, (Ishigami, Miwa, Nagatani, & Yoshida, 2006; Yoshida, Watanabe, Mizuno, & Ishigami, 2006) applied terramechanic soil-wheel theory from flat terrain to analyze and model slope traversability which was validated experimentally. One limitation of the proposed models is that they are based on terramechanics theory developed for flat terrain, and may induce a buildup of error when used for estimations on sloped terrain. However, there is research ambiguity in using SWTB force data to directly predict the slip required for a full rover platform to climb a slope and validate the result experimentally. Moreover, this prediction is likely to be influenced by the wheel width to diameter ratio. This work aims to experimentally compare the DB.P generated by different wheels on slope and flat terrain. Furthermore, another key contribution of this thesis is to evaluate the influence of diameter and width wheel parameters on slope climbing ability and predictions.

### **2.3 Full Rover Mobility Predictions**

For research involving the use of single wheel data for predicting the performance rover mobility, it is important to consider how applicable and accurate the results will be in capturing the real mobility of 4 or 6 wheeled vehicles. One difference between single wheel and full rover mobility is the vertical load distribution of the rover weight among the wheels. Moreover, another difference comes from the multi-path effect, where the front wheel drives on undisturbed soil whereas the rear wheels drive over soil with different physical properties such as compaction. The multi-path effect is especially present when performing skid steer point turns with all the wheels being exposed to it after the rover completes a quarter turn. In past research single wheel experiments are commonly used to tune single wheel terramechanics models which are then modified to incorporate full rover behavior. The full rover models are then validated with real full rover experiments in points turns or slope climbing.

Effati et al. (2020); Fiset, Effati, and Skonieczny (2023); Flippo and Miller (2014) have experimentally shown that single wheel data can accurately predict full rover skid steer power consumption. Ishigami et al. (2006) focused on using single wheel data to validate their single wheel model which was later expanded into an articulated multi-body model. One avenue where there is the possibility of further work is using the forces generated from SWTBs to directly predict the slip required for a full rover model to do a successful point turn. Another area for further work is investigating the effect of multi-path on rovers during skid steer turns.

Similarly, there is recent work into investigating the influence of weight distribution on rovers during slope traversal and the multi-path effect. Senatore et al. (2014) performed simulations which were then validated using experiments that considered the uneven normal load distribution across the rover wheels during slope climbing. The results of this research suggested that for their rover configuration, soil and experimental conditions single wheel test can predict full rover performance without knowing the distribution of the vertical load across the rover axles. On the other hand, Ghotbi, González, Kövecses, and Angeles (2016) used single wheel and full rover simulations, both validated by experiment, to show that vertical load distributions does influence slope climbing ability. Furthermore, investigation of the multi-path effect showed that if it is considered the optimal vertical load placement should be shifted towards the rear wheels. On the other hand if the multi-path effect is not considered an even vertical load distribution is optimal. Overall, further research is required to investigate the influence of multi-path effect and vertical load distribution in the context of using single wheel experiments to predict full rover slope climbing abilities. Moreover, limited work has been done to use single wheel force results to directly predict the slip required for a full rover platform to climb a slope of a specific inclination.

## **2.4 Effect of Reduced Gravity**

A common difficulty in most extra-planetary research is considering the influence of reduced gravity on the vehicle's systems and mobility. Correctly predicting the soil-wheel interaction under reduced gravity can be done through soil simulant design (Oravec, Zeng, & Asnani, 2010), through soil modeling simulation techniques including: discrete element method (DEM) (Johnson et al.,

2015), material point method (MPM) and elastoplastic (Azimi, Kövecses, & Angeles, 2013; Ghotbi et al., 2018), through semi-empirical modeling (Kovács et al., 2020), through scaling laws (Slonaker et al., 2017), by reduced-mass engineering models (Toupet et al., 2018) and more recently by geometrical magnetic-similitude-gravity model testing method (GMMT method) (Li et al., 2022).

Currently, the best way to replicate reduced gravity on earth is by using parabolic flights, which generate 20 to 30 seconds of reduced gravity (Daca & Skonieczny, 2022a). The influence of reduced gravity on mechanical soil properties and deformation under wheel load provides non-trivial results and motivates further research in this field (Daca, Tremblay, & Skonieczny, 2022).

### 2.4.1 Soil Simulants

There are ongoing efforts to design simulants to have similar properties to samples retrieved from the moon. These simulants sometimes attempt to take into account the influence of reduced gravity on granular materials. A key goal of most simulants is to be available in large quantities for use in lunar in-situ resource utilization research and traction experiments. The Glen Research Center - 1 (GRC-1) simulant was designed by (Oravec et al., 2010) to replicate the cone penetration measurements collected by the Apollo mission. GRC-1 was primarily designed for usage in lunar vehicle traction testing, with the assumption that the mechanical response of the lunar soil during penetration readings replicates vehicle wheel loading.

A previous parabolic flight campaign using GRC-1 (Daca, Tremblay, & Skonieczny, 2022) showed that cone index values at 1/6-g show a significant decrease in cone index gradient (G) when compared to 1-g conditions. Furthermore, when 1/6-g wheel experiments were compared to 1-g experiments at equal cone index gradient G, it was found that in 1-g GRC-1 over-predicts the drawbar pull and tractive abilities of wheels (Daca, Tremblay, & Skonieczny, 2022).

Many more simulants including GRC-3, BP-1, DNA-1A, LSS-ISAC-1, JLU-H and CUMT-1 (He, Zeng, & Wilkinson, 2013; Li et al., 2022; Sandeep, Marzulli, Cafaro, Senetakis, & Pöschel, 2019; Suescun-Florez, Roslyakov, Iskander, & Baamer, 2014; Sun et al., 2022; Venugopal, Prabu, Muthukumar, & Annadurai, 2020), were created on the basis of the properties of samples from the Apollo missions. Generally, the above simulants are developed with a focus on matching the chemical composition with a smaller priority given to mineral constituent and particle morphology.

This was addressed during the development of a new high fidelity simulant PolyU-1 that used samples from China's Chang'e-5 sample return mission (C. Zhou et al., 2022). By studying the lunar regolith under micro-CT imaging technology, the three-dimensional geometric characteristics were determined. The result was a simulant similar in mineral constituent, particle morphology, physical and mechanical properties. Generally, when using specific soil simulant it is important to consider what assumptions were used during their creation and how it can influence the accuracy with which they replicate reduced gravity conditions.

#### **2.4.2 Reduced-mass engineering models**

One of the simplest ways to account for reduced gravity when predicting rover or wheel mobility is the use of reduced-mass engineering models. In these models, the vertical wheel loads mimic the loads that would be experienced in the reduced gravity environment. This approach has seen wide usage to perform mobility experiments of Mars exploration rovers (Toupet et al., 2018), and captures the effect of reduced gravity on the wheel loads. However, a major shortcoming of this approach is that it does not accurately reflect the influence of reduced gravity on the granular material itself and the wheel-soil interactions. Experiments conducted by (Kobayashi, Fujiwara, Yamakawa, Yasufuku, & Omine, 2010), isolated the influence of reduced gravity on the wheel (vertical load) from the effect it has on the soil particles themselves. It was observed that when both were subjected to reduced gravity influence, the resulting wheel mobility was impaired. Yet, when the influence of reduced gravity was applied only to the wheel, the mobility improved. This highlights that predictions for motion in reduced gravity must consider the effects of reduced gravity on the wheels and soil particles (Niksirat et al., 2020).

#### **2.4.3 Granular Scaling Laws**

Another method, that has shown a promising ability to reliably predict wheel performance for reduced gravity, is granular scaling laws (GSL), which are based on a similar theory to aero and hydrodynamic scaled testing in wind tunnels. Using scaled models to study wheel performance in loose soil has seen wide usage even during the early stage of terramechanics (Bekker, 1956, 1969). With many works (Clark Jr, Simon, & Roma, 1965; Lessem, 1972; Nuwal, 2022) dedicated to scaled

model testing of agricultural, army and planetary vehicles and further dimensional analysis of the results to understand the mobility capabilities of the full sized platform. Recently, Slonaker et al proposed comprehensive scaling relations that can predict the mobility of a full sized wheel based on a scaled model or predict the mobility in one gravity level based on experiments conducted in a different gravity (Slonaker et al., 2017). The scaling laws were originally validated using discrete element method (DEM) simulations (Slonaker et al., 2017; Zhang, Townsend, & Kamrin, 2020), and then further explored in parabolic flight campaigns. Parabolic flights with scaled rover models (Kuroda, Teshima, Sato, & Kubota, 2004, 2005) showed that the slip ratio closely followed the scaling laws. Parabolic flight experiments by (Daca & Skonieczny, 2022a) have shown that scaling laws combined with representative soil simulants in earth experiments can correctly predict soil behavior in low gravity. These experiments have shown that the performance margins of a wheel can be approximated using scaling laws as a pessimistic bound and equal (i.e. Lunar) loading as the optimistic bound; wheel performance in low gravity experiments was between these bounds and closer to the scaling law predictions.

#### **2.4.4 Geotechnical Magnetic Similitude Models**

Geotechnical magnetic-similitude-gravity model testing method (GMMT method) is a novel way to replicate the influence of reduced gravity on lunar regolith in 1-g conditions. This method uses the superposition of a magnetic force acceleration and acceleration due to earth gravity to create a new gravitational acceleration inside the material. To accurately capture the influence of reduced gravity the simulant used should be magnetically-sensitive granular media (MSG media). This led to the development of a simulant with relatively large magnetic permeability (Li et al., 2022) to be used in GMMT models.

#### **2.4.5 Soil modeling techniques**

Simulation and modeling can also be used to predict the influence of reduced gravity on soil properties and soil-wheel interactions. Particle based methods based on continuum mechanics and discrete mechanics have shown a good ability to model soil deformation and separation (Jasoliya, Untaroiu, & Untaroiu, 2024). The most popular methods are currently discrete element method

(DEM) (Lan et al., 2024), which uses thousands/millions of discrete, minuscule particles, material point method (MPM) (de Vaucorbeil, Nguyen, Sinaie, & Wu, 2020), which combines methods of the Lagrangian material points and background Eulerian grid to discretize continuous fields. Importantly, the force of gravity on the soil is a parameter that can be set for both techniques. There is also development of additional modeling techniques such as the smoothed particle hydrodynamics (SPH) model (El-Sayegh, El-Gindy, Johansson, & Öjjer, 2018; Gheshlaghi & Mardani, 2021; Lescoe, 2010), and techniques using elasto-plasticity theory that uses the description of soil wheel interactions (Azimi et al., 2013). These techniques provide a computationally efficient solution and can be integrated into multi-body simulation environments of rovers (Tasora, Mangoni, Negrut, Serban, & Jayakumar, 2018). With the development of new and improvement of previous modeling and simulation tools, it's very important to consider how the predictions compare to experimental data and how each model was validated.

## 2.5 Simulations of Soil Flow Properties

Observation of soil motion through glass sidewall dates to the origins of terramechanics research (Bekker 1948). Recently, imaging techniques adapted from fluid flow experiments such as particle image velocimetry (PIV) (White, Take, & Bolton, 2003) and particle tracking velocimetry (PTV) (Adamczyk & Rimai, 1988) have shown to provide information about soil particle motion directly underneath the wheel (Gnanamanickam, Lee, Sullivan, & Chandrasekar, 2009; Murthy, Gnanamanickam, Saldana, & Chandrasekar, 2009). A limitation of using these techniques is the requirement for specialized equipment such as high speed cameras, multiphase LED lamps, pulsed lasers and others (Cowen, Monismith, Cowen, & Monismith, 1997). Furthermore, these techniques also had to sacrifice data resolution and accuracy (Gachet, Klubertanz, Vulliet, & Laloui, 2003; White et al., 2003) due to estimating velocity once in grid squares of sizes between 8 x 8 to 30 x 30 pixels. Current research has shown that many of the limitations associated with PIV and PTV could be solved with a newly proposed soil optical flow technique (SOFT) (Moreland et al., 2012; Moreland, Skonieczny, Wettergreen, Creager, & Asnani, 2011; Skonieczny et al., 2014). SOFT is based on a dense motion estimation algorithm developed using computer vision to estimate the velocity at

each pixel resulting in substantially higher resolution. Previous work have utilized SOFT techniques to show the soil flow velocity and shear interface underneath a wheel on flat terrain. However, to the author's knowledge, no work has been done to evaluate sloped terrain soil interactions using soil imaging techniques. This research aims to investigate the soil flow changes between flat and slope terrain using SOFT with the aid of SWTB with soil imaging capabilities to gather experimental data.

# Chapter 3

## Research Methodology

### 3.1 Experimental Apparatus

The experiments completed in the scope of this thesis utilized a large SWTB, with a glass side to allow for soil imaging and soil flow recording. To evaluate skid steering, the yaw of the wheel with respect to the vertical was adjusted to reproduce forces the wheel would experience during a point turn. To evaluate slope climbing, the SWTB was inclined at a predefined angle from the horizontal. Validation of single wheel results were completed by using an experimental rover platform from Clearpath Robotics.

#### 3.1.1 Single Wheel Gantry

Single wheel tests were conducted in a test bed with a linearly operated gantry as seen in Fig. 3.1. The test area is 2 m long by 2 m wide and is filled with GRC-1 lunar simulant to a depth around 25 cm. For single wheel experiments the coordinate axis is defined with the direction of motion parallel to the soil surface as the  $x$ -axis, the perpendicular (normal) direction to the soil surface as the  $y$ -axis and the lateral direction as the  $z$ -axis. This definition stays true even as the test bed is tilted to different angles from the horizontal. The wheel is constrained to a specific pre-set motion in the  $x$  and  $z$  direction but can move freely in the  $y$  direction by means of a 4-bar mechanism to maintain a constant normal load (Daca, Nassiraei, et al., 2022). The wheel is moved by translating the gantry at a specific velocity in the  $x$  direction and rotating the wheel at a set angular velocity.

Changing the relationship between the linear motion of the gantry in the  $x$ -direction and the angular velocity of the wheel allows to test different slip conditions. Moreover, counterweight was used on the 4-bar mechanism to adjust the vertical loading to run tests with different loading conditions (GSL and Equal Load).

For single wheel tests, collected data consists of motor rotations and current, sinkage ( $y$  direction) recorded using 100 mm ALPS 10 kO slide potentiometer, and force data in all 3 directions collected using an ATI Delta IP60 combined with a National Instruments USB-6210 (resolution of 0.0625 N in all 3 directions). Before all tests the wheel is raised in the air and the force torque sensor bias is zeroed.

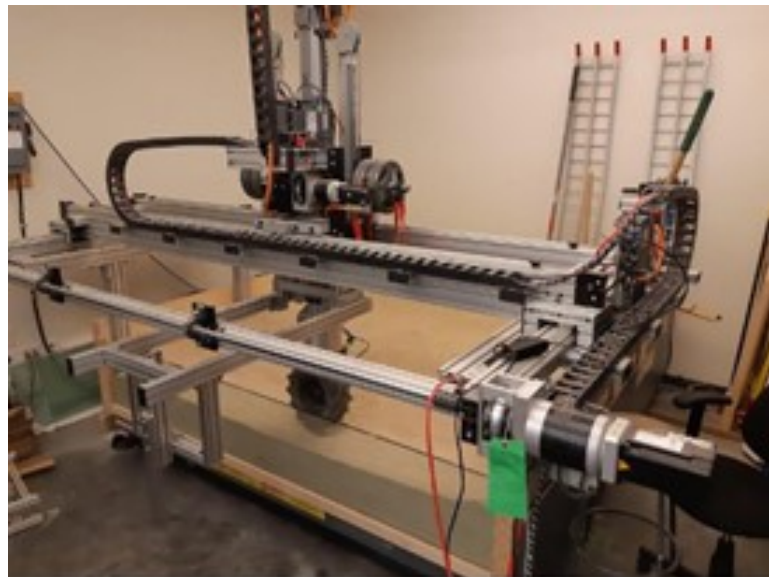


Figure 3.1: Single wheel test apparatus

### 3.1.2 Full Rover Test Environment and Data Gathering

The test bed for full rover testing utilized the same test area as for single wheel tests. The entire soil test bed is mounted on a hydraulic tilt-bed whose angle relative to the horizontal is set after soil preparation. The soil preparation and operating conditions were kept consistent between both sets of experiments. During full rover experiments, the set parameters were the wheel angular velocity, the soil density (compaction level), and the slope angle. The data was gathered using Leica Total Station which records the  $x, y, z$  coordinates of a reference point (prism) on the rover

at approximately 0.2 second intervals. During tests, the  $x, y, z$  position of the rover was recorded as it traveled up the slope. Knowing the total time of motion and the change in position, the rover's velocity was determined. The obtained slip was validated by observing the rover tracks and the total time required to perform the maneuver.

### 3.1.3 Husky Rover

Full rover experiments using a Husky Rover Fig. 3.2 were completed to evaluate predictions for slope climbing and point turn maneuvers. In these experiments, the required slip to perform the maneuver was investigated and compared to the estimations gathered from single wheel experiments.

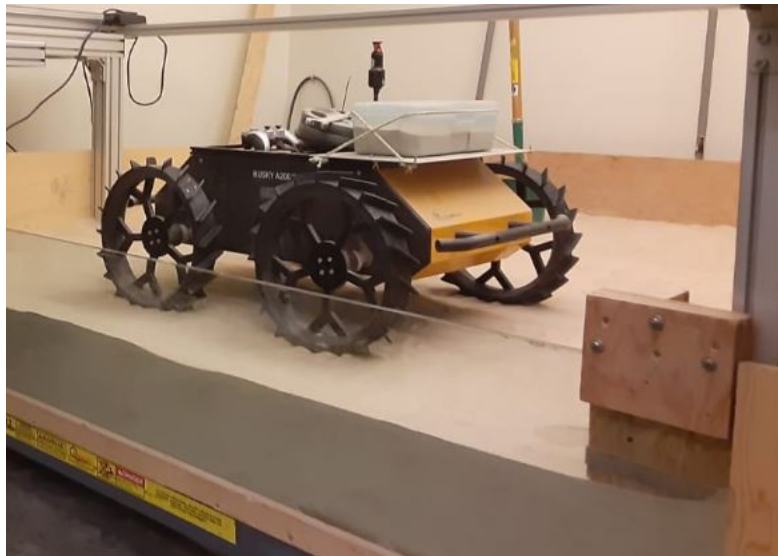


Figure 3.2: Husky rover test platform during experiments

### 3.1.4 Soil Preparation

Before each single wheel or full rover test trial, the sand was flattened, compacted, and characterized using a cone penetrometer to ensure test repeatability. Data collected during Apollo lunar missions, as well as previous studies (Oravec et al., 2010), suggest that a relative density (DR) of around 30% is required to approximate lunar conditions using GRC-1 simulant. For the experiments conducted in this work a Cone Index Gradient (G) of 3.9 to 4.3 was achieved in GRC-1, corresponding to 28 to 31% soil relative density.

### 3.1.5 Experimental Wheel Design

The base wheels considered in this study were rigid and limited to a 300 mm outer diameter (i.e. diameter to the grouser tips). These wheels were designed based on the CSA LRV mission. With many of the dimensions and design choices being based on technical requirements. The key aspect being varied between the wheel used in this study is related to grouser geometry, which is subject to many variables. One option initially considered in preliminary work was the use of trapezoidal and saw-tooth grousers. However, preliminary trials suggested Slanted and V-offset grouser geometries were better in skid-steer turns than trapezoidal grouser geometry.

Slanted and V-offset grousers were both shown to produce lower side-slip along a slope by (Nagaoka et al., 2019). This among other factors makes them good candidates for both slope climbing and point turn maneuvers. The V-offset and Slanted grouser configurations that form the basis for this study are shown in Fig. 3.3, and are described in further detail in the remainder of this section.

Grousers play an important role in both the maximum slope and point turn rover maneuvers. The following geometric parameters shown in Fig.1.2 play a critical role in grouser design: grouser height ( $h_g$ ), grouser spacing (represented by angle  $\beta$ ), grouser slant angle ( $\zeta$ ), and grouser thickness ( $t$ ). V-offset grousers also have a parameter that defines the offset spacing ( $a$ ). The offset spacing was approximated based on agricultural wheel design literature (Nakashima et al., 2013). This approximation was then cross-referenced with other wheel designs such as the Lunakhod and Curiosity to get the final value.

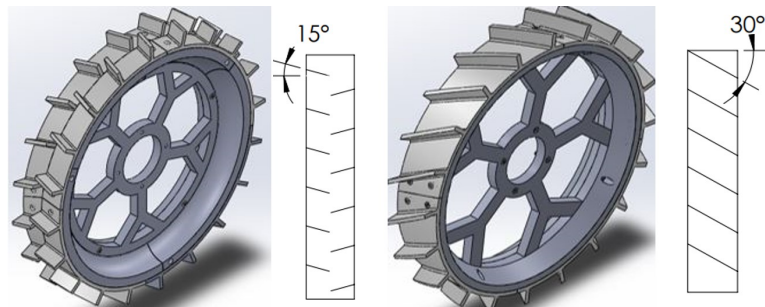


Figure 3.3: V-offset (left) and Slanted (right) grousers

### **Grouser height ( $h_g$ )**

Grouser height is defined as the distance from the inter-grouser surface of the wheel to the outer tip of the grouser (see Fig. 1.2). Previous literature gives guidelines for the grouser height based on the terrain inclination (Inotsume, Moreland, Skonieczny, & Wettergreen, 2019) the rover will be traveling on. The general relationship between grouser height and terrain inclination is shown in Table 3.1. Given functional requirements of a 25 degree slope for the CSA mission, we can assume that other missions will have similar objectives. Based on this the grouser design height was chosen to be 16 mm (12% of the nominal wheel radius) for both grouser designs.

Table 3.1: Grouser height to slope angle relationship

slope angle (degrees $^\circ$ )	< 10	10-20	> 20
grouser height	3-5% radius	6-9% radius	10% radius

### **Grouser spacing angle ( $\beta$ )**

Using methodology from (Sutoh et al., 2013) the grouser spacing angle  $\beta$  can be found using the initial static sinkage of the wheel without grousers. Based on wheel vertical loading the static sinkage angle ( $\theta_{st}$ ) was initially estimated to be 30 degrees which represents 5.97% of the wheel radius. A manufactured grouser-wheel prototype showed that the required grouser spacing angle ( $\beta$ ) has to be less than 19.8 degrees.

This result was validated again by the methodology developed by (Skonieczny et al., 2012) which produced an angle of 20.1 degrees. To satisfy all methodologies and to ensure that the chosen number ( $\beta$ ) is a factor of 360, the grouser spacing angle ( $\beta$ ) was chosen to be 18. This resulted in 20 evenly spaced grousers on the wheel.

### **Grouser slant angle ( $\zeta$ )**

The grouser slant angle effect was studied for Slanted and V-offset grouser types. The grouser slant angle ( $\zeta$ ) as seen in Fig. 1.2, affects drawbar pull, sinkage as well as tractive efficiency. This phenomenon was studied in previous work (Inotsume et al., 2019; Nagaoka et al., 2019) which

showed that a steeper grouser slant angle saw a decrease in drawbar pull compared to straight grouser especially at high slip. Grousers with a smaller angle showed better performance at higher slip. Given the design constraints of the wheel we can expect that it may have to operate at mild to high slip conditions. With this in mind a lower grouser slant angle was selected to increase straight line and slope performance in V-offset grousers. Another factor that contributes to the grouser slant angle design is the point turn slip angle ( $\alpha$ ). This parameter is defined as the angle between the wheel and its direction of travel. The point turn slip angle depends on the physical dimensions of the proposed full rover. Using CSA proposed dimensions as shown in Fig. 3.6 the slip angle is 36.5 degrees. Previous studies on skid steering (Inotsume et al., 2019; Nagaoka et al., 2019) have shown good drawbar pull during point turns when the grouser slant angle is set close to the slip angle. Therefore for the design of the Slanted grouser the slant angle was set to 30 degrees.

### **Grouser thickness (t)**

In this study, PLA being the grouser material imposes a minimum thickness of the grouser to maintain structural integrity compared to other designs (e.g. metals). Given a lack of literature in planetary grouser thickness, studies of agricultural grousers (Nakashima et al., 2013) was used to evaluate the effect of grouser thickness to height ratio on gross traction of the wheel. It showed that a ratio of 0.3 or more between grouser thickness and height starts having a negative influence on the traction of the wheel. For this reason, the grouser thickness ratio is chosen to be smaller than 0.3 and to ensure structural integrity with PLA: 3.5 mm (ratio of 0.22) was selected. This was the overall thickness of the Slanted and V-offset grouser designs (and was the minimum thickness for the preliminary trapezoidal study).

### **Final wheel dimensions and CAD**

Both the Slanted-grouser and V-offset-grouser wheels were designed to have 300 mm outer diameter and 268 mm nominal diameter (i.e. to the inter-grouser surface of the wheel) that accounts for 16 mm grousers. The width of the original wheel tested in single wheel tests was 50 mm as shown in Fig. 3.4.

To account for the size difference between the concept rover and the experimental platform the

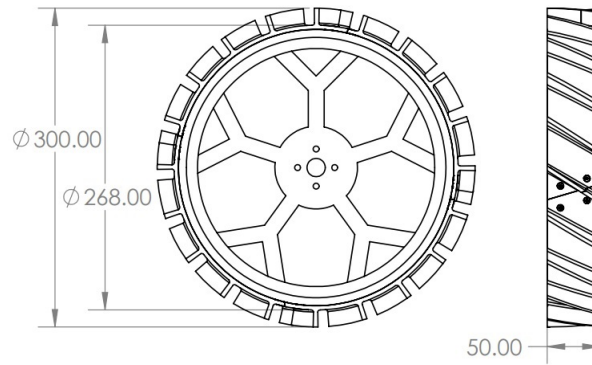


Figure 3.4: CAD drawing of original wheel used in single wheel experiments

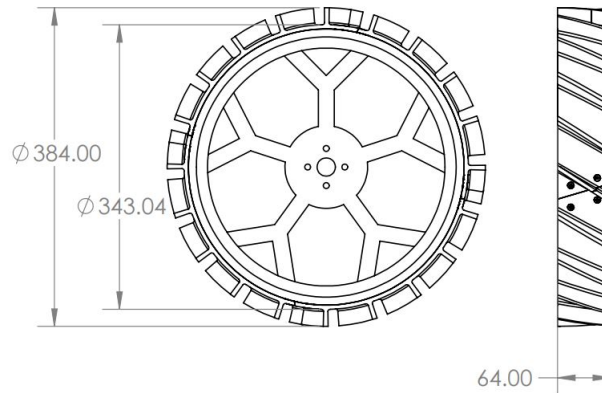


Figure 3.5: CAD drawing of GSL scaled wheel used in single wheel experiments

dimensions of the wheel was updated according to granular scaling laws (GSL) as described in Section 3.2, i.e. scaled by a factor of 1.28. This results in the final dimensions of 384 mm outer diameter, 343 mm nominal diameter and a 64 mm width for the wheel as shown in Fig. 3.5. These scaled wheels were used for full rover experiments (Section 4), single wheel test to evaluate the weight distribution on sloped terrain (Section 4.4) and diameter over width ratio (Section 4.5).

## 3.2 GSL and Equal Load Approximations

Granular scaling laws (GSL) utilize principles analogous to those of aerodynamic similitude (e.g. scaled plane models in wind tunnels) but for machine-soil interactions. In GSL certain experimental variables are fixed, while others can be changed. To satisfy GSL, all non-dimensional terms

on the right-hand side of Equation (4) must be kept constant between two different conditions (e.g. Earth and Moon). The dimensions of the variables in (4) are listed in Table 3.2.

For full rover experiments, the ClearPath Husky UGV platform with 3D printed wheels made from PLA was used. As shown in Fig. 3.6 the increased size of the platform compared to the CSA lunar concept necessitates geometric scaling. The constraining factor is the Husky's wheelbase (the wheel center to center distance lengthwise along the rover's side). The Husky wheelbase is 28% bigger, therefore this same scaling needs to be applied to other critical geometric parameters: wheel radius ( $r$ ), wheel width ( $D$ ) and track width (distance center to center widthwise across the rover). To get all geometric parameters correct, 28% larger wheels and additional 3D printed spacers (for track width) were printed. These larger wheels were then used for both single wheel and full rover experiments.

$$\left[ \frac{F_d}{Mg}, \frac{z}{L}, \frac{P}{Mg\sqrt{Lg}} \right] = \Omega \left( \sqrt{\frac{g}{L}} t, f, \frac{g}{L\omega^2}, \frac{\rho DL^2}{M}, \frac{V}{\sqrt{Lg}} \right) \quad (4)$$

Given the differences in  $D$  and  $L$  between the two conditions to keep the 4th term of Equation 4 constant, the mass ( $M$ ) variable must be adjusted. The adjustment is by a factor of 2.1 ( $1.28^3$ ) relative to the lunar concept model. After all calculations and adjustments due to GSL the final weight of the rover was 63 kg, wheel diameter excluding grousers at 343 mm, and full rover footprint (excluding bumpers) of 896 mm by 755.2 mm as shown in Fig. 3.6.

Lastly, to take the different gravity between Earth and Lunar conditions into account, the 3rd term of Equation 4 was evaluated. In this term, only the angular velocity ( $\omega$ ) can be changed, with values of  $L$  and  $g$  already constrained. To keep the dimensionless term constant the angular velocity needs to be multiplied by 2.175. All variables and non-dimensional terms for the two considered conditions are listed in Table 3.2.

### 3.3 Using Single Wheel Tests to Evaluate Mobility of a Wheel Design

Two different normal loading methods were used for both designs. This gives the upper and lower bounds of the wheel's performance: equal (Lunar) loading, and the use of Granular Scaling Laws (GSL). Previous research (Daca & Skonieczny, 2022a) shows that experiments using the equal

Table 3.2: GSL variables

Variables	Condition 1: Lunar	Condition 2: Earth SWT	Condition 3: Earth FRT
$g (m/s^2)$	1.62	9.81	9.81
$L (m)$	0.268	0.268	0.343
$D (m)$	0.050	0.050	0.064
$v (m/s)$	0.05	0.05	0.1392
$\omega (rad/s)$	0.3731	0.8116	0.8116
$M (kg)$	30	30	63
$\rho (kg/m^3)$	1745	1745	1745
$g/L\omega^2$	43.416	43.416	43.416
$\rho DL^2/M$	0.0998	0.0998	0.0998

load method in 1-g provide an optimistic estimate of the wheel's performance in reduced-g. With this method the vertical force applied on the wheel in Earth gravity is the same as the force that the wheel would experience in lunar gravity, but the soil does not directly experience any effects of reduced gravity. On the other hand, GSL provides a more accurate and a more conservative prediction of the wheel's performance (Daca & Skonieczny, 2022b). Thus, the actual performance that would occur in lunar gravity is expected to fall within the range of performance achieved under equal loading and under GSL, but closer to the GSL performance.

The actual values for vertical loading ( $V.Load$ ) are derived using the proposed mass of the rover and the appropriate gravity conditions for GSL and equal loading. With GSL using earth gravity and equal loading as its name states using lunar gravity.

$$V.Load = \frac{Mass * Gravity}{4} \quad (5a)$$

$$V.Load_{GSL} = \frac{30 * 9.81}{4} = 73.8 N \quad (5b)$$

$$V.Load_{EqualLoad} = \frac{30 * 1.62}{4} = 12.15 N \quad (5c)$$

### 3.3.1 Predicting Full Rover Point Turn Ability

To predict full rover point turn ability we evaluate the wheel's performance in single wheel experiments. For this purpose the entire 4-bar mechanism was rotated to ensure the correct point turn angle is achieved. For our experiments the setup is rotated 36.5 degree relative to the x-axis,

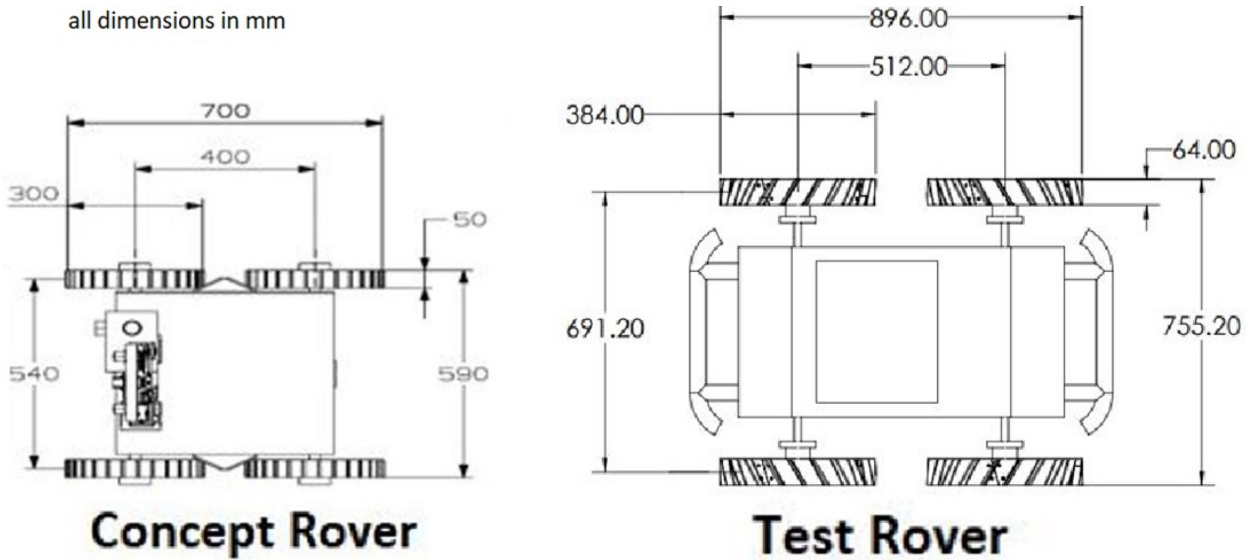


Figure 3.6: Husky rover and wheel dimensions used during experimentation, scaled relative to the LRM CSA lunar concept rover

while  $x$  was kept as the direction of motion. This is defined as testing with a slip angle, and is akin to what the wheel experiences when the rover undergoes a point turn. The assumption to be validated during these experiments is that single wheel experiments can accurately predict full rover point turn ability and the slip required for it.

The primary metric to evaluate point turn ability in single wheel tests is the tangent turning force,  $F_{TTF}$ . It is visualized in Fig. 1.3. The tangent turning force is composed of the tangential components of the net tractive force generated by the wheel,  $F_x$ , and the lateral resistance force,  $F_z$  in our F/T sensor frame definition as shown in Equation 2.

### 3.3.2 Predicting Full Rover Slope Climbing Ability

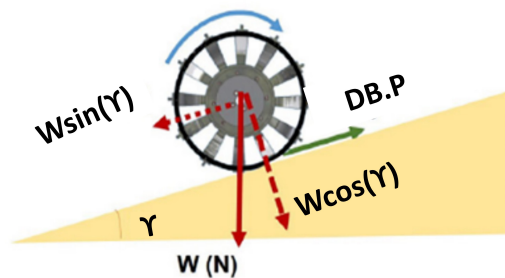


Figure 3.7: Forces experienced by wheel on sloped terrain

The primary forces acting on a wheel during slope motion are shown below in Fig. 3.7. The results obtained from single wheel flat-ground tests were used as a basis to estimate the slope climbing abilities of the rover. Drawbar pull generated by the wheel has previously been used to approximate the maximum slope a rover can climb (Freitag et al., 1970). During single wheel experiments the drawbar pull force:  $DB.P=F_x$ ; lateral force:  $F_y$ , and vertical force:  $W = F_z$ , were collected throughout the wheel's motion. The Drawbar Pull coefficient ( $DB.P_{coeff}$ ) was found by  $F_x/F_z$ . The main force to overcome is gravity and so a general relationship between slope angle  $\gamma$  and  $DB.P_{coeff}$  is found in Equation 6.

$$\gamma = \tan^{-1}\left(DB.P_{coeff}\right) \quad (6)$$

Thus for any slope angle, the required  $DB.P_{coeff}$  can be found. For example, a slope of 15 degrees requires a  $DB.P_{coeff} = 0.27$ .

### 3.3.3 Sub Surface Soil Flow Imaging

By looking at the subsurface soil flow underneath a wheel in flat and slope terrain, we can better predict the slope climbing ability of a full rover platform. Soil response during wheel motion can be used to understand soil-wheel and soil-soil behavior in different conditions (Skonieczny et al., 2014, 2012). To capture soil behavior, a high-speed camera was attached to the horizontal axis which moved next to the wheel. As shown in Fig. 3.8 the camera was pointed at the glass wall capturing the full range of soil wheel interactions. Two external LED lights were placed on a linear rail at an around 90 degree angle to the glass to increase illumination and contrast. The data was collected at a rate of 37 frames per second.

The collected video data was analyzed using a soil flow optical technique (SOFT) discussed in detail in Chapter 2. The settings and tuning of the algorithm were previously done in similar experiments (Niksirat, 2018; Skonieczny et al., 2014) and shown in Table 3.3. The results produced two displacement fields, horizontal and vertical in units of pixels. These displacement fields produce velocity vectors which are averaged over multiple seconds to eliminate noise and negligible differences in soil state.



Figure 3.8: Soil Imaging Attachment to SWTB

Table 3.3: Tuning Parameters used in the SOFT Algorithm

Regularization parameter, $\lambda$	0.1
Pyramid levels	3
Spacing of pyramid levels	2
Maximum number of iterations	10

To compare estimated flow fields, the magnitudes of the velocities at each slip were normalized with respect to rim speed. The rim speed is defined from the tangential wheel rim velocity relative to the wheel hub ( $L\omega$ ) minus the hub velocity. The hub velocity decreases when slip increases, but is constant for every slip value.

## Chapter 4

# Results

The two different grousers designed for the LRM CSA missions, Slanted and V-offset, were experimentally evaluated to determine their performance in slope climbing and point turns. The two different grouser designs were chosen based on literature studies covered in Section 2.2.1 of grouser designs for small light weighed skid steer rovers. Single wheel tests using a linear gantry test bed described in Section 2.2.2 were done to determine the performance of both grousers. The experiments were modeled such that the performance of the wheel would approximate the expected lunar performance. This was done by using lunar simulants, gravity approximation methods and using 1-1 a wheel model. The results from single wheel tests were analyzed and used to predict the performance of a full rover model using the prediction methods outlined in Section 3.3. The best performing grouser was used for further full rover experimental validation. Full rover point turns and slope experiments were completed using the same area filled with GRC-1 as for single wheel experiments. When transitioning between single wheel to full rover experiments additional factors such as multi path and weight distribution need to be considered. Furthermore, the diameter and width of the wheel influence the prediction accuracy. To determine the effect, additional experiments targeting the influence of wheel width and diameter were performed. Different diameters and widths were evaluated for their impact on the slope climbing estimation. Additionally, this thesis uses soil imaging techniques to see if substantial differences in soil flow are observed as the terrain inclination changes.

## 4.1 Comparing Slanted and V-Offset Grouser Designs for Point Turns and Slope Climbing

The effect of different grouser geometry on the mobility of a wheel moving through lunar based simulants was examined. Specifically, the tractive properties of Slanted and V-offset grousers were evaluated experimentally to validate the design against representative tractive requirements for lunar rovers. The two types of grousers were evaluated on flat terrain in a lunar mobility soil simulant (GRC-1) for their ability in straight line driving and point turns. The experiments were done utilizing Equal Load and Granular Scaling Law approximations for the loading conditions, as described in Section 3.2. These two approximation methods gave the upper and lower bounds of the wheel’s mobility, respectively. The evaluation criteria consisted of drawbar pull and sinkage for straight line tests as well as tangent turning force for point turns.

To evaluate the ability of the wheel to climb a slope, straight line experiments were performed and force data was gathered to compute the drawbar pull coefficient. To evaluate point turn ability the wheel was rotated correspond to what the wheel experiences when the rover undergoes a point turn, as shown in Fig. 1.3.

### 4.1.1 Single Wheel Experiments

Both grouser designs (Slanted and V-Offset) were tested under 4 different conditions (two vertical loads and two slip angles) as shown in the table 4.1. Each condition had sub tests at 4 different slip ratios of: 0.05, 0.20, 0.40 and 0.60. Experiments at each slip ratio were performed three times with the average slip being used in further analysis.

Table 4.1: Single wheel experimental conditions

Conditions	Loading Type	Slip Angle
1	Equal Loading (12N)	No Slip Angle
2	Equal Loading (12N)	36.5 Slip Angle
3	GSL Loading (74N)	No Slip Angle
4	GSL Loading (74N)	36.5 Slip Angle

For all experiments the slip ratio  $i_x$ , is controlled by the velocity of the gantry,  $v_x$ , and angular

velocity of the wheel,  $\omega$ , as shown in Equations 7 and 8.

$$v_{ref} = r\omega \quad (7)$$

$$i_x = 1 - \left( -\frac{v_x}{v_{ref}} \right), v_x \leq v_{ref} \quad (8)$$

As previously discussed in Section 3.2, the angular velocity and other geometric parameters of the wheel are set based on GSL. It is useful to note that, conveniently, this type of scaling keeps the slip ratio the same between lunar and Earth conditions. Moreover, for single wheel experiments in this Section the physical dimension of the wheel are the 1-1 based on theoretical LRM dimensions. The soil density,  $\rho$ , is prepared to be constant between two conditions based on G values of 3.9 to 4.3. The experimental conditions are thus approximately representative of the lunar conditions, in accordance with GSL.

#### 4.1.2 Single Wheel Results: Drawbar Pull Coefficient

The drawbar pull coefficient ( $DB.P_{coeff}$ ), defined as drawbar pull force (net forward force in forward driving on flat terrain) divided by wheel load, describes the tractive performance of a wheel and informs its likely slope climbing performance. In similarity with previous studies in the literature, the  $DB.P_{coeff}$  increases as slip values increase, regardless of the grouser design or loading condition. Consistent with past studies described in Section 2, Equal Loading provided more optimistic tractive performance compared to GSL. Grouser design had little impact on straight line drawbar pull results, as shown in Fig. 4.1; at higher slip the effect that different grouser shapes had on the  $DB.P_{coeff}$  was less than 5%.

#### 4.1.3 Single Wheel Results: Sinkage

Sinkage is another important metric given its link to possible rover entrapment. Sinkage increases at high slip, with a wheel excavating soil from beneath itself, and this general trend was observed across grouser shapes, loading conditions, and slip angles, as shown in Fig. 4.2 and Fig. 4.3. Grouser shape showed no direct influence on sinkage in straight line tests. In point turn single wheel

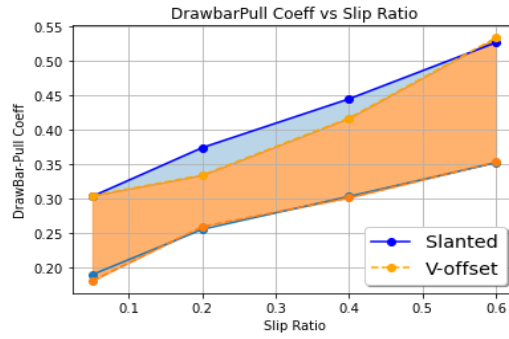


Figure 4.1: Drawbar pull vs Slip data for equal loading (upper bounds) and GSL (lower bounds) experiments for Slanted and V-offset grouser designs.

experiments (i.e. slip angle of 36.5 degrees) Slanted grousers showed significantly lower sinkage compared to V-offset grousers.

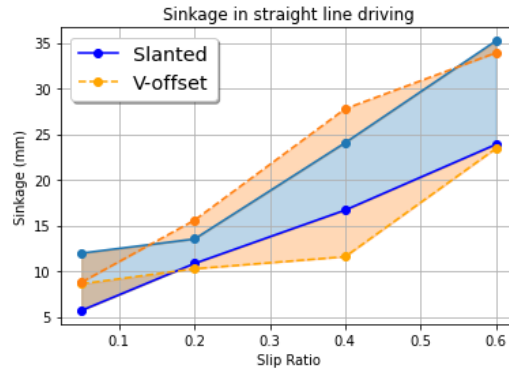


Figure 4.2: Sinkage obtained during single wheel experiments, with the higher sinkage corresponding to GSL conditions and lower sinkage to Equal Load

#### 4.1.4 Single Wheel Results: Tangent Turning Force

Tangent turning force can be used to directly evaluate a vehicle's ability to perform a point turn and is defined in Section 3.3.1. To achieve self-propelled point turning,  $F_{TTF}$  must be positive. The slip required for a point turn is when the tangent turning force enters the positive region.

Fig. 4.4 shows that the Slanted grouser wheel clearly achieves positive  $F_{TTF}$  at 0.40 slip ratio and above, even under the pessimistic GSL loading condition. The V-offset grouser wheel, on the other hand, has positive  $F_{TTF}$  at 0.4 slip ratio only under the most optimistic assumption, and barely achieves a positive value at 0.6 slip ratio under the more pessimistic GSL approximation.

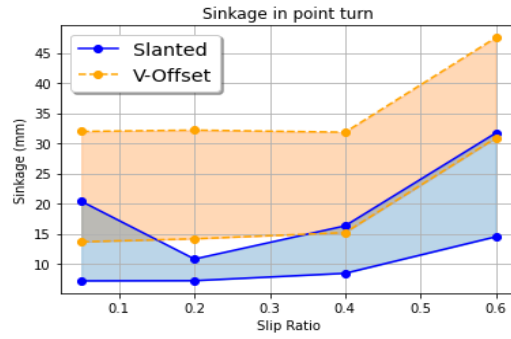


Figure 4.3: Sinkage in point turn driving for single wheel tests, with the higher sinkage corresponding to GSL conditions and lower sinkage to Equal Load

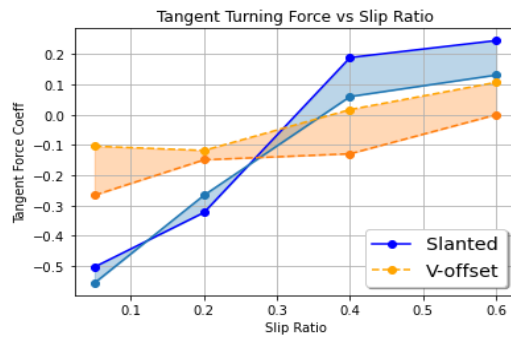


Figure 4.4: Tangent turning force generated by the wheel during single wheel tests with the GSL corresponding to the lower bound and equal load to the upper.

The superiority of the Slanted grouser design could be due to the angle of the grouser (30 degrees) allowing it to have more perpendicular contact with the soil during turns. Moreover, the Slanted grouser had a lower sinkage during slip angle tests which results in a lower lateral resistance force. While a reduction in sinkage can also lead to a lower drawbar pull, the decrease in lateral resistive forces is evidently the dominant effect. The grouser design, angle and orientation have a large effect on point turns.

## 4.2 Single Wheel Tests to Predict Point Turns

Full rover testing was done using the grouser design that satisfied the requirements from single wheel tests and has the best performance. The Slanted grouser design showed very similar abilities in straight line driving and superior in generating positive tangent turning force compared to the v-offset grousers. The focus of the test was to validate the estimations created from single wheel tests

by performing point turns using a Husky rover platform. It must be noted that the orientation of the grousers plays a critical role. The wheels were mounted ensuring that the grouser orientation will provide maximum traction as shown below in Fig. 4.5. With this orientation, each wheel's grousers have the same alignment relative to the wheel's direction of motion (regardless of clockwise or anticlockwise point turning). This ensured that all grousers were aligned at  $36.5^\circ$  during the point turn mimicking the slip angle that was set during single wheel experiments.

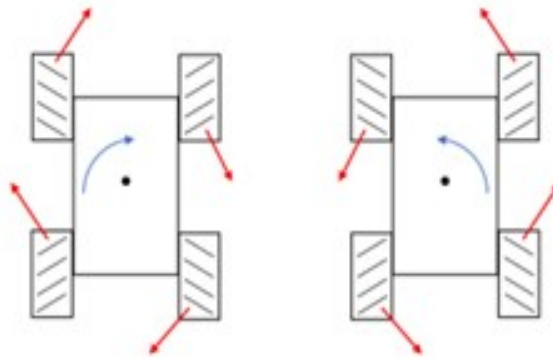


Figure 4.5: Grouser orientation (view from below the rover)

The main parameter used in estimating point turn ability of a full rover platform is the tangent turning force. This force is computed as seen in Section 1.1.2 and once it's positive then a point turn is theoretically possible at this slip ratio. This estimate is validated against the real slip obtained from full rover experiments calculated from the rover velocities.

Experimental results demonstrated good agreement between the two different slip ratios, thus validating the accuracy of the estimation method. This showcased that the slip required to point turns can reliably be estimated based on single wheel data and the tangent turning force approximation method. It must be noted that this is true for light rovers operating on loose soil using GSL approximation methods with Slanted grousers. For heavier rovers or those that include suspension, the prediction might not be as reliable.

#### 4.2.1 Full Rover Point Turn Results: Sinkage

The maximum sinkage for the Slanted grouser during full rover tests was shown to be 42 mm once steady conditions in soil displacement were reached, as shown in Fig. 4.6. This result is the

average result of three trials of point turn tests. Moreover, results that are related to dimensions scaled by GSL need to be multiplied by the inverse of the scaling applied to get the performance of the original wheel (which is 1.28 times smaller). Due to the  $h/L$  term in GSL we can expect the original wheel's sinkage to be 32.8 mm ( $42 \text{ mm} / 1.28$ ). As seen in Fig. 4.3 the sinkage observed during single wheel tests was substantially smaller sinking about 15 mm in the 0.3 to 0.4 slip range. This showed that single wheel tests are not that accurate in predicting sinkage of the full rover platform. This could be caused by the multi path effect and the difference due to the transfer between SWTB and a full rover test platform.

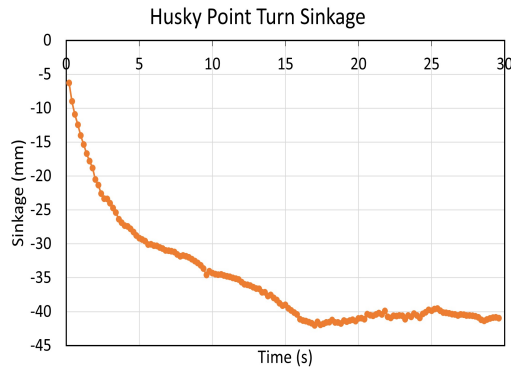


Figure 4.6: Average sinkage obtained during point turn full rover test

#### 4.2.2 Full Rover Point Turn Results: Slip

Full rover tests were consistent with and thus validated the result obtained from single wheel testing for point turn maneuvers. During full rover point turn the slip values varied between 0.25 to 0.4. This was similar to the predicted slip value of 0.35 obtained from single wheel experiments under GSL test conditions. This shows that under the conservative GSL condition single wheel tests can be a good estimate for the performance of the full rover platform. Overall, the results from the full rover testing successfully validated single wheel tests and showed agreement between the two experiments for point turns

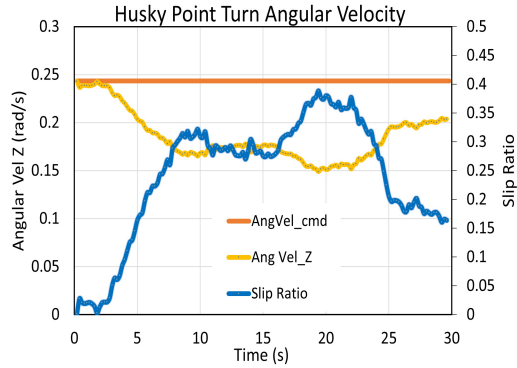


Figure 4.7: Average slip obtained during point turn full rover test

### 4.3 Single Wheel Tests to Predict Slope Climbing

Full rover experiments using a Husky Rover (Fig. 3.2) were done to evaluate slope climbing predictions based on the results from single wheel trials. To approximate slope climbing ability of a full rover platform rover, single-wheel flat-ground test data was paired with a gravity approximation model. The key parameter, the drawbar pull coefficient was calculated as the ratio of horizontal to vertical forces ( $F_x/F_z$ ). By relating  $DB.P_{coeff}$  to the slope angle ( $\gamma$ ) using Equation 6, the required  $DB.P_{coeff}$  for a slope of any inclination can be found. Once the desired  $DB.P_{coeff}$  is found, single wheel data can be used to approximate the slip at which it occurs.

The experimental test results showed that purely single wheel tests did not accurately predict the performance of the rover platform on sloped terrain. This showcased that using purely drawbar pull was not feasible when comparing traversal on flat and sloped terrain for these wheels. Moreover, methods using only force equilibrium as shown in Equation 6 are not sufficient. It is possible that the gravity vector has an important influence on soil interactions, such that the soil on a slope does not provide the same amount of resistance to wheel motion as on flat terrain. Furthermore, rover weight distribution, wheel width to diameter ratio, multi-path and other effects could have a detrimental influence on rover mobility on a slope. These factors were explored and incorporated into further experiments to gain better understanding and to further the development of a more accurate predictive model for rover slope climbing estimates.

### 4.3.1 Full Rover Slope Climbing Results: Slip

During experiments the controlled parameters included; the lunar simulant, the soil density (compaction level), and slope inclination, as well as the commanded rover wheel angular velocity, set in accordance to Condition 2 (GSL) in Table 3.2. During tests, the  $x,y,z$  values of the rover were recorded as it traveled up the slope. Combining travel time with the rover position, the actual rover velocity was determined. The slip was obtained by comparing commanded versus actual velocity. Slip was validated by observing the rover tracks and the total time required to perform the maneuver.

The results in Fig. 4.8 show the rover slip that occurred during the slope climb. Unlike the prediction from single wheel experiments which showed the required slip of around 0.3, the full rover tests showed that a slip ratio of around 0.80 is required to overcome a slope of 15 degrees. This constitutes a slip ratio of approximately 2.5 times the original estimate. This could be caused by the specific soil mechanics interactions that occur on sloped terrain or may be specific to wheels of low width to diameter ratio as will be explored further in Section 4.5. Furthermore, other factors such as weight distribution combined with a multi-path effect may have a negative effect on slope climbing ability as described in Section 2.3. Based on these experimental results it can be noted that the simple force equilibrium model paired with single wheel tests, does not accurately estimate the climbing ability of a full rover platform. If this estimate is to be used a large correction factor (around 2 if based on flat ground tests) should be considered to not overestimate the real rover mobility.

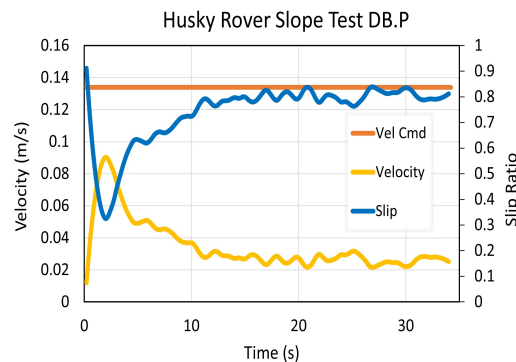


Figure 4.8: Velocity and slip obtained during slope experiments

### 4.3.2 Full Rover Slope Climbing Results: Sinkage

Fig. 4.9 shows that the sinkage for the slope experiment stabilizes around 60 mm. Since single wheel tests were limited to a maximum of 0.6 slip we don't have a direct comparison. Furthermore, similar to point turns we need to apply the inverse GSL scaling to get the correct value. The resulting sinkage would be 46.9 mm, which is what the original wheel should experience. If we extend the line of best fit in Fig. 4.2 then we can estimate that we will reach approximately 45 - 50 mm of sinkage for the single wheel sloped tests at a slip of 0.80.

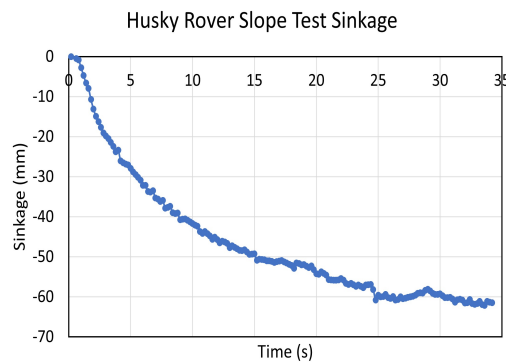


Figure 4.9: Sinkage obtained during slope experiments

## 4.4 Influence of Weight Distribution on Slope Climbing Predictions

To improve the approximation method, the weight distribution of the full rover platform on a sloped terrain was investigated. Previous literature had conflicting conclusions, with work by [Gheshlaghi and Mardani \(2021\)](#) concluding that it has an effect, while [Senatore et al. \(2014\)](#) came to the conclusion that the effects could be neglected. This Section addresses this by performing multiple single wheel experiments with different wheels with two different methods for determining the vertical load. The first method assumes equal weight distribution among all wheels and sets the vertical loading in single wheel experiments to 1/4 of the total vertical load. The other method is to theoretically evaluate the weight distribution of the rover on a slope, thus finding the front wheel and rear wheel vertical loads. The results from these single wheel experiments are then paired with the full platform approximation theory and the slip required to climb different slope terrain was

found. To evaluate if a significant change in prediction error occurs, validation experiments were completed using a husky platform on different slope inclinations.

#### 4.4.1 Weight Distribution Theory

The weight distribution model of a vehicle on a slope was used to create equations in which the vertical forces applied on a front and rear wheel are a function of terrain inclination and location of the center of weight.

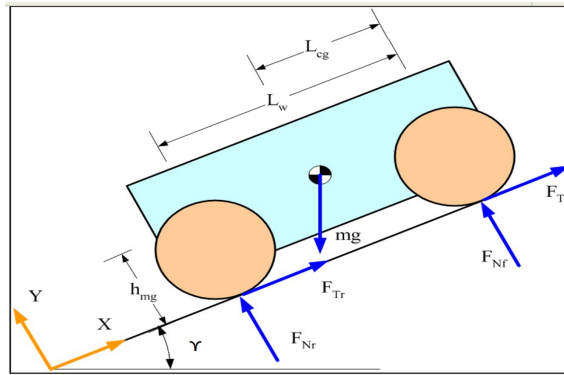


Figure 4.10: Forces Acting on Vehicle on Slope Terrain

As shown in Fig. 4.10 the main forces of interest are the reaction forces on the front ( $F_{Nf}$ ) and rear ( $F_{Nr}$ ) wheels. The calculations were done for a slope of 15 degrees, and the vertical loads were divided by two to get the vertical load acting on a single wheel. The derivation of the front and rear wheel reaction forces are shown below:

$$\sum F_x = 0 = F_{Tr} + F_{Tf} - mgsin\gamma \quad (9)$$

$$\sum F_y = 0 = F_{Nr} + F_{Nf} - mgcos\gamma \quad (10)$$

$$\sum M = 0 = F_{Nr}L_w - mg\left(L_{cg}cos\gamma + h_{mg}sin\gamma\right) \quad (11)$$

Using Equations 10 and 11, the reaction forces can be found for any center of gravity and slope inclination angle ( $\gamma$ ).

$$F_{Nr} = \frac{mg \left( L_{cg} \cos \gamma + h_{mg} \sin \gamma \right)}{L_w} \quad (12)$$

$$F_{Nf} = \frac{mg \left[ \left( L_w - L_{cg} \right) \cos \gamma - h_{mg} \sin \gamma \right]}{L_w} \quad (13)$$

The center of gravity of the rover is in the center of the chassis. Furthermore, with the addition of extra weight to the top of the rover the center of weight is moved slightly higher. To have a conservative assumption the vertical position of center of weight was assumed to be at the top surface of the rover. If the center of weight is in a lower position the distribution would be more even between the front and rear wheels. However, by using the most extreme situation we evaluate the maximum difference in prediction between the two methods. The values used to calculate the vertical load distribution are shown in Table 4.2, with the final values shown in Table 4.3.

Table 4.2: Full Rover Parameters

Mass (kg)	$L_w$ (m)	$L_{cg}$ (m)	$h_{cg}$ (m)
63	0.512	0.256	0.39

Table 4.3: Vertical load on the front and rear axles on sloped terrain

	Distributed Wheel Loading	1/4 Wheel Loading
$F_{Nr}$	420.33N	298N
$F_{Nf}$	176.64N	298N

Thus the resulting vertical load to be applied during single wheel experiments is 149N for 1/4 wheel loading and 210N & 88N for distributed wheel loading.

#### 4.4.2 Slope Climbing Predictions

The two vertical loading methods were applied in single wheel testing and the generated data was used to predict slope climbing for a full rover platform. The main variable used in this prediction is the  $DB.P_{coeff}$ . The  $DB.P_{coeff}$  is a non dimensional term that normalizes the drawbar pull by the vertical load as described in 3.3.2. As shown in Equations 14 there is a direct relationship between

$DB.P_{coeff}$ , slope inclination angle ( $\gamma$ ) and the force required for a rover platform this slope. For test cases evaluated, the data trends of  $DB.P_{coeff}$  vs slip seen were not obviously nonlinear in the fixed interval of slip tested. Therefore, to estimate the DB.P values between the slip ratios tested, a linear line of best fit was used. It must be noted that previous literature (Ding et al., 2011) has shown trends that are obviously non-linear, but all such trends are wheel, soil, and slip interval dependent. Furthermore, a linear line can simplify the comparison between two test conditions (slope and flat), using fewer model parameters.

$$DB.P_{coeff} = \tan(\gamma) \quad (14a)$$

$$F_{slope} = 63 * 9.81 * \sin(\gamma) \quad (14b)$$

An important assumption made when predicting full rover slip from single wheel tests is that all wheels are slipping the same amount during slope traversal. Moreover, the total force required for the rover to travel up the slope is based solely on its weight. Therefore, to predict the slip required for the full platform to climb the slope, we need to approximate the slip at which single wheels generate the equivalent force.

Slip from the distributed front & rear wheel loads can be calculated by summing the interpolation equations and equating them to the desired force. Similarly, this can be done for the 1/4 wheel load. The final equations are shown below in Equation 15.

$$F_{slope} = 4 * VerticalLoad_{1/4} * f(slip_{1/4}) \quad (15a)$$

$$F_{slope} = 2 * \left[ VerticalLoad_{front} * f(slip_{front}) + VerticalLoad_{rear} * f(slip_{rear}) \right] \quad (15b)$$

### 4.4.3 Single Wheel Experiments

Additional single wheel experiments were performed using the vertical load calculated in Section 4.4. The same soil preparation methods and equipment are used for these experiments as in Section 4.1 and are described in detail in Section 3.1.1.

The main difference for this set of experiments is the change in the wheel's physical dimensions

used in single wheel experiments. The difference in wheel dimensions used on the test platform and the original concept are 1.28 according to the GSL scaling method described in Section 3.2. To reduce error accumulation from GSL and error from other sources single wheel tests were completed using the bigger (384 diameter) wheels that are used on the full rover platform. The drawbar pull resulting from these new tests were used for further estimations and comparison between the distributed and 1/4 wheel load methods.

Table 4.4: Experiments Completed to Test Influence of Weight Distribution

	Vertical Load	Slip Ratio Tested	Number of Trials Per Slip Ratio
Tested for Each Wheel	210N, 88N, 149N	0.05, 0.20, 0.40, 0.60	2



Figure 4.11: Wheels used in experiments; Bare, Grouser, Husky from left to right

To gather more data for analysis multiple wheels that were readily available in the lab were tested. The primary difference between the bare and grouser wheel is the exterior surface which can be easily changed without changing the distance to the wheel surface. This setup allows the test of multiple different surface types including different types of grousers or a bare surface. The drawbar pull results from each test were then used in predictions and the accuracy of the predictions was evaluated. Table 4.4 provides a summary of the experiments conducted with each wheel. The specific wheels used in the experiments are shown in Fig. 4.11. The order of experiments is bare wheel, grouser wheel, then husky wheel. This order is used to evaluate the difference in prediction

first using the simplest wheel type. Using a bare wheel simplified theoretical modeling of soil wheel interactions and conclusions made using this wheel can be extrapolated to more complex wheels. Testing the grouser wheel, is done to test a realistic wheel that was designed for the LRM mission to observe if conclusions from the bare wheel hold when the wheel surface changes. Lastly, to make conclusions from this work generally applicable the husky wheel was tested. The husky wheel is different in its physical dimensions, material and wheel surface. This ensures that any conclusions from this work apply to wheels of different types and dimensions.

### **Bare wheel results**

Seen below are the slope climbing predictions from the bare wheel 1/4 and front & rear wheel distribution methods. Data was collected using the SWTB described in Section 3.1.1. Single wheel data was used to predict the slip required for a full rover platform to climb an inclined slope. The resulting slip from both methods was compared to full rover experiments and the error from each method was analyzed.

Table 4.5: Force Required to Climb the Slopes Tested for Bare Wheel

Wheel Loading Method	Slope 3.5°	Slope 5°	Slope 6.5°	Slope 10°
Force Required	37.7 N	53.9 N	70.0 N	107.3 N

Solving Equations 14 and 15 we can approximate the slip required for our rover to climb a slope of any angle. The slope inclination angle was chosen to correspond to the predicted values of slip between 30 and 80 percent. These values are chosen based on operational slip values for a rover during a possible mission. The Table 4.5 captures the required force for a full platform to climb the selected slope inclinations. Single wheel predictions were then calculated using the data from Table 4.5 as inputs to Equation 14. The estimated slip to climb the slope was then determined and is shown in Table 4.6.

Once the required slope angles were determined, full rover validation experiments were performed with two trials per slope angle. The average slip was taken from the steady state region of the rover slope climb. The average of both trials was used as the final value to compare against single wheel predictions as shown in Table 4.6.

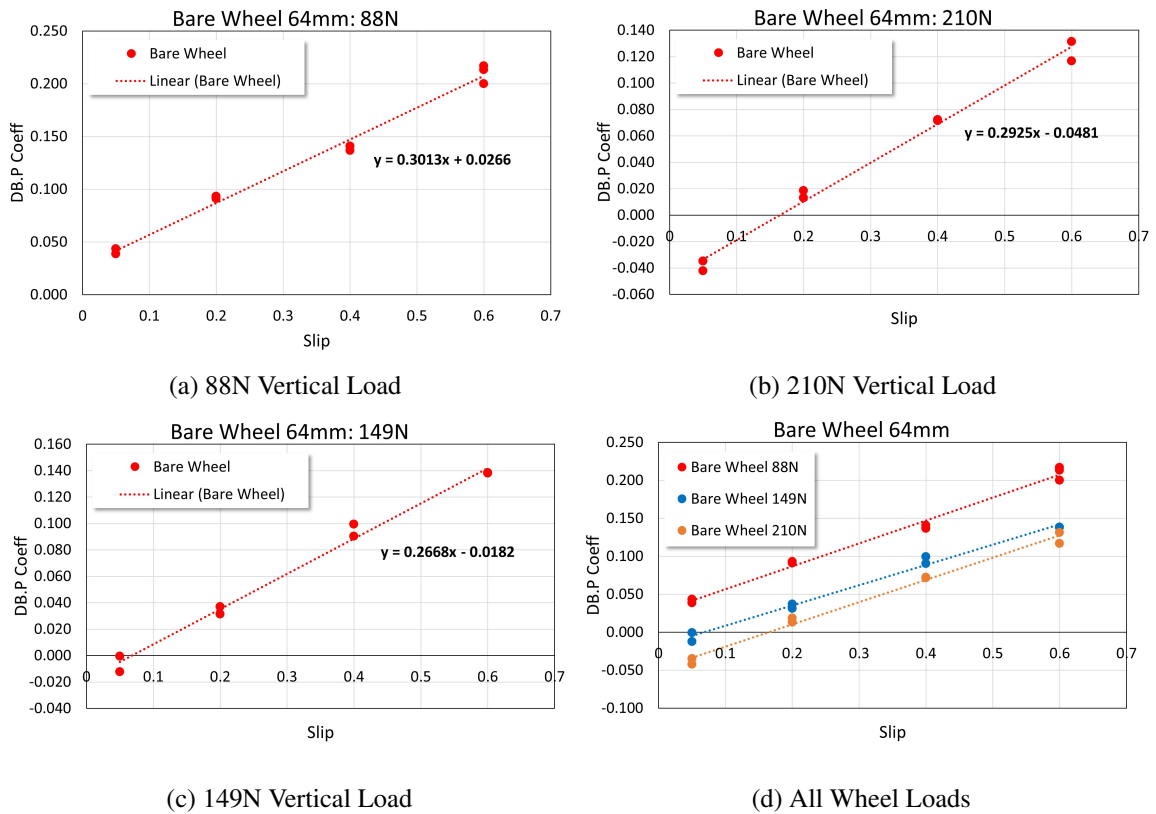


Figure 4.12: Bare Wheel  $DB.P_{coeff}$  vs slip

Analyzing the slip predictions generated by each method we observe that the difference between them is negligible for the first three tests, being less than 2%. This value is less than sensor noise and data variability due to soil preparation and other experimental inconsistencies. However, for the slope inclination of 10 degree the difference is 4.5%. This difference value still falls within the expected range of variation due to uncertainties in an experiment of this type. Looking at Fig. 4.12d we can observe that  $DB.P_{coeff}$  increases as the vertical weight decreases. The 149 N vertical load data is closer to the 210 N vertical load data, indicating that the increase in  $DB.P_{coeff}$  is not directly proportional to the decrease in vertical load for this wheel type. Therefore, the theoretical total force generated by the wheels from the front & rear distribution should be very similar to the 1/4 distribution given the increased weight of the rear wheel (210 N). With the 1/4 method being slightly more conservative in their predictions. Lastly, when evaluating the accuracy of the predictions, a large error was seen with values differentiating up to 35%. This was not seen in previous literature and may be related to the influences of multipath effect, specific soil-wheel and

Table 4.6: Bare Wheel Estimated Slip Compared to Actual Slip Required to Climb Slope

Wheel Loading Method	Slope 3.5	Slope 5	Slope 6.5	Slope 10
Prediction using Front & Rear	30.3%	39.5%	48.6%	69.8%
Prediction using 1/4	30.5%	40.7%	50.8%	74.3%
<b>Full Rover Results</b>	<b>52.6%</b>	<b>75.5%</b>	<b>79.2%</b>	<b>87.3%</b>

soil-soil interaction on slope terrain and the wheel's physical properties.

### Grouser wheel results

This Section shows results for experiments using the grouser wheels. The theory and experimental setup are the same as in Section 4.4.3. The purpose of testing the grouser wheel is to observe whether the conclusions of Section 4.4.3 will hold when the wheel surface is changed. The addition of grousers complicates and changes soil wheel interactions and soil flow underneath the wheel.

Table 4.7: Force Required to Climb the Slopes Tested for Grouser Wheel

Wheel Loading Method	Slope 10°	Slope 12.5°	Slope 15°
Force Required	107.3 N	133.8 N	160.0 N

Table 4.7 shows the force required for a full platform using grouser wheels to climb a slope. Knowing the force we can estimate the appropriate slip required to climb the specific slope. Table 4.8 shows the result of single wheel slip predictions and the full rover validation experiments for every slope inclination.

Table 4.8: Grouser Wheel Estimated Slip Compared to Actual Slip Required to Climb Slope

Wheel Loading Method	Slope 10°	Slope 12.5°	Slope 15°
Prediction using Front & Rear	17.2%	30.5%	43.6%
Prediction using 1/4	17.4%	29.8%	42.0%
<b>Full Rover Results</b>	<b>39.6%</b>	<b>60.0%</b>	<b>80.6%</b>

Grouser wheel results followed very similar trends to the bare wheel. The observed difference between the two prediction methods was once again negligible. Furthermore, the  $DB.P_{coeff}$  versus vertical load shown in Fig. 4.13d had the same relationship as the bare wheel. One difference from the bare wheel was that the front & rear method was not more conservative in their predictions.

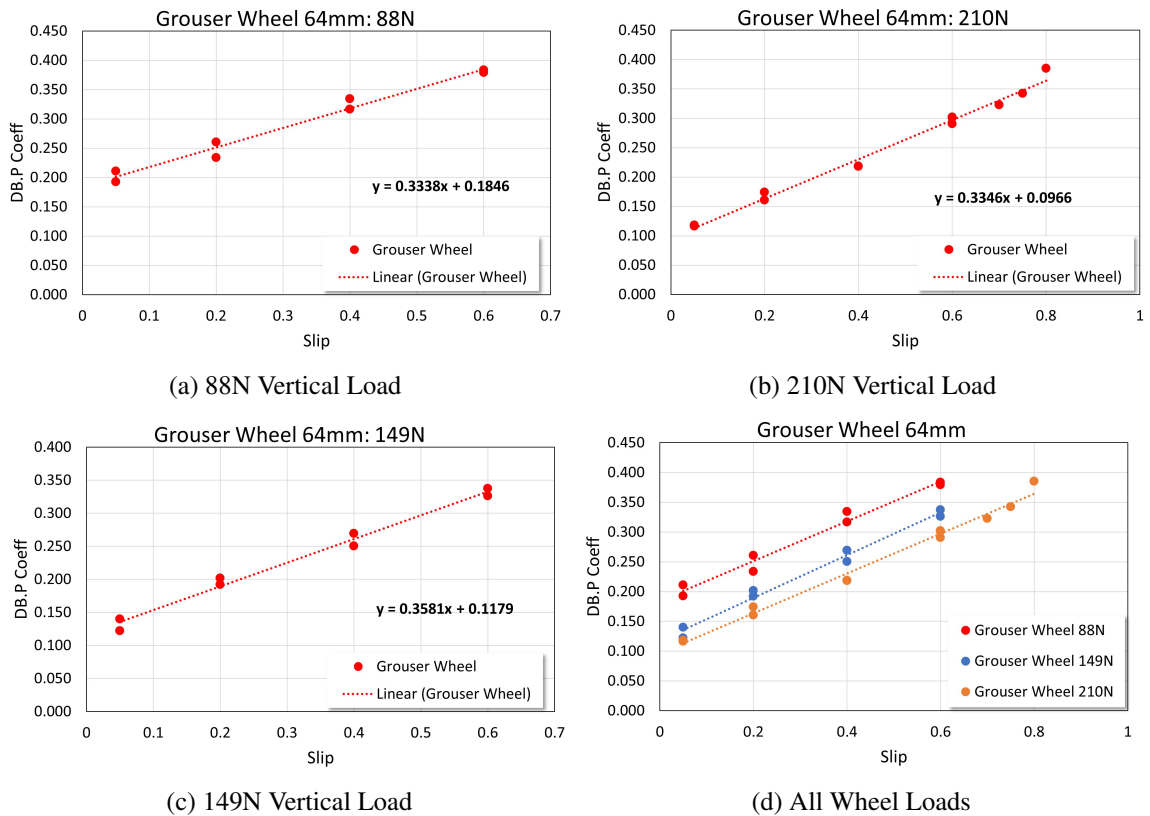


Figure 4.13: Grouser Wheel  $DB.P_{coeff}$  vs slip

However, when comparing the estimations to actual rover climbing slip there was a large error which was consistent with the bare wheel.

### Husky wheel results

Lastly, the husky wheel was tested with the appropriate results presented in this Section. The husky wheel was tested to ensure the conclusions from Sections 4.4.3 and 4.4.3 apply to more than one wheel type.

Table 4.9: Force Required to Climb the Slopes Tested For Husky Wheel

Wheel Loading Method	Slope $5^\circ$	Slope $10^\circ$	Slope $12.5^\circ$
Force Required	53.9 N	107.3 N	133.8 N

Table 4.9 shows the force required for a rover using husky wheels to climb a slope. Table 4.10 displays single wheel slip estimations and slip experienced by the full rover platform for every slope

climb.

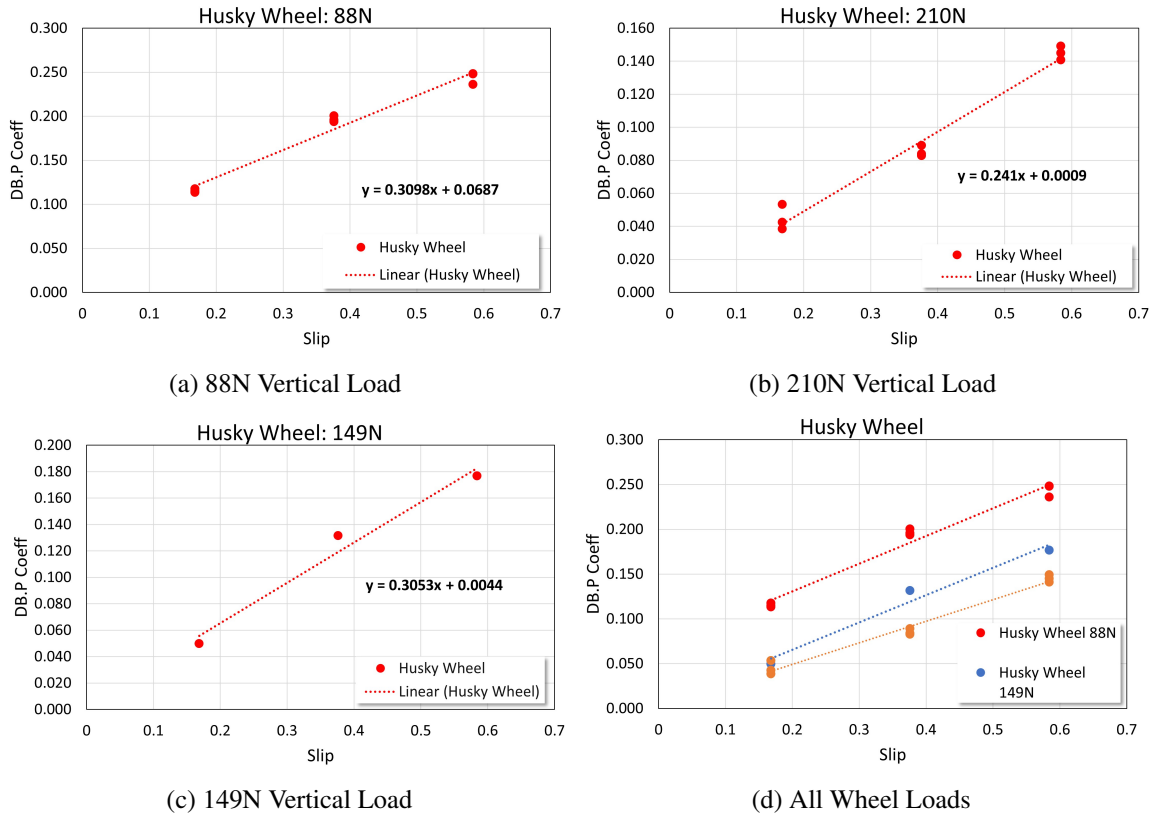


Figure 4.14: Husky Wheel  $DB.P_{coeff}$  vs slip

Table 4.10: Husky Wheel Estimated Slip Compared to Actual Slip Required to Climb Slope

Wheel Loading Method	Slope 5°	Slope 10°	Slope 12.5°
Prediction using Front & Rear	26.6%	60.9%	77.9%
Prediction using 1/4	28.2%	57.5%	72.1%
<b>Full Rover Results</b>	<b>20.0%</b>	<b>65.0%</b>	<b>78.0%</b>

After reviewing the results it was clear that in the case of the husky wheel there was very little difference between predictions from the 1/4 and front & rear wheel distribution methods. Similarly to the bare wheel, the largest differences in predictions were observed at higher slip values. However, even at these high slip values the difference was 6 % at most. One thing to note is that these predictions are most accurate in the mid slip regions (20 to 60% slip). This region is characterized by a mostly linear like relationship between  $DB.P_{coeff}$  and slip. The results from the 1/4 vertical load method were non-conservative, which is similar to the grouser wheel. When comparing single

wheel predictions to full rover results it can be seen that they are a lot closer than with the previous wheels tested. With single wheel predictions for the 5 degree slope over predicting the slip required for a full rover platform. The other test cases showed prediction errors of up to 8 % from the 1/4 method and only 4% using the distributed method. Showing that for the case of the husky wheel the front & rear method provides a slightly more accurate result.

#### 4.4.4 Prediction Accuracy Evaluation

Overall, for all the experiments involving the three different wheel types there was little difference between predictions from 1/4 and front & rear distribution. The difference between the two methods range between 1 % and 6 %, which is around the levels of noise seen in the experiments. The source of this noise is mainly due to manual soil preparation which can cause the average slip values between experiments to differ from each other up to 5%. Moreover, there is some small amount of noise due to data collecting sensors but this is substantially smaller than the variability in soil preparation. This experimental validation support claims made by [Senatore and Iagnemma \(2014\)](#) that vertical wheel load distribution does not have a large impact on slope climbing predictions. Therefore, for any future work in this thesis 1/4 vertical load distribution methods are deemed appropriate to use as the primary method of collecting single wheel data for slope climbing predictions. Using the 1/4 method requires two times fewer experiments, resulting in substantial time and resource savings.

The difference of error in predictions from single wheel test data is primarily seen in the bare and grouser wheel. These wheel have a large diameter and a small width compared to the Husky wheel. Moreover, they are made from a completely rigid material (PLA) compared to the standard rubber husky tire.

Table 4.11: Single Wheel Prediction Error for Front & Rear Method: Absolute Difference

Wheel Type	Slope 3.5°	Slope 5°	Slope 6.5°	Slope 10°	Slope 12.5°	Slope 15°
Bare Predictions Error	21.3%	36.0%	30.6%	17.5%	-	-
Grouser Predictions Error	-	-	-	22.4%	29.5%	37.0
Husky Predictions Error	-	-9.4%	-	4.8%	1.6%	-

Table 4.12: Single Wheel Prediction Error for Front & Rear Method: Percent Difference

Wheel Type	Slope 3.5°	Slope 5°	Slope 6.5°	Slope 10°	Slope 12.5°	Slope 15°
Bare Predictions Error	41.2%	47.7%	38.6%	20.0%	-	-
Grouser Predictions Error	-	-	-	56.5%	49.2%	45.9%
Husky Predictions Error	-	-54.7%	-	7.3%	2.0%	-

The prediction error was evaluated for front & rear, the error is calculated using two metrics absolute and percent difference.

$$Error_{Percent} = \frac{SingleWheelSlip - FullRoverSlip}{FullRoverSlip} \quad (16a)$$

$$Error_{Absolute} = SingleWheelSlip - FullRoverSlip \quad (16b)$$

The results using both metrics were reported in Tables 4.11 and 4.12 respectively. Similarly, the prediction error for the 1/4 method was calculated using both metrics and shown below in Tables 4.13 and 4.14.

Table 4.13: Single Wheel Prediction Error for 1/4 Method: Absolute Difference

Wheel Type	Slope 3.5°	Slope 5°	Slope 6.5°	Slope 10°	Slope 12.5°	Slope 15°
Bare Predictions Error	21.1%	34.8%	28.4%	13.0%	-	-
Grouser Predictions Error	-	-	-	22.2%	30.3%	38.6%
Husky Predictions Error	-	-11.0%	-	8.15%	7.4%	-

Table 4.14: Single Wheel Prediction Error for 1/4 Method: Percent Difference

Wheel Type	Slope 3.5°	Slope 5°	Slope 6.5°	Slope 10°	Slope 12.5°	Slope 15°
Bare Predictions Error	40.8%	46.1%	35.8%	14.9%	-	-
Grouser Predictions Error	-	-	-	56.1%	50.4%	47.9%
Husky Predictions Error	-	-64.0%	-	12.4%	9.3%	-

The predictions made from both methods substantially overestimated the real performance of the rover platform for the bare and grouser wheels. With the actual slip to climb the slope differing by 0 to 56 percent and -33 to 56 absolute error respectively. This indicated that purely using DB.P was not feasible when comparing traversal on flat and sloped terrain between single wheel and full rover

test cases for the wheels designed for CSA LRM. The dimensions of these wheels differ from the wheels previously used with the gravity approximation methods (Sutoh et al., 2011). The primary difference is the diameter over width ratio. This ratio is a value of around 6 for the CSA LRM wheels, while in most previous studies this ratio was always under 3. The Husky wheel showed a good consensus between the predictions and the full rover slip. The diameter to width ratio of the Husky wheels is 2.63 which is closer to the ratio of the wheels used in previous studies. This could be one of the reasons for the higher accuracy of the prediction method.

The gravity vector likely has a major influence on soil interactions. The soil on a slope does not provide the same resistance to wheel motion as on flat terrain resulting in lower DB.P generated. Furthermore, rover weight distribution, multi-path and other effects could negatively influence slope mobility when transitioning from single wheel to a full rover test case. The wheel's dimensions, particularly its radius-to-width ratio, may further affect the flow of soil beneath it and influence approximations.

## **4.5 Influence of Diameter over Width Ratio on Slope Climbing Predictions**

The tractive properties of a wheel are heavily influenced by its physical parameters and the shape of the exterior surface as previously shown by (Inotsume et al., 2019; Skonieczny et al., 2012; Sutoh et al., 2013, 2012). Among them are two parameters: the width and the diameter which heavily influence the DB.P generated by the wheel. The exact influence of these parameters was explained in Section 2.2.1. Experiments in Section 4.3 have indicated that these two parameters might influence the accuracy of full rover slope predictions using single wheel data. To investigate the influence of these parameters a ratio (diameter/width) was defined. When using this ratio in Section 4.4.4 it was seen that the accuracy was better for wheel with a smaller ratio. To isolate the influence of this ratio, experiments using two wheels which differed solely by the dia/width ratio were completed.

Previously, most of the rovers designed and sent on missions have used wheels with a diameter to width ratio below 3. This leads experiments and research to use these mission proven wheels in

Table 4.15: Diameter to Width Ratio of Wheel used Previously

Rover	Lunahkods	Sojourner	Curiosity	SFR
Diameter (mm)	510	130	500	550
Width (mm)	200	79	400	200
Dia/Width Ratio	2.55	1.65	1.25	2.75

their research. A summary of the diameter to width ratio of wheels from previous years is shown in Table 4.15. Therefore, in experiments involving single wheel and full rover mobility certain aspects that are specific to low width high diameter wheels might have been missed. Given the heightened interest in micro rover for future lunar and other extra-planetary exploration understanding the relationship between diameter/width and mobility predictions is important.

Two different wheels were used for these experiments. Both wheels were 3D printed from PLA material and had the same inner structure with the main difference being the tractive surface. The modular design of the wheels allows modification of the tractive surface with little effort. This resulted in the following four different wheels used in experiments: bare wheel and grouser wheel each with 64 and 128 mm widths. Each wheel was subjected to single wheel and full rover experiments to determine the influence of the diameter/width ratio. Furthermore, the vertical load chosen for the experiments was 1/4 vertical load. This decision was based on the experimental results from Section 4.4.4 which showcased that using 1/4 versus distributed vertical weight loading techniques made little difference in slope climbing prediction error. To gather the required data for predicting slope climbing performance, each wheel was tested using a SWTB at the slip ratios shown in Table 4.16.

Table 4.16: Single Wheel Experiments Completed to Test Influence of Diameter over Width

	Vertical Load	Slip Ratio Tested (%)	Number of Trials Per Slip Ratio
Tested for Each Wheel	149N	0.05, 0.20, 0.40, 0.60	2

Similarly, Table 4.17 shows all the slope inclinations for which data was gathered using the Husky rover.

Table 4.17: Full Rover Experiments Completed to Test Influence of Diameter over Width

	Slope Inclination $\gamma$ (deg $^{\circ}$ )	Number of Trials Per Slope Inclination
Grouser Wheel 64mm	10, 12.5, 15	2 to 3
Grouser Wheel 128mm	10, 15, 17	2 to 3
Bare Wheel 64mm	3.5, 5, 6.5, 10	2 to 3
Bare Wheel 128mm	5, 6, 7, 10	2 to 3

### 4.5.1 Diameter over Width Effect on Slope Climbing

To evaluate the influence of the diameter to width ratio, the absolute (16b) and relative errors (16a) were compared between the different wheels tested.

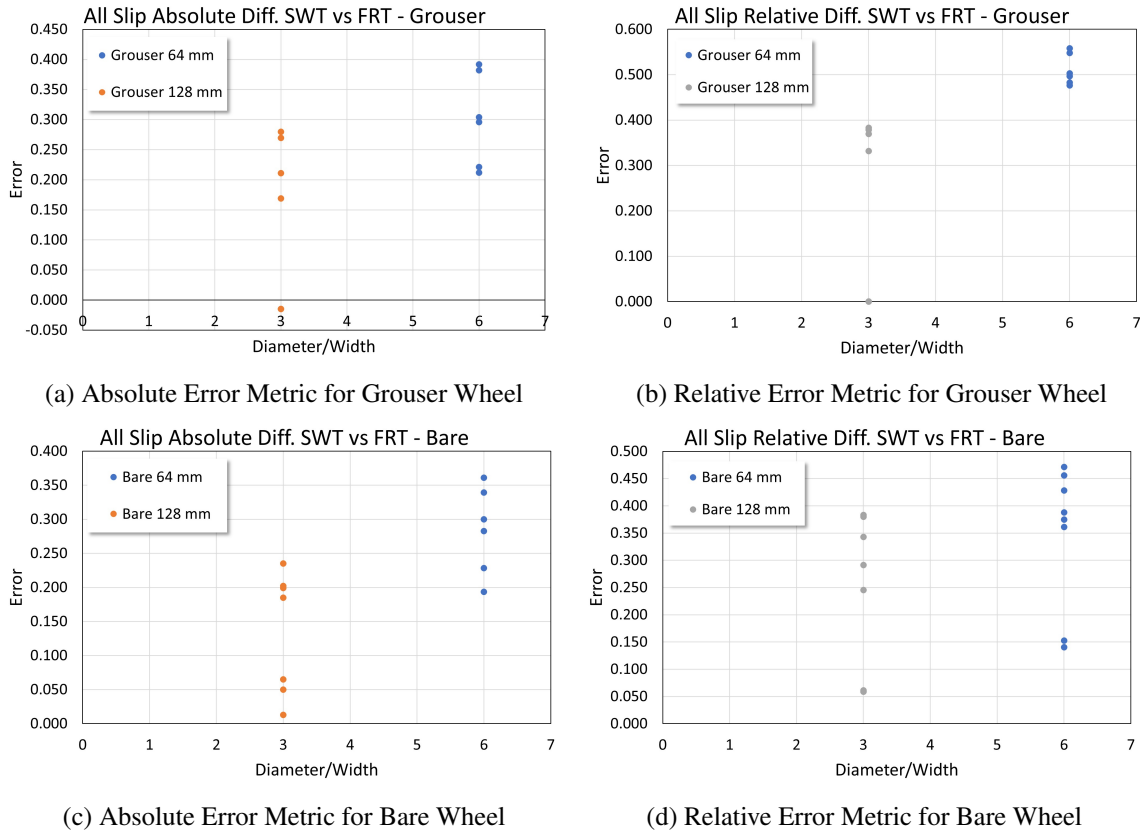


Figure 4.15: All Slip Data for Grouser and Bare Wheels (including edge values)

Shown in Fig. 4.15 is the complete data of the predictions compared against the full rover validation experiments. However, it was observed that trends across all wheels were different for very low slip (< 30%) and very high (> 70%) slip values when compared to mid range slip values

(30-70 %). This is supported when looking at the prediction error plotted against the prediction shown in Fig. 4.16. Moreover, the error metrics for data sets seem to suggest that in mid slip region the errors are within a smaller distribution than at the extreme slip regions. For these reasons, and since operationally the mid range slip ratios is of the most interest, the statistical analysis completed between the different wheels included only mid slip values.

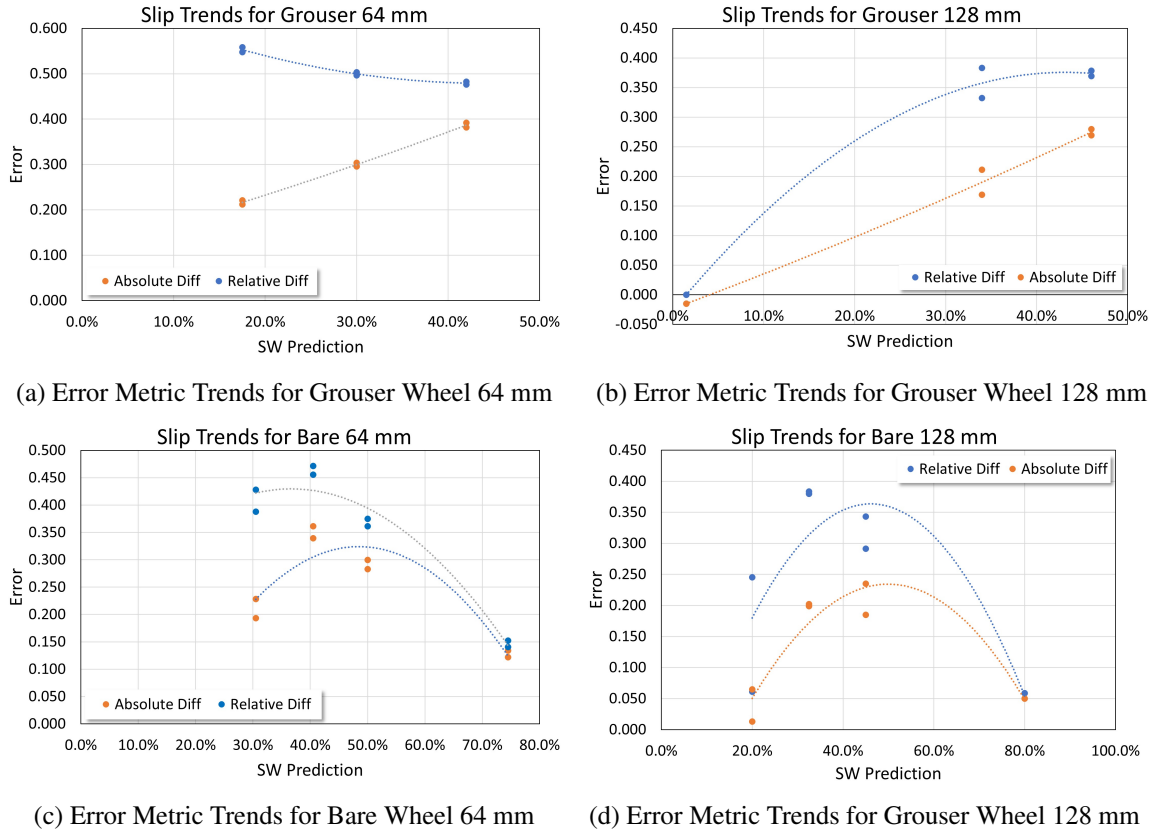


Figure 4.16: Slip Data Trends, Mid vs Boundary

These adjusted results shown in Fig. 4.17 were statistically analyzed to determine if there was evidence to conclude that the diameter to width ratio has an effect on the slope climbing prediction error.

The statistical analysis was performed using a paired T-test. This method requires the data to follow a normal distribution. Therefore, as an initial step all datasets were tested for normality using an Anderson Darling test. Table 4.18 shows the dataset for each wheel and the results of the Anderson Darling test. The null hypothesis tested was that with a confidence of 95% the dataset

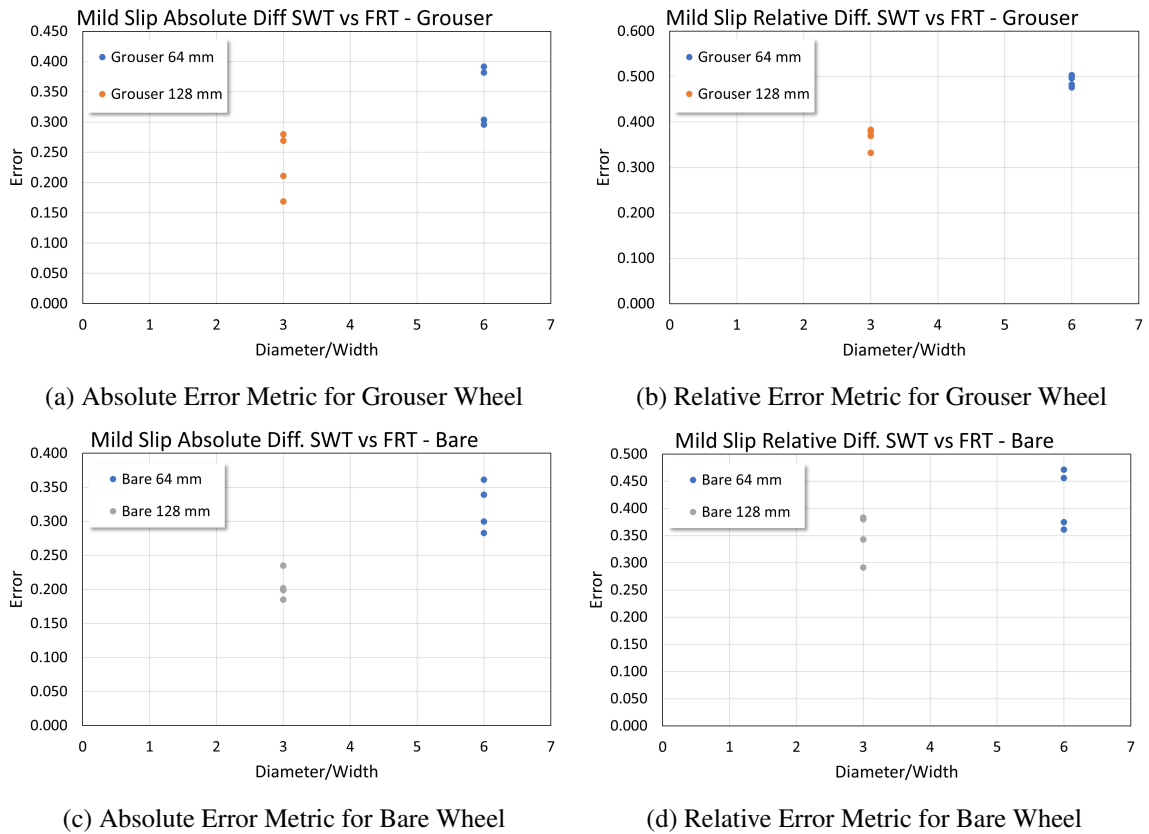


Figure 4.17: Mild Slip Data for Grouser and Bare Wheels

follows a normal distribution. To achieve this confidence level, the resulting p-value must be greater or equal to 0.05. The results showed that all datasets fulfilled the conditions for normality, and therefore a paired T-test can be used.

The T-test calculations shown in Table 4.19 were completed with a null hypothesis stating that for the two datasets 64mm and 128mm the mean difference is equal to zero at a confidence of 95%. To have statistical significance the p-value must be equal to or less than 0.05, which would result in an h-value of 1. Thus rejecting the null hypothesis and showing that there is a statistical difference between the two datasets. The result of the statistical analysis strongly suggests that the diameter/width of the wheel has a non-negligible influence on prediction error.

Table 4.18: Anderson Darling Test for all Wheels

Data Set	Data	Mean	Anderson Darling Test	
			h	p
Grouser 64 ABS	0.296, 0.304, 0.392, 0.382	0.344	0	0.1532
Grouser 128 ABS	0.169, 0.211, 0.269, 0.280	0.232	0	0.5508
Bare 64 ABS	0.361, 0.339, 0.283, 0.300	0.321	0	0.7471
Bare 128 ABS	0.202, 0.199, 0.235, 0.185	0.205	0	0.3518
Grouser 64 Per	0.496, 0.503, 0.483, 0.476	0.490	0	0.7930
Grouser 128 Per	0.332, 0.383, 0.369, 0.378	0.366	0	0.1701
Bare 64 Per	0.471, 0.456, 0.361, 0.375	0.416	0	0.3518
Bare 128 Per	0.383, 0.380, 0.343, 0.291	0.349	0	0.3339

Table 4.19: T-Test for all Wheels

T-Test		
Data Set Name	h Value	p Value
Grouser Abs	1	8.63E-4
Grouser Per	1	0.0031
Bare Abs	1	0.0175
Bare Per	1	0.0268

#### 4.5.2 Improving Prediction Using Diameter/Width Value

The statistical analysis has shown that increasing the diameter to width ratio has an influence on prediction error. The relationship nature is hard to identify given only four points of data for rigid rover wheels as shown in Fig. 4.18, which evaluates the maximum absolute and relative errors. The original husky wheel, an inflated rubber wheel has a substantially lower error. However, the rigid wheels were designed specifically with lunar exploration in mind and can be more representative of the wheels that will be used for exploration purposes compared to the husky wheel. The rigid wheels dataset can be used to find the appropriate equation for a correction factor. The correction factor can then be calculated based on the diameter to width ratio of the wheel. Adding a correction factor, the accuracy of predictions with single wheel data and the simple gravity approximation model can be improved.

The data gathered in this study can be used to develop a relationship between prediction error and diameter over width D/W value. By knowing the specific diameter and width of the wheels we can estimate the expected error with the following Equation 17



(a) Absolute Error Metric for Grouser Wheel (b) Relative Error Metric for Grouser Wheel

Figure 4.18: Mild Slip Data for Grouser and Bare Wheels

$$Error_{ABS} = 0.0397 * D/W + 0.1384 \quad (17a)$$

$$Error_{REL} = 0.0346 * Dia/D + 0.2794 \quad (17b)$$

The relative error values can be used to select an appropriate correction factor (C.F) as shown in Equation 17. Thus, single wheel test slip can be multiplied by a correction factor found from the error to get an updated and more accurate full rover slip prediction as shown in Equation 19. With SWTS meaning single wheel test slip, FRTS meaning full rover test slip.

$$C.F = \frac{1}{1 - Error_{REL}} \quad (18)$$

$$FRTS = SWTS * C.F \quad (19)$$

Using a correction factor can get a more representative slip required for the full platform to climb the slope. For example, for the Dia/D ratio of 6 the calculated FS of 1.95 reduced the slip error of the prediction to 0.02 for the slope inclination of 12.5 degrees. Table 4.20 shows the improvements achieved by using the FS.

Table 4.20: Slip Error for Grouser Wheel 64 mm after Adding a Correction Factor

FS = 1.94			
Slope <sup>o</sup>	SWT Predicted Slip	Corrected by FS	FRT Slip
10	17.5	34.1	39.6
12.5	30.0	58.5	60.0
15	42.0	81.9	80.7

## 4.6 Single Wheel Experiments on Sloped Terrain

To investigate the large difference in predictions seen in Section 4.4.4, single wheel experiments on sloped terrain were completed and compared to flat ground data. The wheel was tested utilizing GSL conditions on sloped terrain (15 degrees) under 4 different slip ratios: 0.05, 0.2, 0.4, 0.6 and these results were compared to flat ground experiments collected previously. Two trials were conducted for each different slip ratio. The vertical loading was 149N, 88N and 210N which corresponded to the 1/4 and distributed vertical load distributions covered in Section 4.4.

### 4.6.1 Data Collection on Sloped Terrain

The SWTB available at Concordia University is mounted on a hydraulic tilt-bed, giving it the rare ability to be inclined to a desired slope after soil preparation, as shown in Figure 4.19. Certain adjustments are needed to ensure accurate data collection by the force sensor on sloped terrain. When the test bed is inclined, it induces forces due to gravity that affect the readings. These forces come primarily from the wheel weight and mechanical setup (4-bar mechanism). To account for these forces, once the test bed is inclined, the wheel is lifted from the soil to isolate the forces that occur on the incline due to the setup's weight. These forces act in the x direction parallel to the soil. The force-torque sensor is then zeroed at this instant and the wheel is lowered back into the soil after. Excluding noise, only the force in the y-axis direction is present during the test's initial conditions. This ensures consistency between flat and sloped terrain data collection and allows for a direct one-to-one comparison.

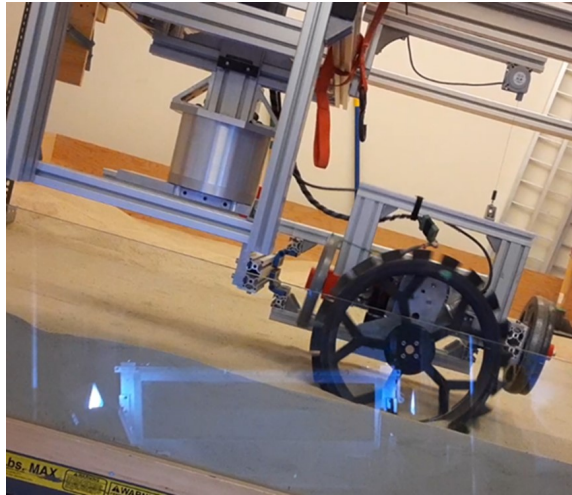


Figure 4.19: Single Wheel Experiments on Incline Terrain

#### 4.6.2 Results: Drawbar Pull Coefficient

The drawbar pull coefficient described in Section 3.3.2 describes the tractive performance of a wheel and informs its likely slope climbing performance. Figure 4.20 shows the  $DB.P_{coeff}$  increases as slip values increase. The main contribution covered in this section is the comparison between single-wheel test data on flat ground and on a 15-degree slope. All other test variables are kept constant to isolate and focus on the change from flat to sloped terrain. The results in Fig. 4.20 show data gathered using the SWTB in this experimental campaign. The experimental data from inclined terrain is compared with previously collected flat ground data for the same wheel and vertical loading. The  $DB.P_{coeff}$  decreased by between 6% to 27% for sloped terrain compared to flat terrain. The exact DB.P, the percentage and absolute differences between flat and sloped terrain are shown in Tables 4.21, 4.22 and 4.23.

Table 4.21: Single Wheel Test Data for Flat and Slope Terrain for 88N Vertical Load

Slip Ratio	0.05	0.2	0.4	0.6
Flat terrain DP Coeff	0.202	0.247	0.325	0.381
Sloped terrain DP Coeff	0.166	0.231	0.294	0.355
Decrease sloped to flat (%)	18	6	10	7
Absolute difference	0.035	0.016	0.031	0.026

The absolute difference between the  $DB.P_{coeff}$  ranged from 0.016 to 0.045. This difference

Table 4.22: Single Wheel Test Data for Flat and Slope Terrain for 149N Vertical Load

Slip Ratio	0.05	0.2	0.4	0.6
Flat terrain DP Coeff	0.131	0.197	0.260	0.332
Sloped terrain DP Coeff	0.105	0.175	0.221	0.288
Decrease sloped to flat (%)	20	11	15	13
Absolute difference	0.026	0.022	0.039	0.044

Table 4.23: Single Wheel Test Data for Flat and Slope Terrain for 210N Vertical Load

Slip Ratio	0.05	0.2	0.4	0.6	0.70	0.75	0.8
Flat terrain DP Coeff	0.117	0.167	0.218	0.298	0.323	0.342	0.385
Sloped terrain DP Coeff	0.085	0.122	0.198	0.239	0.255	0.291	0.323
Difference sloped to flat (%)	27	27	9	20	21	15	16
Absolute difference	0.032	0.045	0.021	0.059	0.068	0.051	0.062

showcased a clear decrease in performance between these two operating conditions. This showcased that a wheel's ability to generate DB.P decreases when operating on sloped terrain by a non-negligible amount. This most likely is a contributing factor in why there was such a high error between single wheel flat ground predictions and actual full rover slope performance.

### 4.6.3 Sinkage

Sinkage results are shown in Fig. 4.21, as expected sinkage increases as the slip rises. The difference between sinkage on flat and sloped terrain was small. This difference was seen more clearly at lower slips with 13% to 22% higher sinkage on sloped terrain for slips between 0.05 and 0.4. However, at 0.6 there was almost no difference between the sinkage. Moreover, when reviewing the sinkage for all the vertical loading it was observed that there is little difference between 149N and 210N. This can suggest that for this wheel, sinkage increases substantially between the vertical load of 88N and 149N but then hits a saturation area where no additional sinkage occurs with increasing the vertical load. This saturation could be due to specific soil density of the soil and the constant angular velocity of the wheel.

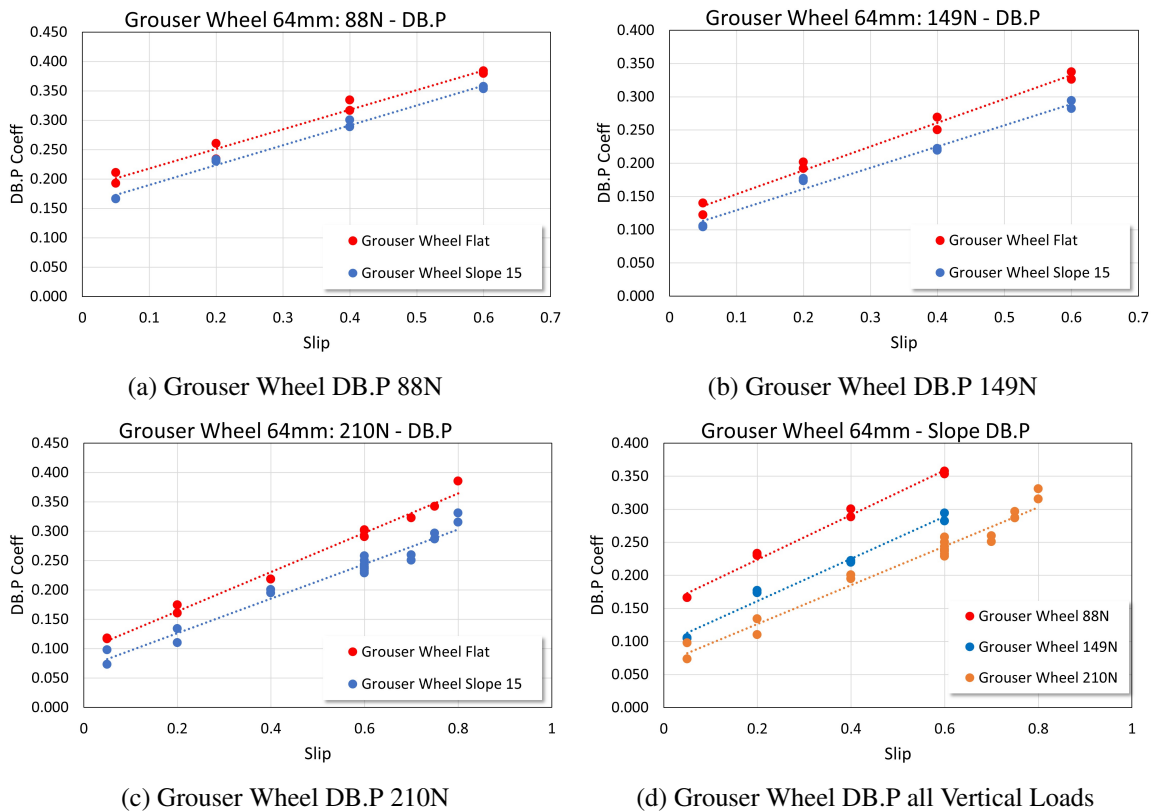


Figure 4.20: Comparing Force Generated by Grouser Wheel on Flat and Slope Terrain

## 4.7 Soil Imaging Comparison between Flat and Sloped Terrain

Additional insight into the reason behind the reduction in DB.P between slope can be gained by using sub surface soil imaging. Soil imaging shows the direction and magnitude of the soil flow. By using soil imaging we can extract parameters such as the dynamic sinkage, entrance and exit angles of the wheel. These parameters play an important role in the classical terramechanic models when calculating the force a wheel generates.

By performing experiments on terrain inclined at different angles we aim to see if there parameters change substantially. If a clear pattern between slope inclination and the parameters emerges, these parameters can be used in terramechanic models to calculate the force this wheel should generate. Further validation can be done by comparing these forces to the actual force generated by the wheel during the experiment.

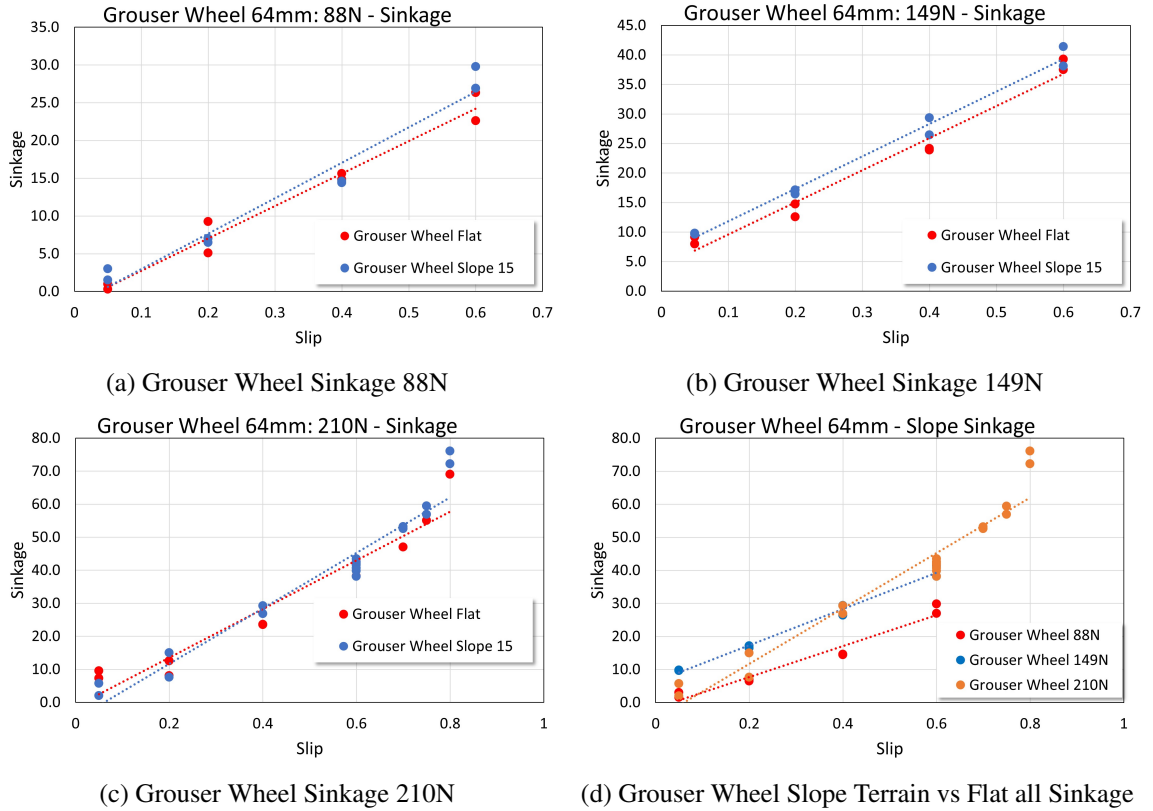


Figure 4.21: Comparing Grouser Wheel Sinkage on Slope Terrain

#### 4.7.1 Drawbar Pull Equations

To determine the traveling performance two main forces are used, the drawbar pull and vertical load. Numerical simulations are done to calculate these forces which are then evaluated against experimental results. The terramechanics model shown in Fig. 4.22, shows the stresses and other critical parameters present in calculating the drawbar pull. To calculate the DB.P, terramechanics models use the normal and shear stresses underneath the wheel as it rotates. The numerical value of DB.P ( $F_x$ ) is calculated based on integrating the normal and shear stresses from entry angle  $\theta_1$  to exit angle  $\theta_2$  as shown below:

$$F_x = rb \int_{\theta_1}^{\theta_2} [\tau_x(\theta) \cos\theta - \sigma(\theta) \sin(\theta)] d\theta \quad (20)$$

Similarly, the vertical force  $F_z$  is obtained using the same method as in Equation 20 where b and r are defined as the wheel width and wheel radius:

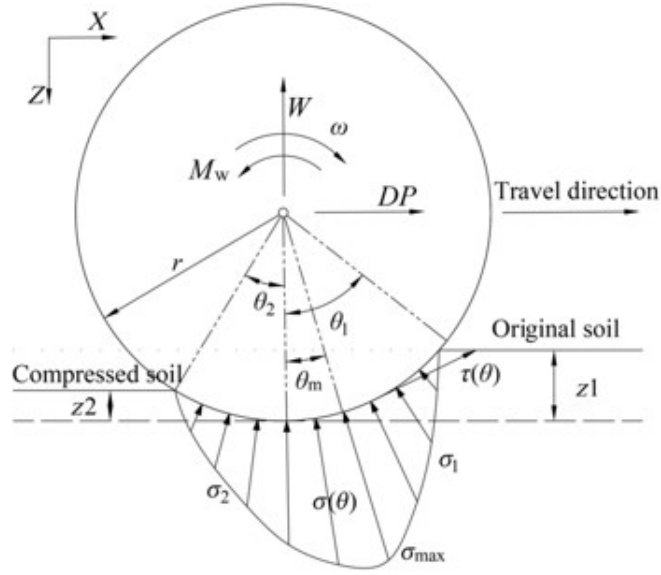


Figure 4.22: Terremechanic Model of Wheel

$$F_z = rb \int_{\theta_1}^{\theta_2} [\tau_x(\theta) \sin\theta + \sigma(\theta) \cos(\theta)] d\theta \quad (21)$$

Furthermore, the normal stress  $\sigma(\theta)$  is found in 22 given that  $\theta_m < \theta < \theta_f$ . On the other hand, if  $\theta_2 < \theta < \theta_m$  the normal stress is given by 23.

$$\sigma(\theta) = \sigma_{max} \left( \frac{\cos\theta - \cos\theta_1}{\cos\theta_m - \cos\theta_1} \right)^n \quad (22)$$

$$\sigma(\theta) = \sigma_{max} \left[ \frac{\cos\left[\theta_1 - \frac{\theta - \theta_2}{\theta_m - \theta_2} (\theta_1 - \theta_m)\right] - \cos\theta_1}{\cos\theta_m - \cos\theta_1} \right]^n \quad (23)$$

Where  $\theta_m$  specifies the wheel angle at which the normal stress is maximized. The maximum stress angle depends on the entrance angle and two tuning parameters  $c_1$  and  $c_2$  and is shown in Equation 24. Where  $i$  represents the wheel slip.

$$\theta_M = (c_1 + c_2 i) \theta_1 \quad (24)$$

With the use of soil imaging, the entrance and exit angles can be found. The entrance angle is directly related to the parameters  $c_1$  and  $c_2$ . The primary interest is to observe if the entrance

and exit angles will substantially change as the slope inclination increases. If there is a noticeable change in the entrance angle then this can be a possible explanation for the decrease of the draw-bar pull on slope terrain. Furthermore, if the entrance angle can be directly related to the slope angle, terramechanic models that calculate forces on slope terrain can be expanded to consider this relationship.

#### 4.7.2 Soil Imaging Experiments

Novel single wheel soil imaging experiments were performed on sloped terrain using a SWTB. These types of experiments can be used to understand the difference in soil wheel interactions as the slope inclination changes. Table 4.24 shows the slope inclination and the slip ratio at which the experiments were completed.

Table 4.24: Single Wheel Test Completed for Soil Imaging Experiments

Wheel Type	Slip Ratio at each Inclination	Slope Inclinations ( $^{\circ}$ )	Vertical Loads Tested
Bare Wheel	5, 20, 40, 60	Flat, 5, 10, 15	210N and 88N

By applying the SOFT technique described in Section 3.3.3 the vectors estimating the horizontal and vertical soil velocity were obtained at every pixel. The average of the vectors was taken for the entire duration that the wheel was in the steady state region. This region was found by reviewing the sinkage and force data recorded during the experiments.

To quantitatively evaluate if soil behavior at the same slip changes as the slope inclination increases we can look at the region where the soil flow shift from clock-wise to counter clock-wise. To determine this location the vectors must be converted from the Cartesian coordinates to Polar coordinates. This conversion requires the location of the wheels center. After using SOFT techniques the output is a greyscale image to which we can apply image processing to determine the boundary of the wheel as shown in Fig. 4.23. Once the edge of the wheel is found, the Hough transform is applied to find the center of the wheel.

Once the center of the circle is found as shown in Fig. 4.24, the coordinates are used to compute the vectors in the polar coordinate frame.

Equations 25 and 26 in combination with Fig. 4.25 show the method for calculating the polar

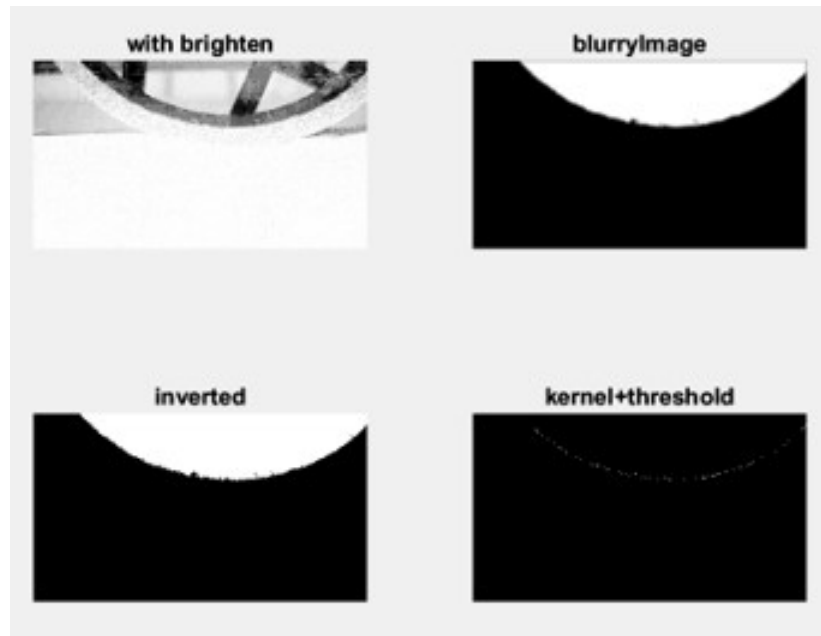


Figure 4.23: Image Processing Applied to GreyScale Image

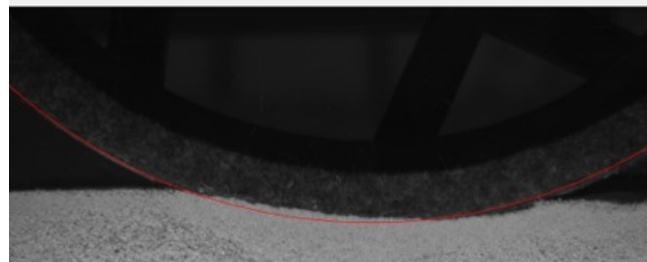


Figure 4.24: Wheel Rim Found After Application of Hough Transform

vectors given the  $U$  and  $V$  vectors at each pixel.

$$t_1 = U \cos(\psi) \quad (25a)$$

$$r_1 = U \sin(\psi) \quad (25b)$$

$$t_2 = V \sin(\psi) \quad (25c)$$

$$r_2 = V \cos(\psi) \quad (25d)$$

$$theta = V \sin(\psi) + U \cos(\psi) \quad (26a)$$

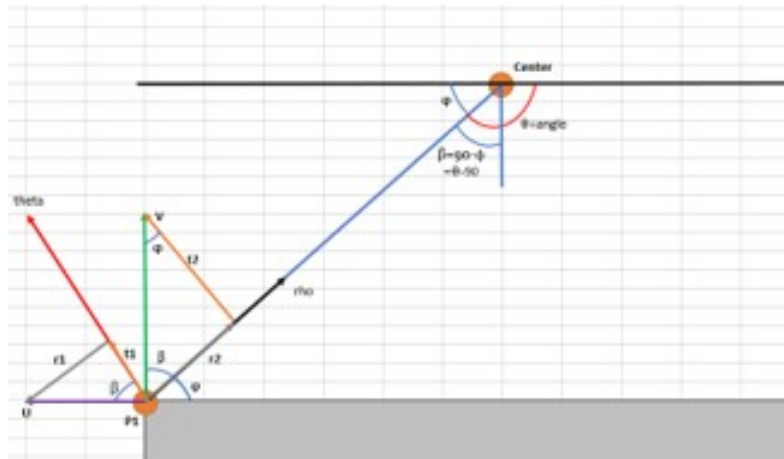


Figure 4.25: Wheel Rim Found After Application of Hough Transform

$$rho = -1 * V \cos(\psi) + U \sin(\psi) \quad (26b)$$

The result shows a vector field containing vectors theta and rho. We can plot the magnitude of the vector field to then evaluate where the flow switches from CW to CCW as shown in Fig. 4.26.

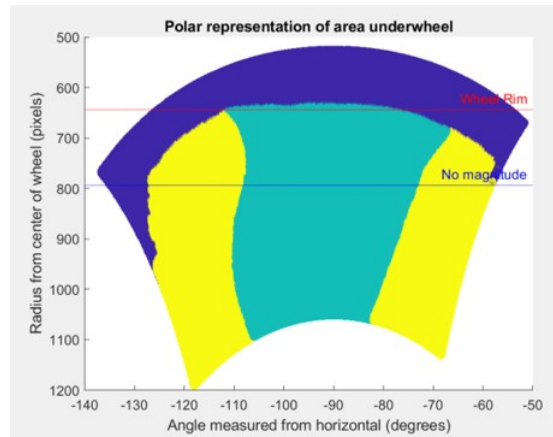


Figure 4.26: Magnitude plot of theta vector with blue representing CCW motion and yellow CW motion

### 4.7.3 Soil Imaging Results

The SOFT algorithm provides Matlab vector plots which can be displayed graphically to indicate the magnitude and direction. In our case this does not provide sufficient data for analysis and the difference between different slope inclinations is hard to see. Fig. 4.27 shows Flat and Slope 15

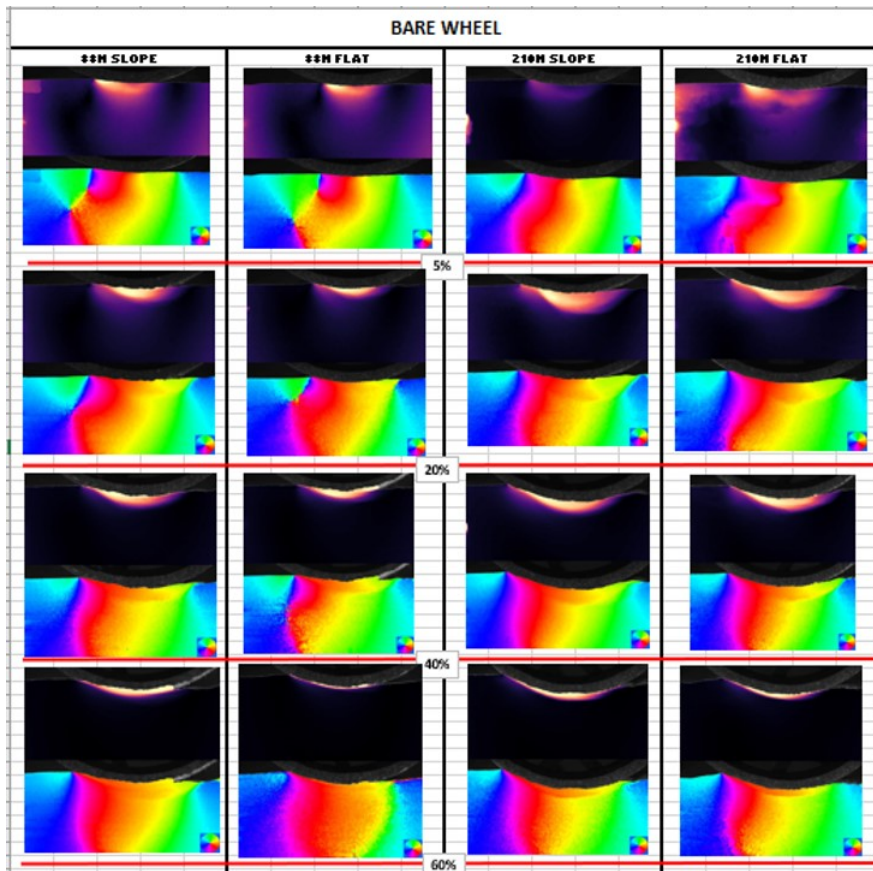


Figure 4.27: Magnitude and Direction Plots for wheel movement from right to left

degree magnitude and direction, however purely from this visualization the difference is not easily seen. After using the transformation described in Section 4.7.2 we can accurately evaluate the location where the soil flow switches direction. Results for all experiments performed in this Section are shown in Table 4.25.

Table 4.25: Single Wheel Test Results, Location in Angle of Flow Switch for 210N

Slip	Flat	Slope 5°	Slope 10°	Slope 15°
Slip 5	-110	-112	-113	-112
Slip 20	-117	-118	-117	-117
Slip 40	-122	-123	-123	-123
Slip 60	-124	-125	-126	-126

After reviewing the results, it was shown that changing the slope inclination did not influence the angle where the flow switched. Furthermore, the variable with the highest effect on flow angle

was wheel sinkage, which was directly associated with wheel slip.

Table 4.26: Single Wheel Test Results, Location in Angle of Flow Switch for 88N

Slip	Flat	Slope 5°	Slope 10°	Slope 15°
Slip 5	-108	-109	-107	-108
Slip 20	-111	-112	-110	-111
Slip 40	-116	-115	-115	-116
Slip 60	-116	-117	-118	-120

## **Chapter 5**

# **Conclusions and Future Work**

Single wheel experiments were completed to evaluate different grouser designs against possible tractive requirements for lunar rovers. Different grousers were compared in their ability to perform important micro-rover maneuvers such as point turns and slope climbing. Simple approximation methods were paired with single wheel data to predict the abilities of a full rover platform. The experiments were done utilizing Equal Load and Granular Scaling Law approximations to ensure the results would be representative of possible lunar operating conditions. These two approximations methods gave the upper and lower bounds of the wheel's mobility, respectively. In addition to GSL, a lunar soil simulant (GRC-1) was used during experiments to find the wheel's tractive properties. The evaluation criteria for single wheel experiments consisted of drawbar pull, sinkage and tangent turning force. For the prediction methods, the accuracy was evaluated using absolute and relative slip differences between the experimental and predicted values.

### **5.1 Advantages of Slanted Grousers over V-offset Grousers for Slope Climbing and Point Turns**

The tractive properties of Slanted and V-offset grousers were experimentally evaluated to determine which grouser would be superior for point turn maneuvers, slope climbing, and other possible tractive requirements for lunar rovers. Each grouser was evaluated using drawbar pull, sinkage and tangent turning force.

Single wheel experiments showed that Slanted grousers were superior in the tangent turning force metric. To achieve a point turn, the tangent turning force must be positive, therefore the grouser design which achieves this at a lower slip is better. As seen in Section 4.1.4, the Slanted grouser wheel generated positive  $F_{TTF}$  at a slip of 0.35 under the conservative GSL conditions, compared to the V-Offset grouser which required a value of 0.6, almost twice the slip to generate a positive  $F_{TTF}$  under the same conservative GSL conditions. The Slanted grouser wheel had lower drawbar pull at low slip values, but had a greater rate of increase as slip increased.

Sinkage data also showed the advantage of Slanted grousers during single wheel experiments. For point turn single wheel experiments the Slanted grouser showed substantially lower sinkage, with the difference ranging between 5 to 20 millimeters.

The Slanted grouser could be superior due to the larger surface of the grouser having perpendicular contact with the soil during turns. Moreover, the Slanted grouser had a lower sinkage during single wheel angle tests which results in a lower lateral resistance force. While a reduction in sinkage can lead to a lower drawbar pull, the decrease in lateral resistive forces appears to be the dominant factor.

Straight-line experiments using the representative approximation method GSL, had nearly identical drawbar pull for both grousers as shown in Section 4.1. In equal load conditions, the Slanted grousers generated slightly more drawbar pull during straight-line tests. The difference in drawbar pull was at slip ratios of 0.2 and 0.4 in equal load conditions, with the Slanted wheel generating up to 20% more. In straight-line driving the difference in sinkage between the designs was minimal, which aligns with the small difference in drawbar pull.

The grouser design, angle and orientation shows a large effect on point turns and a lower effect on straight-line driving and slope climbing, with the Slanted grouser showing an overall better performance.

## **5.2 Predicting Full Rover Point Turns using Single Wheel Experiments**

Full rover experimental data was consistent with and thus validated the results obtained from single wheel testing for point turn maneuvers. During full rover point turns, the slip values varied

between 0.25 to 0.4. This was similar to the predicted slip value of 0.35 obtained from single wheel experiments under GSL test conditions. This shows that using GSL approximations, single wheel tests can be a good estimate for the performance of the full rover platform in point turns.

### **5.2.1 Estimating Point Turn Performance**

1. To predict the slip full a platform requires for a point turn, single wheel test beds with a 4-bar mechanism to ensure constant vertical load are recommended. To simulate the point turn, the entire 4-bar mechanism should be rotated to correspond to the desired point turn angle  $\alpha$ .

2. Force data from SWTB experiments are used to compute the Tangent Turning Force and at each of the set slip ratios. The slip predicted from SWTB was experimentally shown to be very similar when compared to validation experiments using a full rover platform as shown in Chapter 4, section 4.2.

3. Sinkage, on the other hand, was not accurately predicted from SWTB data. Even after correcting for GSL scaling, the sinkage of the full rover platform was around 2 times more than the predicted values. Given this error, a 2.5 correction factor could be applied to any prediction that include sinkage values to ensure the results are more accurate and conservative. The results presented in Chapter 4 sub section 4.2.1 provide starting points for this correction factor.

## **5.3 Predicting Full Rover Slope Climbing using Single Wheel Experiments**

The following subsections summarize the results and remaining challenges for predicting rover slope climbing.

### **5.3.1 Single Wheel Experiments on Flat Versus Slope Terrain**

Single wheel experiments on flat terrain were completed with three different vertical loads: 88N, 149N, and 210N. Flat terrain results were compared to the equivalent experiments on terrain inclined at a 15 degree angle. The primary interest is determining if any non-negligible change in drawbar pull occurs. Experimental results in Section 4.6 show that drawbar pull drops by 6 to 27

% when transitioning to sloped terrain. Similarly, the sinkage on sloped terrain was also slightly higher, with the difference ranging between 0 to 22%. Furthermore, sinkage saw a large increase between 88N to 149N loadings. However, between 149N and 210N sinkage saw very little change. The difference between slope and flat terrain for single wheel experiments was found to be non-negligible. This difference can influence slope climbing estimations from flat terrain data if not properly accounted for.

### **5.3.2 Evaluating Slope Climbing Ability using Single Wheel Experiments**

Single wheel experiments were done to get an initial estimate of the wheel's slope climbing abilities. Results were used in the prediction model to estimate the slope climbing ability of a full rover platform with similar properties. The predictions indicated that a full rover platform should climb a slope of 15 degrees at slip of around 0.3 as shown in Section 4.3.1. These predictions substantially underestimated the required slip required for the full rover platform, with the actual slip to climb a slope of 15 degrees being around 0.8. This indicated that using purely DB.P is not sufficient for all cases when comparing traversal single wheel tests on flat and full rover tests sloped on terrain.

### **5.3.3 Influence of Vertical Load Distribution Methods on Slope Climbing Predictions**

Two different vertical load techniques were investigated to see their impact on slope climbing predictions. The vertical loading methods used were based on 1/4 or front and rear weight distribution for a rover platform inclined on a slope of 15 degrees. When using the DB.P data collected from each method to predict slope climbing performance, the difference in slip predictions between the two methods was small ranging between 1 and 6 % as described in Section 4.4.4. This value was less than the variance of drawbar pull in single wheel experiments. Therefore, for the experimental conditions tested there is no substantial difference between the two vertical load methods for slope climbing predictions. Furthermore, this supports the claims made by (Senatore & Iagnemma, 2014) that vertical wheel load distribution does not have a large influence on slope climbing estimations. So estimations for full rover slope climbing abilities can be made with 1/4 vertical weight

distribution without large accuracy loss.

### 5.3.4 Soil Imaging

Single Wheel soil imaging experiments were completed for flat and terrain inclined at 5, 10 and 15 degrees. The tests were done to observe if the location of maximum stress underneath the wheel is influenced by slope inclination. To evaluate the collected data, the experiments were paired with the analysis technique SOFT as described in Section 4.7. The analysis showed that with the current experimental data and using the described analysis no observable pattern emerges. The stress profile underneath the wheel may be influenced by slope, but would require more precise experiments and further analysis to uncover.

### 5.3.5 Estimating Slope Climbing Performance

1. Slope climbing predictions can be completed using single wheel test data on flat terrain, though with caution. Experiments have shown that using 1/4 vertical loads or distributed vertical loads has little influence on prediction error and the predicted slip for the full rover platform to climb the slope. This is shown in Section 4.4.

2. Force data is gathered from SWTB generated by the wheel at every slip. The drawbar pull should be normalized by vertical load giving the drawbar pull coefficient  $DB.P_{coeff}$ . Furthermore, using the single gravity approximation model (Sutoh et al., 2011) we can find the drawbar pull coefficient required to climb an inclined slope. Then single wheel experimental data paired with a simple gravity equilibrium model is used to provide an initial approximation of the slip required for the full rover platform to climb a slope inclined at the desired angle as shown in Section 3.3.2.

3. The slip predicted using this method can be substantially lower than the actual slip required to climb the slope based on experimental results in Section 4.3.1 and Section 4.4. A possible method to correct for this error is to evaluate the diameter to width ratio (Dia/D) of the wheel. Then, based on this ratio, to apply the correction factor to the slip predicted using SWTB. The suggested values for wheels similar to those used in this thesis are shown in Section 4.5.2. This correction should make the predicted slip for the full rover platform to climb the slope more accurate and more conservative.

## 5.4 Diameter and Width Experiments and Influence on Slope Climbing Predictions

The diameter over width value was shown to be related to the slope climbing prediction error. To isolate the influence of diameter/width ratio (Dia/D) wheels were tested with a ratio of 3 and 6, while the rest of the variables were kept constant. The wheels were tested using GSL approximation and the 1/4 vertical loading method. This resulted in four datasets, which after analysis showed that a larger ratio was correlated with a higher prediction error. The error increased by at least 10% when changing the ratio from 3 to 6. Moreover, this result was statistically significant, which was proven using a T-Test as shown in Section 4.5.1.

To increase prediction accuracy a correction factor based on the collected data could be applied. Given that only two data points are available the nature of the relationship (e.g. linear vs nonlinear) between diameter/width ratio and prediction error cannot be determined. However, for the experimental conditions and wheel type in this thesis a linear correction be used as a basis for determining the required correction factor as shown in Section 4.5.2. For a diameter/width ratio of 6, we can calculate the correction factor to be 1.95. By applying the correction factor calculated from the relative error, the prediction error from single wheel data can be substantially reduced. As seen in Table 4.20 the correction factor reduced the slip error to values within 0.05 slip instead of previously having around 2 times slip error.

## 5.5 Sources of Error and Limitations

The experiments performed on this thesis were done in a 1-g environment using SWTB, GSL approximations and GRC-1 lunar regolith simulant. The conclusions made are based on these conditions and might be influenced if experimental conditions or different gravity approximations are used.

Sources of error in the experiments include noise in sensor readings and variance in soil preparation. Sensor noise magnitude should be low enough to not have substantial influence on the conclusions drawn from experiments given the specific sensor used. The soil preparation of the test

area was done manually, therefore there is a some variance in soil compaction levels. This influences individual runs due to a variance of the soil compaction on the wheel path, as well as across multiple runs. The cone penetrometer index gradient (G) for each run was recorded and experiments were completed only if the values across the whole test region ranged from 3.8 to 4.3.

## **5.6 Future Work**

Experiments and research completed in this thesis have shown the need for additional investigation in the following avenues:

1. Experiments and theory to investigate the disparity between sinkage prediction and full rover experiments in point turns. Further work is required to validate if the sinkage error between SWTB predictions and FRT is consistent across different wheel types and experimental conditions. Once a pattern is found this can expand the current predictions by including sinkage.

2. The current relationship between diameter to width ratio and prediction error is based on a sample of four different rigid wheels. Further experiments and research could be useful to validate this relationship across a wider scope of wheel designs and grouser shapes. Introducing more data points validates the proposed relationship and increases its usefulness.

3. Experiments to expand the relationship between sinkage predicted from SWTB data and the actual sinkage observed during full rover slope tests.

# References

- Adamczyk, A., & Rimai, L. (1988). 2-dimensional particle tracking velocimetry (ptv): technique and image processing algorithms. *Experiments in fluids*, 6(6), 373–380.
- Arvidson, R. E., Bell III, J. F., Bellutta, P., Cabrol, N. A., Catalano, J. G., Cohen, J., ... Yen, A. S. (2010). Spirit mars rover mission: Overview and selected results from the northern home plate winter haven to the side of scamander crater. *Journal of Geophysical Research: Planets*, 115(E7). Retrieved from <https://agupubs.onlinelibrary.wiley.com/doi/abs/10.1029/2010JE003633> doi: <https://doi.org/10.1029/2010JE003633>
- Azimi, A., Kövecses, J., & Angeles, J. (2013). Wheel–soil interaction model for rover simulation and analysis using elastoplasticity theory. *IEEE Transactions on robotics*, 29(5), 1271–1288.
- Bauer, R., Leung, W., & Barfoot, T. (2005). Experimental and simulation results of wheel-soil interaction for planetary rovers. In *2005 iee/rsj international conference on intelligent robots and systems* (pp. 586–591).
- Bekker, M. G. (1956). Theory of land locomotion: the mechanics of vehicle mobility. (*No Title*).
- Bekker, M. G. (1969). *Introduction to terrain-vehicle systems*. MICHIGAN UNIV ANN ARBOR. Retrieved from <https://api.semanticscholar.org/CorpusID:131292053>
- Clark Jr, J. M., Simon, H., & Roma, C. (1965). Correlation of prototype and scale model vehicle performance in clay soils. *SAE Transactions*, 272–294.
- Costes, N. C., Farmer, J. E., & George, E. B. (1972). Mobility performance of the lunar roving vehicle: Terrestrial studies: Apollo 15 results. In *Nasa technical report ; r-401*. Retrieved from <https://searchworks.stanford.edu/view/8724076>
- Cowen, E., Monismith, S., Cowen, E., & Monismith, S. (1997). A hybrid digital particle tracking

- velocimetry technique. *Experiments in fluids*, 22(3), 199–211.
- Daca, A., Nassiraei, A. A. F., Tremblay, D., & Skonieczny, K. (2022). Comparison of wheel load application methods in single-wheel testbeds. *Journal of Terramechanics*. Retrieved from <https://api.semanticscholar.org/CorpusID:244687031>
- Daca, A., & Skonieczny, K. (2022a, 06). Evaluating 1-g testing methods for predicting planetary rover mobility in reduced gravity. In *16th symposium on advanced space technologies in robotics and automation (astra) 2022*.
- Daca, A., & Skonieczny, K. (2022b, 04). Experimentally evaluating granular scaling laws for predicting lunar-gravity wheel performance in cohesive regolith. In *Earth and space 2022*. doi: 10.1061/9780784484470.004
- Daca, A., Tremblay, D., & Skonieczny, K. (2022). Experimental evaluation of cone index gradient as a metric for the prediction of wheel performance in reduced gravity. *Journal of Terramechanics*, 99, 1-16. Retrieved from <https://www.sciencedirect.com/science/article/pii/S0022489821000720> doi: <https://doi.org/10.1016/j.jterra.2021.09.003>
- de Vaucorbeil, A., Nguyen, V. P., Sinaie, S., & Wu, J. Y. (2020). Chapter two - material point method after 25 years: Theory, implementation, and applications. In S. P. Bordas & D. S. Balint (Eds.), (Vol. 53, p. 185-398). Elsevier. Retrieved from <https://www.sciencedirect.com/science/article/pii/S0065215619300146> doi: <https://doi.org/10.1016/bs.aams.2019.11.001>
- Deng, Z., Gao, H., Tao, J., Iagnemma, K., & Liu, G. (2014, 08). Interaction mechanics model for rigid driving wheels of planetary rovers moving on sandy terrain with consideration of multiple physical effects. *Journal of Field Robotics*, 32. doi: 10.1002/rob.21533
- Ding, L., Gao, H., Deng, Z., Nagatani, K., & Yoshida, K. (2011). Experimental study and analysis on driving wheels' performance for planetary exploration rovers moving in deformable soil. *Journal of Terramechanics*, 48(1), 27-45. Retrieved from <https://www.sciencedirect.com/science/article/pii/S0022489810000601> doi: <https://doi.org/10.1016/j.jterra.2010.08.001>
- Ding, L., Yang, H., Gao, H., Li, N., Deng, Z., Guo, J., & Li, N. (2017). Terramechanics-based

- modeling of sinkage and moment for in-situ steering wheels of mobile robots on deformable terrain. *Mechanism and Machine Theory*, 116, 14-33. Retrieved from <https://www.sciencedirect.com/science/article/pii/S0094114X16302968> doi: <https://doi.org/10.1016/j.mechmachtheory.2017.05.011>
- Effati, M., Fiset, J.-S., & Skonieczny, K. (2020). Considering slip-track for energy-efficient paths of skid-steer rovers. *Journal of Intelligent & Robotic Systems*, 100, 335–348.
- El-Sayegh, Z., El-Gindy, M., Johansson, I., & Öijer, F. (2018). Off-road soft terrain modeling using smoothed particle hydrodynamics technique. In *International design engineering technical conferences and computers and information in engineering conference* (Vol. 51784, p. V003T01A030).
- Fiset, J.-S., Effati, M., & Skonieczny, K. (2023). Power and energy consumption of skid-steer rovers turning on loose soil. *Journal of Field Robotics*, 40(2), 193–214.
- Flippo, D., Heller, R., & Miller, D. (2009, 01). Turning efficiency prediction for skid steer robots using single wheel testing. In (p. 479-488). doi: 10.1007/978-3-642-13408-1\_43
- Flippo, D., & Miller, D. (2014). Turning efficiency prediction for skid steering via single wheel testing. *Journal of Terramechanics*, 52, 23-29. Retrieved from <https://www.sciencedirect.com/science/article/pii/S0022489814000020> doi: <https://doi.org/10.1016/j.jterra.2014.02.001>
- Freitag, D. R., Green, A. J., & Melzer, K.-J. (1970). *Performance evaluation of wheel for lunar vehicles*. (Tech. Rep.). Huntsville, AL: Marshall Space Flight Center. National Aeronautics and Space Administration.
- Freitag, D. R., & Knight, S. J. (1964). A technique for estimating the slope-climbing ability of wheeled vehicles in sand. *SAE Transactions*, 72, 178–185. Retrieved 2024-11-17, from <http://www.jstor.org/stable/44562942>
- Gachet, P., Klubertanz, G., Vulliet, L., & Laloui, L. (2003). Interfacial behavior of unsaturated soil with small-scale models and use of image processing techniques. *Geotechnical Testing Journal*, 26(1), 12–21.
- Gao, H., Guo, J., Ding, L., Li, N., Liu, Z., Liu, G., & Deng, Z. (2013). Longitudinal skid

- model for wheels of planetary exploration rovers based on terramechanics. *Journal of Terramechanics*, 50(5), 327-343. Retrieved from <https://www.sciencedirect.com/science/article/pii/S0022489813000773> doi: <https://doi.org/10.1016/j.jterra.2013.10.001>
- Gheshlaghi, F., & Mardani, A. (2021). Prediction of soil vertical stress under off-road tire using smoothed-particle hydrodynamics. *Journal of Terramechanics*, 95, 7–14.
- Ghotbi, B., González, F., Kövecses, J., & Angeles, J. (2016). Mobility evaluation of wheeled robots on soft terrain: Effect of internal force distribution. *Mechanism and Machine Theory*, 100, 259–282.
- Ghotbi, B., Kovács, L., González, F., Niksirat, P., Skonieczny, K., & Kövecses, J. (2018). Including the effect of gravity in wheel/terrain interaction models. In *Proceedings of the in proceedings of the 14th international symposium on artificial intelligence, robotics and automation in space (i-sairas)*.
- Gnanamanickam, E. P., Lee, S., Sullivan, J. P., & Chandrasekar, S. (2009). Direct measurement of large-strain deformation fields by particle tracking. *Measurement science and technology*, 20(9), 095710.
- Harvey, B. (2007, 01). Soviet and russian lunar exploration. *Soviet and Russian Lunar Exploration*, by B. Harvey. Berlin: Springer, 2007. ISBN 978-0-387-21896-0.
- He, C., Zeng, X., & Wilkinson, A. (2013, 07). Geotechnical properties of grc-3 lunar simulant. *Journal of Aerospace Engineering*, 26, 528-534. doi: 10.1061/(ASCE)AS.1943-5525.0000162
- Iizuka, K., Kunii, Y., & Kubota, T. (2008). Study on wheeled forms of lunar robots considering elastic characteristic for traversing soft terrain (effect of elastic wheel considering in interaction between wheel and soft soil). *Nihon Kikai Gakkai Ronbunshu, C Hen/Transactions of the Japan Society of Mechanical Engineers, Part C*, 74(12), 2962–2967.
- Iizuka, K., Sato, Y., Kuroda, Y., & Kubota, T. (2006a). Experimental study of wheeled forms for lunar rover on slope terrain. In *9th ieee international workshop on advanced motion control, 2006*. (p. 266-271). doi: 10.1109/AMC.2006.1631669
- Iizuka, K., Sato, Y., Kuroda, Y., & Kubota, T. (2006b). Study on wheel of exploration robot on sandy terrain. In *2006 ieee/rsj international conference on intelligent robots and systems*

(p. 4272-4277). doi: 10.1109/IROS.2006.281956

- Iizuka, K., Yoshida, T., & Kubota, T. (2011). Effect of tractive given by grousers mounted on wheels for lunar rovers on loose soil. *IECON 2011 - 37th Annual Conference of the IEEE Industrial Electronics Society*, 110-115. Retrieved from <https://api.semanticscholar.org/CorpusID:35780523>
- Inotsume, H., Moreland, S., Skonieczny, K., & Wettergreen, D. (2019). Parametric study and design guidelines for rigid wheels for planetary rovers. *Journal of Terramechanics*, 85, 39-57. Retrieved from <https://www.sciencedirect.com/science/article/pii/S0022489818301368> doi: <https://doi.org/10.1016/j.jterra.2019.06.002>
- Irani, R. A., Bauer, R. J., & Warkentin, A. (2011a). A dynamic terramechanic model for small lightweight vehicles with rigid wheels and grousers operating in sandy soil. *Journal of Terramechanics*, 48, 307-318. Retrieved from <https://api.semanticscholar.org/CorpusID:110975852>
- Irani, R. A., Bauer, R. J., & Warkentin, A. (2011b). A dynamic terramechanic model for small lightweight vehicles with rigid wheels and grousers operating in sandy soil. *Journal of Terramechanics*, 48, 307-318. Retrieved from <https://api.semanticscholar.org/CorpusID:110975852>
- Ishigami, G., Miwa, A., Nagatani, K., & Yoshida, K. (2006, 01). Terramechanics-based analysis on slope traversability for a planetary exploration rover. *Proceedings of the International Symposium on Space Technology and Science*.
- Ishigami, G., Miwa, A., Nagatani, K., & Yoshida, K. (2007). Terramechanics-based model for steering maneuver of planetary exploration rovers on loose soil. *Journal of Field Robotics*, 24(3), 233-250. Retrieved from <https://onlinelibrary.wiley.com/doi/abs/10.1002/rob.20187> doi: <https://doi.org/10.1002/rob.20187>
- Jasoliya, D., Untaroiu, A., & Untaroiu, C. (2024). A review of soil modeling for numerical simulations of soil-tire/agricultural tools interaction. *Journal of Terramechanics*, 111, 41-64. Retrieved from <https://www.sciencedirect.com/science/article/pii/S002248982300085X> doi: <https://doi.org/10.1016/j.jterra.2023.09.003>
- Johnson, J. B., Kulchitsky, A. V., Duvoy, P., Iagnemma, K., Senatore, C., Arvidson, R. E., &

- Moore, J. (2015). Discrete element method simulations of mars exploration rover wheel performance. *Journal of Terramechanics*, 62, 31-40. Retrieved from <https://www.sciencedirect.com/science/article/pii/S0022489815000154> (Planetary Rovers and Machine-Regolith Interactions) doi: <https://doi.org/10.1016/j.jterra.2015.02.004>
- Kassel, S. (1971). *Lunokhod-1 soviet lunar surface vehicle*. Santa Monica, CA: RAND Corporation.
- Kobayashi, T., Fujiwara, Y., Yamakawa, J., Yasufuku, N., & Omine, K. (2010). Mobility performance of a rigid wheel in low gravity environments. *Journal of Terramechanics*, 47(4), 261–274.
- Kovács, L. L., Ghotbi, B., González, F., Niksirat, P., Skonieczny, K., & Kövecses, J. (2020). Effect of gravity in wheel/terrain interaction models. *Journal of Field Robotics*, 37(5), 754–767.
- Kuroda, Y., Teshima, T., Sato, Y., & Kubota, T. (2004). Mobility performance evaluation of planetary rover with similarity model experiment. In *Ieee international conference on robotics and automation, 2004. proceedings. icra '04. 2004* (Vol. 2, p. 2098-2103 Vol.2). doi: 10.1109/ROBOT.2004.1308133
- Kuroda, Y., Teshima, T., Sato, Y., & Kubota, T. (2005). Mobility performance evaluation of planetary rovers in consideration of different gravitational acceleration. In *2005 ieee/rsj international conference on intelligent robots and systems* (p. 2991-2996). doi: 10.1109/IROS.2005.1545177
- Lan, Q., Wang, Z., Ding, L., Yang, H., Gao, H., Richter, L., & Deng, Z. (2024). Dem simulation and continuation algorithm of granular physical field for planetary wheel-terrain interaction. *Powder Technology*, 433, 119197. Retrieved from <https://www.sciencedirect.com/science/article/pii/S0032591023009804> doi: <https://doi.org/10.1016/j.powtec.2023.119197>
- Lescoe, R. (2010). *Improvement of soil modeling in a tire-soil interaction using finite element analysis and smooth particle hydrodynamics* (Unpublished master's thesis). Pennsylvania State University.
- Lessem, A. S. (1972). *Operations and maintenance manual for a scale-model lunar roving vehicle*

- (Tech. Rep.). Huntsville, AL: Marshall Space Flight Center. National Aeronautics and Space Administration.
- Li, R., Zhou, G., Yan, K., Chen, J., Chen, D., Cai, S., & Mo, P.-Q. (2022). Preparation and characterization of a specialized lunar regolith simulant for use in lunar low gravity simulation. *International Journal of Mining Science and Technology*, 32(1), 1-15. Retrieved from <https://www.sciencedirect.com/science/article/pii/S2095268621001002> doi: <https://doi.org/10.1016/j.ijmst.2021.09.003>
- Liu, J., Gao, H., & Deng, Z. (2008). Effect of straight grousers parameters on motion performance of small rigid wheel on loose sand. *Information Technology Journal*, 7, 1125-1132. Retrieved from <https://api.semanticscholar.org/CorpusID:61026394>
- Lyasko, M. (2010). Lsa model for sinkage predictions. *Journal of Terramechanics*, 47(1), 1-19. Retrieved from <https://www.sciencedirect.com/science/article/pii/S0022489809000871> doi: <https://doi.org/10.1016/j.jterra.2009.06.004>
- Männel, A. (2016). *Modeling of the wheel-soil contact for planetary exploration rovers* (Unpublished doctoral dissertation). Technische Universität München.
- Meirion-Griffith, G., & Spenko, M. (2011). A modified pressure–sinkage model for small, rigid wheels on deformable terrains. *Journal of Terramechanics*, 48(2), 149-155. Retrieved from <https://www.sciencedirect.com/science/article/pii/S0022489811000024> doi: <https://doi.org/10.1016/j.jterra.2011.01.001>
- Ming, D. (1992). Lunar sourcebook. a user's guide to the moon: Edited by grant heiken, david vaniman and bevan m. french. pp. 736. cambridge university press. 1991. £50.00, us 59.50 isbn 0 521 33444 6. *Endeavour*, 16(2), 96. Retrieved from <https://www.sciencedirect.com/science/article/pii/016093279290014G> doi: [https://doi.org/10.1016/0160-9327\(92\)90014-G](https://doi.org/10.1016/0160-9327(92)90014-G)
- Moreland, S., Skonieczny, K., Inotsume, H., & Wettergreen, D. (2012). Soil behavior of wheels with grousers for planetary rovers. In *2012 IEEE Aerospace Conference* (pp. 1–8).
- Moreland, S., Skonieczny, K., Wettergreen, D., Creager, C., & Asnani, V. (2011, 01). Soil motion analysis system for examining wheel-soil shearing. *17th International Conference of the International Society for Terrain Vehicle Systems 2011, ISTVS 2011*.

- Murthy, T. G., Gnanamanickam, E. P., Saldana, C., & Chandrasekar, S. (2009). Deformation field in indentation of granular materials. In *Aip conference proceedings* (Vol. 1145, pp. 263–266).
- Nagaoka, K., Sawada, K., & Yoshida, K. (2019). Shape effects of wheel grousers on traction performance on sandy terrain. *Journal of Terramechanics*, 90, 23-30. Retrieved from <https://www.sciencedirect.com/science/article/pii/S0022489819301041> (Modeling, Visualization, and Verification in Terrain-Machine Interactions) doi: <https://doi.org/10.1016/j.jterra.2019.08.001>
- Nakashima, H., Fujii, H., Oida, A., Momozu, M., Kawase, Y., Kanamori, H., ... Yokoyama, T. (2007). Parametric analysis of lugged wheel performance for a lunar microrover by means of dem. *Journal of Terramechanics*, 44(2), 153-162. Retrieved from <https://www.sciencedirect.com/science/article/pii/S0022489806000498> doi: <https://doi.org/10.1016/j.jterra.2005.11.001>
- Nakashima, H., Yoshida, T., Wang, X., Shimizu, H., Miyasaka, J., & Ohdoi, K. (2013). On a gross traction generated at grouser for tracked agricultural vehicles. *IFAC Proceedings Volumes*, 46(4), 311-316. Retrieved from <https://www.sciencedirect.com/science/article/pii/S1474667016335625> (5th IFAC Conference on Bio-Robotics) doi: <https://doi.org/10.3182/20130327-3-JP-3017.00071>
- Nassiraei, A., & Skonieczny, K. (2020, 10). Grousers improve drawbar pull by reducing resistance and generating thrust at the front of a wheel. *Journal of Terramechanics*, 91, 73-84. doi: 10.1016/j.jterra.2020.05.005
- Niksirat, P. (2018). *Characterizing the effect of reduced gravity on rover wheel-soil interactions* (Master's thesis, Concordia University). Retrieved from <https://spectrum.library.concordia.ca/id/eprint/985320/> (In Press)
- Niksirat, P., Daca, A., & Skonieczny, K. (2020). The effects of reduced-gravity on planetary rover mobility. *The International Journal of Robotics Research*, 39(7), 797–811.
- Nuwal, A. (2022). *Evaluation of off-road uninhabited ground vehicle mobility using discrete element method and scalability investigation* (Unpublished doctoral dissertation). Cranfield University.
- Oravec, H., Zeng, X., & Asnani, V. M. (2010). Design and characterization of grc-1: A soil for lunar

- terramechanics testing in earth-ambient conditions. *Journal of Terramechanics*, 47, 361-377. Retrieved from <https://api.semanticscholar.org/CorpusID:129856595>
- Pandey, K., & Ojha, T. (1978). Effect of design parameters on the performance of rigid traction wheels on saturated soils. *Journal of Terramechanics*, 15(3), 145–156.
- Reece, A. R. (1965). Principles of soil-vehicle mechanics. *Proceedings of the Institution of Mechanical Engineers: Automobile Division*, 180(1), 45-66. Retrieved from [https://doi.org/10.1243/PIME\\_AUTO\\_1965\\_180\\_009\\_02](https://doi.org/10.1243/PIME_AUTO_1965_180_009_02) doi: 10.1243/PIME\\_AUTO\\_1965\\_180\\_009\\_02
- Sandeep, C. S., Marzulli, V., Cafaro, F., Senetakis, K., & Pöschel, T. (2019). Micromechanical behavior of dna-1a lunar regolith simulant in comparison to ottawa sand. *Journal of Geophysical Research: Solid Earth*, 124(8), 8077-8100. Retrieved from <https://agupubs.onlinelibrary.wiley.com/doi/abs/10.1029/2019JB017589> doi: <https://doi.org/10.1029/2019JB017589>
- Schäfer, B., Gibbesch, A., Krenn, R., & Rebele, B. (2010, January). Planetary rover mobility simulation on soft and uneven terrain. *Vehicle System Dynamics, International Journal of Vehicle Mechanics and Mobility*, 48(1), 149-169. doi: 10.1080/00423110903243224
- Senatore, C., & Iagnemma, K. (2014, 02). Analysis of stress distributions under lightweight wheeled vehicles. *Journal of Terramechanics*, 51, 1–17. doi: 10.1016/j.jterra.2013.10.003
- Senatore, C., Stein, N., Zhou, F., Bennett, K., Arvidson, R., Trease, B., ... Iagnemma, K. (2014). Modeling and validation of mobility characteristics of the mars science laboratory curiosity rover. In *Proc. proceedings of the 12th international symposium on artificial intelligence, robotics and automation in space (i-sairas)*.
- Skonieczny, K., Moreland, S. J., Asnani, V. M., Creager, C. M., Inotsume, H., & Wettergreen, D. S. (2014). Visualizing and analyzing machine-soil interactions using computer vision. *Journal of Field Robotics*, 31. Retrieved from <https://api.semanticscholar.org/CorpusID:18696719>
- Skonieczny, K., Moreland, S. J., & Wettergreen, D. S. (2012). A grouser spacing equation for determining appropriate geometry of planetary rover wheels. *2012 IEEE/RSJ International Conference on Intelligent Robots and Systems*, 5065-5070. Retrieved from <https://api>

[.semanticscholar.org/CorpusID:15927645](https://api.semanticscholar.org/CorpusID:15927645)

- Skonieczny, K., Niksirat, P., & Nassiraei, A. A. F. (2019). Rapid automated soil preparation for testing planetary rover-soil interactions aboard reduced-gravity aircraft. *Journal of Terramechanics*, 83, 35–44.
- Slonaker, J., Motley, D. C., Zhang, Q., Townsend, S., Senatore, C., Iagnemma, K., & Kamrin, K. (2017, Jun). Publisher's note: General scaling relations for locomotion in granular media [phys. rev. e 95, 052901 (2017)]. *Phys. Rev. E*, 95, 069902. Retrieved from <https://link.aps.org/doi/10.1103/PhysRevE.95.069902> doi: 10.1103/PhysRevE.95.069902
- Suescun-Florez, E., Roslyakov, S., Iskander, M., & Baamer, M. (2014, 07). Geotechnical properties of bp-1 lunar regolith simulant. *Journal of Aerospace Engineering*, 28, 04014124. doi: 10.1061/(ASCE)AS.1943-5525.0000462
- Sullivan, R., Anderson, R., Biesiadecki, J., Bond, T., & Stewart, H. (2011). Cohesions, friction angles, and other physical properties of martian regolith from mars exploration rover wheel trenches and wheel scuffs. *Journal of Geophysical Research: Planets*, 116(E2). Retrieved from <https://agupubs.onlinelibrary.wiley.com/doi/abs/10.1029/2010JE003625> doi: <https://doi.org/10.1029/2010JE003625>
- Sun, X., Zhang, R., Li, X., Zou, M., Wang, C., & Chen, L. (2022). Jlu-h: A novel lunar highland regolith simulant for use in large-scale engineering experiments. *Planetary and Space Science*, 221, 105562. Retrieved from <https://www.sciencedirect.com/science/article/pii/S0032063322001489> doi: <https://doi.org/10.1016/j.pss.2022.105562>
- Sutoh, M., Nagaoka, K., Nagatani, K., & Yoshida, K. (2013). Design of wheels with grousers for planetary rovers traveling over loose soil. *Journal of Terramechanics*, 50(5), 345-353. Retrieved from <https://www.sciencedirect.com/science/article/pii/S0022489813000499> doi: <https://doi.org/10.1016/j.jterra.2013.05.002>
- Sutoh, M., Yajima, R., Nagatani, K., & Yoshida, K. (2011). Traveling performance estimation for planetary rovers over slope. *2011 IEEE/SICE International Symposium on System Integration (SII)*, 884-889. Retrieved from <https://api.semanticscholar.org/CorpusID:42466717>

- Sutoh, M., Yusa, J., Ito, T., Nagatani, K., & Yoshida, K. (2012). Traveling performance evaluation of planetary rovers on loose soil. *Journal of Field Robotics*, 29. Retrieved from <https://api.semanticscholar.org/CorpusID:2885692>
- Sutoh, M., Yusa, J., Nagatani, K., & Yoshida, K. (2010). Traveling performance evaluation for planetary rovers on weak soil. *Journal of Field Robotics*, 546–551.
- Tasora, A., Mangoni, D., Negrut, D., Serban, R., & Jayakumar, P. (2018, 08). Deformable soil with adaptive level of detail for tracked and wheeled vehicles. *International Journal of Vehicle Performance*, 5, 1-16. doi: 10.1504/IJVP.2019.10018134
- Toupet, O., Biesiadecki, J., Rankin, A., Steffy, A., Meirion-Griffith, G., Levine, D., ... Maimone, M. (2018). Traction control design and integration onboard the mars science laboratory curiosity rover. In *2018 IEEE Aerospace Conference* (pp. 1–20).
- Venugopal, I., Prabu, T., Muthukkumaran, K., & Annadurai, M. (2020). Development of a novel lunar highland soil simulant (lss-isac-1) and its geotechnical properties for chandrayaan missions. *Planetary and Space Science*, 194, 105116. Retrieved from <https://www.sciencedirect.com/science/article/pii/S0032063320303299> doi: <https://doi.org/10.1016/j.pss.2020.105116>
- Watyotha, C., Gee-Clough, D., & Salokhe, V. (2001). Effect of circumferential angle, lug spacing and slip on lug wheel forces. *Journal of Terramechanics*, 38(1), 1-14. Retrieved from <https://www.sciencedirect.com/science/article/pii/S0022489800000082> doi: [https://doi.org/10.1016/S0022-4898\(00\)00008-2](https://doi.org/10.1016/S0022-4898(00)00008-2)
- White, D., Take, W., & Bolton, M. (2003). Soil deformation measurement using particle image velocimetry (piv) and photogrammetry. *Geotechnique*, 53(7), 619–631.
- Wiendieck, K. W. (1971). *Prediction of the slope-climbing capability of elastic-rim wheels* (Tech. Rep.). Huntsville, AL: Marshall Space Flight Center. National Aeronautics and Space Administration.
- Wong, J. (2022). *Theory of ground vehicles*. Wiley. Retrieved from <https://books.google.ca/books?id=CW96EAAAQBAJ>
- Wong, J. Y. H., & Reece, A. R. (1967). Prediction of rigid wheel performance based on the analysis

- of soil-wheel stresses part i. performance of driven rigid wheels. *Journal of Terramechanics*, 4, 81-98. Retrieved from <https://api.semanticscholar.org/CorpusID:109496918>
- Yoshida, K., & Ishigami, G. (2004). Steering characteristics of a rigid wheel for exploration on loose soil. In *2004 IEEE/RSJ International Conference on Intelligent Robots and Systems (IROS)* (IEEE Cat. no. 04ch37566) (Vol. 4, pp. 3995–4000).
- Yoshida, K., Watanabe, T., Mizuno, N., & Ishigami, G. (2006). Terramechanics-based analysis and traction control of a lunar/planetary rover. In S. Yuta, H. Asama, E. Prassler, T. Tsubouchi, & S. Thrun (Eds.), *Field and service robotics: Recent advances in research and applications* (pp. 225–234). Berlin, Heidelberg: Springer Berlin Heidelberg. Retrieved from [https://doi.org/10.1007/10991459\\_22](https://doi.org/10.1007/10991459_22) doi: 10.1007/10991459\_22
- Zhang, Q., Townsend, S., & Kamrin, K. (2020, 11). Expanded scaling relations for locomotion in sloped or cohesive granular beds. *Physical Review Fluids*, 5. doi: 10.1103/PhysRevFluids.5.114301
- Zhou, C., Jia, Y., Liu, J., Li, H., Fan, Y., Zhang, Z., ... Zou, Y. (2022). Scientific objectives and payloads of the lunar sample return mission—chang’e-5. *Advances in Space Research*, 69(1), 823-836. Retrieved from <https://www.sciencedirect.com/science/article/pii/S0273117721006931> doi: <https://doi.org/10.1016/j.asr.2021.09.001>
- Zhou, F., Arvidson, R., Bennett, K., Trease, B., Lindemann, R., Bellutta, P., ... Senatore, C. (2014, 01). Simulations of mars rover traverses. *Journal of Field Robotics*, 31. doi: 10.1002/rob.21483